

Geology of the Boyongan and Bayugo Porphyry Cu-Au Deposits: An Emerging Porphyry District in Northeast Mindanao, Philippines*

David P. Braxton,^{1,2,†,**} David R. Cooke,^{1,3} Allan M. Ignacio,^{1,***} and Patrick J. Waters^{4,****}

¹Centre of Excellence in Ore Deposits (CODES), University of Tasmania, Private Bag 79, Hobart, 7001, Tasmania, Australia

²Anglo American, Group Exploration and Geosciences, 20 Carlton House Terrace, London SW1Y 5AN, United Kingdom

³Transforming the Mining Value Chain, an Australian Research Council Industrial Transformation Research Hub, University of Tasmania, Hobart, Tasmania 7001, Australia

⁴Anglo American Exploration (Philippines) Inc., 21 Outlook Drive, Baguio City 2600, Philippines

Abstract

The Boyongan and Bayugo porphyry Cu-Au mineral deposits, discovered under postmineralization cover during the previous decade, are part of an emerging belt of intrusion-centered Au-rich Cu mineral deposits and prospects in the Surigao district of northeast Mindanao, Philippines. Since their formation in the early Pleistocene, exhumation and weathering of these deposits have led to the development of a 600-m-thick oxidation profile at Boyongan and a modest (30–70 m) oxidation profile at Bayugo. Debris flows, volcanic material, and fluvio-lacustrine sediments accumulating in the actively extending Mainit graben subsequently covered the weathered deposits, preserving their supergene profiles.

The mineral deposits formed in association with a composite diorite complex containing at least 12 discrete intrusive stages. Three premineralization diorite porphyry stocks and a silt-sand matrix breccia complex represent early stages of magmatism and brecciation. Significant Cu and Au introduction followed these events and occurred in association with small early-mineralization diorite porphyry stocks at Boyongan and Bayugo. Within the diorite complex, the two mineral deposits are spatially distinct, separated by approximately 1 km of premineralization diorites. Inter- and late-mineralization intrusions were emplaced as the magmatic-hydrothermal system waned.

A characteristic progression of vein and K silicate alteration styles affected each of the synmineralization intrusions. Rare comb quartz unidirectional solidification textures (stage 0) mark the transition from magmatic to hydrothermal conditions. Quartz-poor wispy magnetite-biotite-K-feldspar veinlets characterize stage 1. Stage 2 veins consist of quartz with selvage and/or disseminated magnetite or biotite and K-feldspar halos. Stage 3 quartz veins have K-feldspar halos but generally lack magnetite and biotite. Stage 4 veins consist of massive bornite-chalcopyrite and chalcopyrite-pyrite with K-feldspar halos. Stage 3 quartz veins and stage 4 sulfide veins host Cu-Au mineralization of the greatest volumetric significance, reflecting the general paucity of sulfide in the earlier vein stages. Despite the simplicity of this sequence, detailed paragenetic reconstructions reveal that this characteristic progression of veining and K silicate alteration was repeated with the emplacement of each synmineralization intrusive event, revealing multiple magmatic-hydrothermal cycles of alteration and mineralization.

At Boyongan and Bayugo, intense and pervasive illite alteration, in association with pyrite, chalcopyrite, and tetrahedrite-tennantite, developed in narrow structures crosscutting quartz-K-feldspar veins. Debris flows in the burial sequence above and adjacent to the Boyongan/Bayugo complex also contain abundant clasts with intense, pervasive illite and alunite-pyrophyllite-dickite-kaolinite alteration assemblages that have overprinted K silicate-style quartz veins.

In both mineral deposits, Cu and Au are associated with intense quartz-vein stockworks composed primarily of K silicate stage 3 veins. Despite this association, not all of these quartz-vein stockworks contain Cu and Au to the same tenor. Quartz-vein stockworks in the eastern high grade of Boyongan have been intersected over a vertical interval of 800 m, having affected much of the early-mineralization stock. However, hypogene Cu grades exceed 0.5% by weight only in the upper 300 m of the stockwork (in the cupola of the early-mineralization stock). Superior grade development in high-grade zones at Boyongan, locally exceeding 2% Cu and 3 g/t Au, developed where fertile vein stages from two or more magmatic-hydrothermal cycles affected the same wall rock.

The documented paragenetic relationships demonstrate multiple discrete cycles of K silicate-stage veining and alteration associated with each synmineralization intrusive event. All such events predate formation of feldspar-destructive illite-smectite-chlorite, illite-pyrite, and quartz-alunite-clay assemblages. Existing geochronological constraints on the timing of magmatism and hydrothermal activity demonstrate that these repeated cycles supporting superior grade development transpired extremely rapidly, in a period of less than 200,000 years (2.3–2.1 Ma). Geologic and geochronological constraints on the life cycle of Boyongan and Bayugo describe an extremely dynamic history of emplacement, exhumation, weathering, and burial over a period of 2.3 m.y. The study illustrates the spectrum of metallogenic processes operative over a geologically brief period and highlights some of the key elements responsible for formation of superior grades and for deposit preservation in an extensional setting.

† Corresponding author: e-mail, dave.braxton@angloamerican.com

* Electronic appendices for this paper can be found at www.economicgeology.org.

** Present address: Anglo American, Group Exploration and Geosciences, 20 Carlton House Terrace, London SW1Y 5AN, United Kingdom.

*** Present address: Aranz Geo (AUS) Pty Ltd. 2F, 25 Cantonment St, Fremantle WA 6160, Australia.

**** Present address: Locrian Resources Inc. 400, 255-17 Avenue SW-Calgary, Alberta T2S 2T8, Canada.

Introduction

Located in the northeast of the island of Mindanao, Boyongan and Bayugo are two Cu-Au porphyry mineral deposits discovered by Anglo American in 2000 and 2003, respectively, beneath postmineralization cover in the historic Surigao Au district of the southern Philippines (Fig. 1). Recent mineral resource estimates for Boyongan (measured, indicated, and inferred at 0.5% Cu equiv cutoff grade) stand at 299 million tons (Mt) grading 0.51% Cu and 0.70 g/t Au, while similar estimates for Bayugo total 132 Mt grading 0.67% Cu and 0.67 g/t Au (Philex, 2011).

Since their formation in the early Pleistocene, the Boyongan and Bayugo mineral deposits were exhumed and subsequently buried beneath postmineralization cover in the active Mainit graben system. During its geologically brief exposure, a 600-m-thick supergene profile developed at Boyongan, this being the deepest pervasive oxidation profile of any porphyry system described to date (Braxton et al., 2009). This paper provides a detailed geologic description for these deposits and their evolution in this emerging Cu-Au district.

Discovery history

With the genetic association of epithermal Au and porphyry Cu-Au systems in mind, Anglo American Exploration (Philippines) Inc. (Anglo American) targeted the Surigao Au district (northeast Mindanao) for porphyry Cu-Au potential in 1997. In January 1998, Anglo American, operating a joint venture with partner Philex Gold (Philex), began a program of reconnaissance-scale geologic mapping and stream sediment geochemistry over Philex's tenements in the Surigao peninsula. This work highlighted several low-level stream sediment Au and Cu anomalies as well as extensive trains of diorite boulders containing intense quartz vein stockwork in the Bagacay and Magpayang drainage areas, located northwest and south, respectively, of the Bayugo and Boyongan deposits (Fig. 2). The exploration team then carried out a dipole-dipole induced-polarization (IP) survey over a 10-km² area around Bagacay. Drilling results in the vicinity of the altered boulder trains (Fig. 2A) failed to intersect a porphyry system but did reveal intensely veined diorite porphyry cobbles and boulders in the cover sequence. These results suggested that the mineralized and altered boulders had been transported by active streams reworking Pleistocene conglomeratic and debris-flow facies in the postmineralization cover. Continued prospecting for the bedrock source of the mineralized boulders highlighted sparse diorite porphyry float in the Boyongan area, leading to the decision to conduct a 13-km ridge-and-spur soil sampling program in conjunction with ground magnetic and IP geophysical surveys. The geochemical survey results defined discrete Au and base-metal anomalies within restricted Pliocene or older inliers and also within the actively eroding paleo-debris flows in the cover sequence. Diamond drilling at Boyongan commenced in mid-2000, with the first hole (TSD01) targeting a magnetic feature. The hole intersected barren magnetite-bearing basaltic rocks of the Oligocene-Miocene Bacuag Formation beneath cover. Scout drilling continued, and in August 2000 diamond drill hole TSD06 intercepted the Boyongan mineral deposit beneath 57 m of volcanic and sedimentary postmineralization cover. The discovery hole

intercepted 362 m of K silicate-altered diorite breccia, with grades of 0.8% Cu and 1.9 g/t Au (Fig. 2).

In parallel with a resource scoping drilling program at Boyongan, exploration for additional porphyry centers in the district continued with a series of low-density (~1-km spacing) scout drill holes designed to sample the pre-Quaternary bedrock over a ~40-km² NW-trending structural corridor centered on Boyongan (Fig. 2D). A key result of this program was recognition that chalcocite in hole TSD29, drilled several hundred meters to the northwest of the Boyongan system, likely reflected provenance from a second porphyry system. In mid-2003 hole JSD15 (drilled ~1,200 m northwest of Boyongan) encountered a 600-m interval of hypogene Cu sulfides grading 0.3% Cu and 0.3 g/t Au from 400-m depth. This hole confirmed the discovery of a second blind porphyry Cu-Au system, termed Bayugo (Fig. 2).

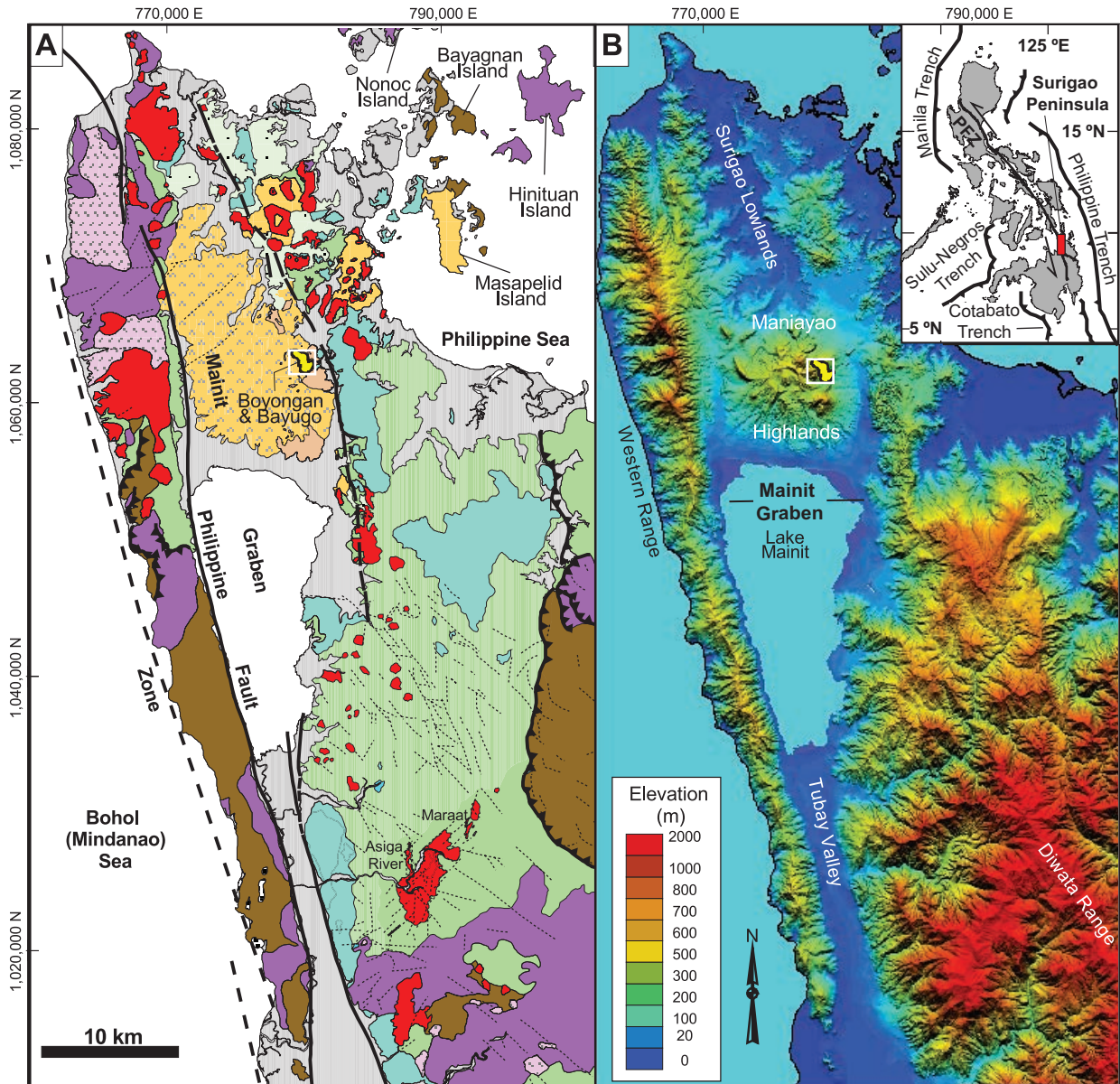
Regional Tectonic Setting

The Philippine archipelago currently lies at the juncture of two major tectonic plates: the Philippine Sea plate to the east, and the Eurasia plate to the west. Caught between these two converging plates is the Philippine mobile belt (Gervasio, 1966), an actively deforming tectonic collage of oceanic crustal blocks surrounded on most sides by destructive plate margins. Four major subduction zones currently consume oceanic crust beneath the Philippines (Fig. 1B, inset). To the west, collision of the Philippines and Eurasia plates is driving E- and NE-directed subduction of South China, Sulu, and Celebes oceanic crust at the Manila, Negros-Sulu, and Cotabato trenches, respectively. Suture (collision) zones in Mindoro, Panay, and Mindanao connect these subduction zones in locations where Eurasia plate continental crustal fragments are colliding with the Philippine oceanic basement. East of the central and southern Philippines, the Philippine trench is consuming the Philippine Sea plate. Farther north, the bathymetric depression of the east Luzon trough may represent an incipient and/or inactive subduction zone (Aurelio, 2000b).

Much of the Philippine archipelago represents a collage of Mesozoic and Tertiary island arcs built on oceanic crust of the Philippine Sea plate. Northeast movement of this plate relative to the Eurasia plate resulted in collision and docking of these arc terranes at the Eurasian continental margin beginning in the late Miocene. Active volcanism throughout much of the Philippines is related to subduction zones beneath the eastern, western, and southern margins of the Philippine mobile belt. Oblique convergence between the Eurasia and Philippine Sea plates has contributed to the development of the Philippine fault, a strike-slip fault zone with dominantly sinistral displacement extending over 1,200 km from Luzon to Mindanao. In the vicinity of the Boyongan and Bayugo deposits, the Philippine fault passes through (and controls the overall shape of) the Surigao peninsula (Fig. 1B). The patterns of physiography, sedimentation, and active volcanism in this region reflect the profound influence of this crustal-scale fault zone.

Philippine porphyry deposits

Porphyry Cu-(Au) deposits (defined herein as low-grade, large-tonnage hydrothermal accumulations of Cu ± Au and/or Mo formed in intimate association with high-level, commonly



Volcanic & Sedimentary Stratigraphy

- Alluvium
- Maniayao Andesite
- Tugunan Fm.
- Timamana Limestone
- Mabuhay Clastics Fm.
- Motherlode Turbidite Fm.¹
- Bacuag Fm.²
- Madanlog Fm.

Hypabyssal Intrusions

- Plio-Pleistocene andesites-diorites
- Miocene (?) diorites

Basement Complex

- Surigao Ophiolite
- Concepcion Schist³

Structures

- Thrust/Reverse Fault
- Major Fault: Observed/Inferred
- Lineament

¹Includes Libas Marl of Mitchell and Leach (1991).

²Includes San Isidro Fm of L. Santos-Ynigo (unpub. report, 1944).

³Includes Sohatan Fm of L. Santos-Ynigo (unpub. report, 1944).

Fig. 1. (A) Generalized geology of the Surigao peninsula, compiled from mapping of L. Santos-Ynigo (unpub. report, 1944) for the Philippine Bureau of Mines and Geosciences (Bureau of Mines and Geosciences, 1983), mapping of United Nations Development Program (1987), and from unpublished mapping by Anglo American Exploration (Philippines) Inc. (B) Digital elevation model of the Surigao peninsula emphasizing the region's principal physiographic elements, modified after unpublished data from Anglo American Exploration (Philippines) Inc. Map Projection: UTM zone 51N, datum: Clark 1864 (Luzon exclusive of Palawan). Inset in (B) shows the tectonic context of the Surigao peninsula in the Philippine mobile belt. Abbreviations: PFZ = Philippine fault zone.

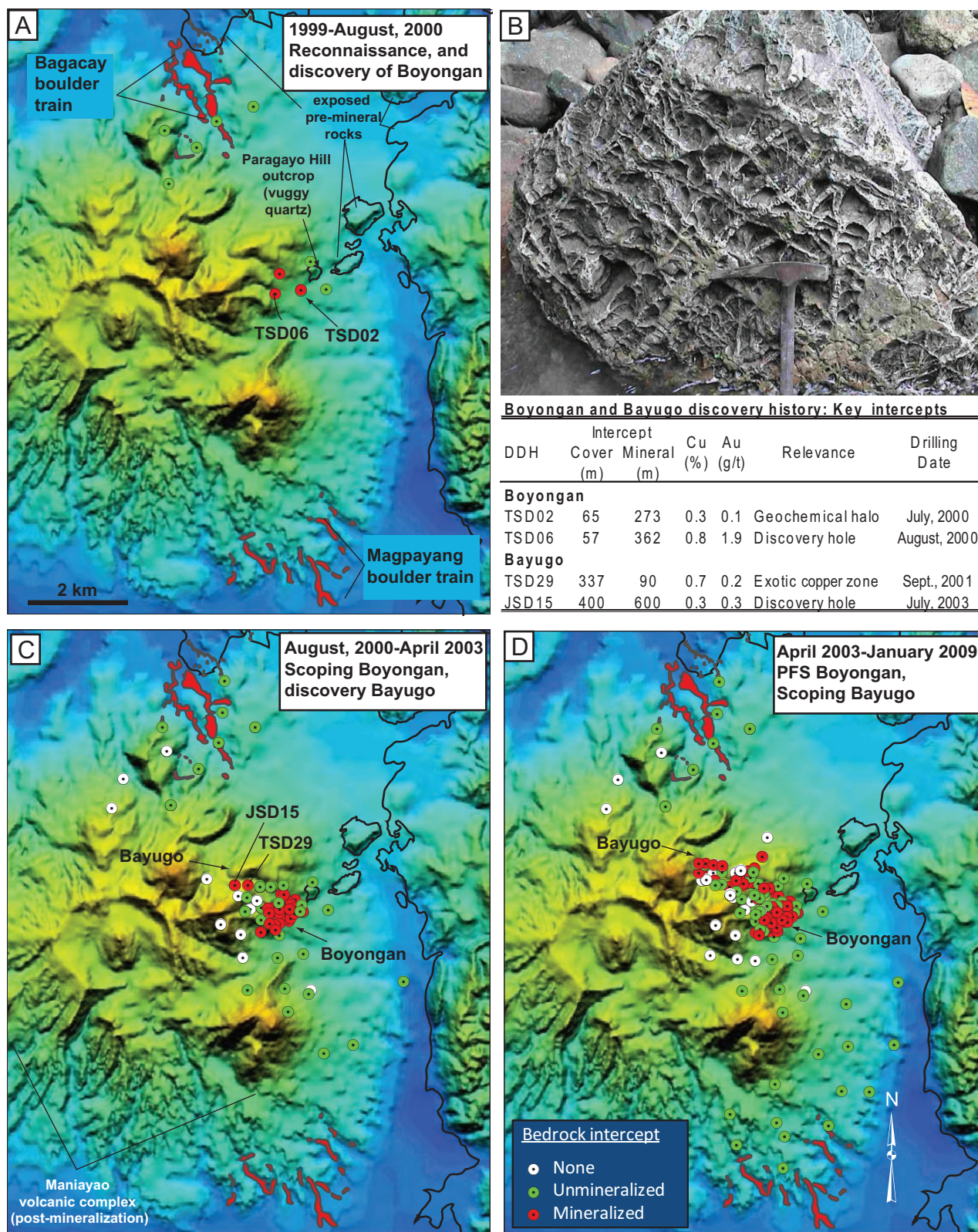


Fig. 2. Key elements of the discovery history, Boyongan and Bayugo. (A) Reconnaissance mapping and geochemical sampling leads to recognition of mineralized boulder fields at Bagacay and Magpayang (shown in red). Black outlines delimit areas of premineralization bedrock outcrop. (B) Scout drilling leads to discovery hole at Boyongan (TSD06). (C) Step-out drilling in TSD29 intersects chalcocite later recognized as evidence for a second porphyry Cu system (Bayugo), as confirmed by JSD15. (D) Scoping of Bayugo confirms presence of chalcocite enrichment zone. Modified after Braxton and Waters (2012). Abbreviations: PFS = prefeasibility study.

porphyritic, intrusive stocks) developed in most of the magmatic arcs within the Philippine archipelago. For clarity, the terms “deposit” or “mineral deposit” as employed broadly in this study follow the terminology defined by the American Geological Institute (1996, p. 347) to refer to “a mineral occurrence of sufficient size and grade that it might, under favorable circumstances, be considered to have economic potential.” More than 50 Philippine porphyry deposits and prospects have been described in some detail (Sillitoe and Gappe, 1984; Hedenquist et al., 1998; Cooke et al., 2005, 2011; Singer et al., 2005a, b, 2008; Braxton, 2007), attesting to the archipelago’s endowment of intrusion-related Cu. Some of these systems relate to older arc configurations, including the Cretaceous Atlas district in Cebu (Walther et al., 1981; Kermtke et al., 1991), the Eocene Canicanian deposit in Polillo (Knittel and Burton, 1985), the early Oligocene Sipalay deposit in southern Negros (Walther et al., 1981), the latest Oligocene Dinkidi deposit in the Didipio region of northern Luzon (Hollings et al., 2011; Wolfe and Cooke, 2011), and the early Miocene Tapian (Marcopper) deposit in Marinduque (Walther et al., 1981). The majority of dated Philippine porphyry deposits are younger than 10 Ma (Sillitoe and Angeles, 1985; Arribas et al., 1995; Bellon and Yumul, 2000; Imai, 2001; Rohrlach, 2002; Chang et al., 2011; Waters et al., 2011; Braxton et al., 2012). Most of these are spatially associated with the Philippine fault zone in Luzon and Mindanao, reflecting a tectonic configuration approaching that of today.

Surigao District Geologic Setting

The Surigao peninsula lies at the northeast tip of Mindanao and defines a NNW-trending salient some 90 km in length and 60 km in width. Three elevated landforms dominate the physiography of the Surigao peninsula. From east to west these are the Diwata Range (or Eastern Cordillera), the Maniayao highlands, and the Western Range (Fig. 1B). An elongate depression defined by the Surigao lowlands in the north and the Tubay Valley in the south separates the Diwata Range from the Western Range. This depression relates to the actively-extending Mainit graben, filled on its southern edge by the prominent freshwater Lake Mainit. The volcanic Maniayao highlands occur at the northern edge of Lake Mainit. They are associated with Pleistocene-Recent extension within the graben and locally reach 660 m above sea level (a.s.l.). Along the western graben margin, transtension along a strand of the Philippine fault (Pubellier et al., 1993) has led to uplift of the Western Range to elevations exceeding 1,000 m a.s.l. Uplift in the Diwata Range on the east side of the peninsula has generated peaks reaching 2,000 m a.s.l.

The stratigraphy of the Surigao peninsula reflects the protracted history of tectonic assembly that took place in the southern Philippines. The brief summary presented here draws largely on the work of L. Santos-Yñigo (unpub. report, 1944), United Nations Development Program (1987), and Mitchell and Leach (1991), supplemented in the vicinity of the Boyongan and Bayugo prospects by our observations from diamond drill core. Figure 3 presents a generalized stratigraphic column for the Surigao peninsula. Thicknesses presented represent estimates of the maximum stratigraphic thicknesses reported in the literature or observed in the field.

Basement complex

Basement rocks in the Surigao peninsula are of two distinct types: (1) greenschist facies metasediments and greenstones and (2) ultramafic rocks with ophiolitic affinities. Drilling and mapping revealed no substantial basement rocks in the vicinity of the Boyongan and Bayugo deposits. However, xenoliths of garnet-amphibolite occur in the Maniayao andesite flows, consistent with the presence of the Surigao ophiolite and/or the Madanlog Formation at depth.

Concepcion schist: L. Santos-Yñigo (unpub. report, 1944) termed this metasedimentary sequence the Sohatan Formation, describing it as a package of metaconglomerates, schists, sandstones, and marbles. United Nations Development Program (1984) added greenstones to the description of the sequence and renamed the package as the Concepcion schist. Their more recent terminology is retained here. The Concepcion schist underlies much of the Western Range, west and south of Lake Mainit, and occurs in the eastern Diwata Range (Fig. 1A). Direct age constraints for the metasedimentary/metavolcanic Concepcion schist in the Surigao peninsula do not exist. However, Cretaceous- to Paleogene-aged sequences of similar rock types underlie much of the eastern Philippines (Fernandez, 1981; Mitchell and Leach, 1991), suggesting a Cretaceous age for the Concepcion schist.

Surigao ophiolite: Extensive, locally serpentized bodies of peridotite, dunite, harzburgite (locally hosting podiform chromite), and gabbro crop out in the Western Range, the Diwata Range east of the Tubay Valley, and in numerous small islands (e.g., Nonoc, Dinagat, and Hinituan Islands) to the northeast of the Surigao peninsula (Fig. 1A). Although the package lacks a complete ophiolite sequence from basal peridotite through capping pillow basalts and sediments, many authors (e.g., Hawkins et al., 1985) consider this mafic-ultramafic package to be a detached fragment of oceanic crust. Mitchell and Leach (1991) interpreted the garnet amphibolite rocks in southern Dinagat Island as a metamorphic sole of the Surigao ophiolite. Like the Concepcion schist, direct age determinations for the Surigao ophiolite have not been reported. Age determinations from pelagic sediments covering mafic-ultramafic sequences elsewhere in the Philippines provide the principal age constraint for Philippine ophiolites (Aurelio, 2000a, and references therein), suggesting minimum ophiolite ages between late Cretaceous and Oligocene. The stratigraphic sequence overlying the Surigao ophiolite constrains the minimum age to pre-late Eocene.

Where contacts are exposed in the Surigao peninsula, mapping has shown the Surigao ophiolite to have been thrust atop the Concepcion schist (Fig. 1A), a relationship common to most of the Philippine basement rocks. Based on this relationship, Mitchell and Leach (1991) argued that most large Philippine ophiolites were emplaced as extensive thrust nappes.

Madanlog Formation

The Madanlog Formation occurs as isolated outcrops containing interstratified conglomerates, black shales, and fossiliferous gray limestones. The sequence nonconformably overlies the basement complex in the Western Range (Fig. 1A) and in an isolated occurrence east of the Mapawa mine (United Nations Development Program, 1987). The conglomerates

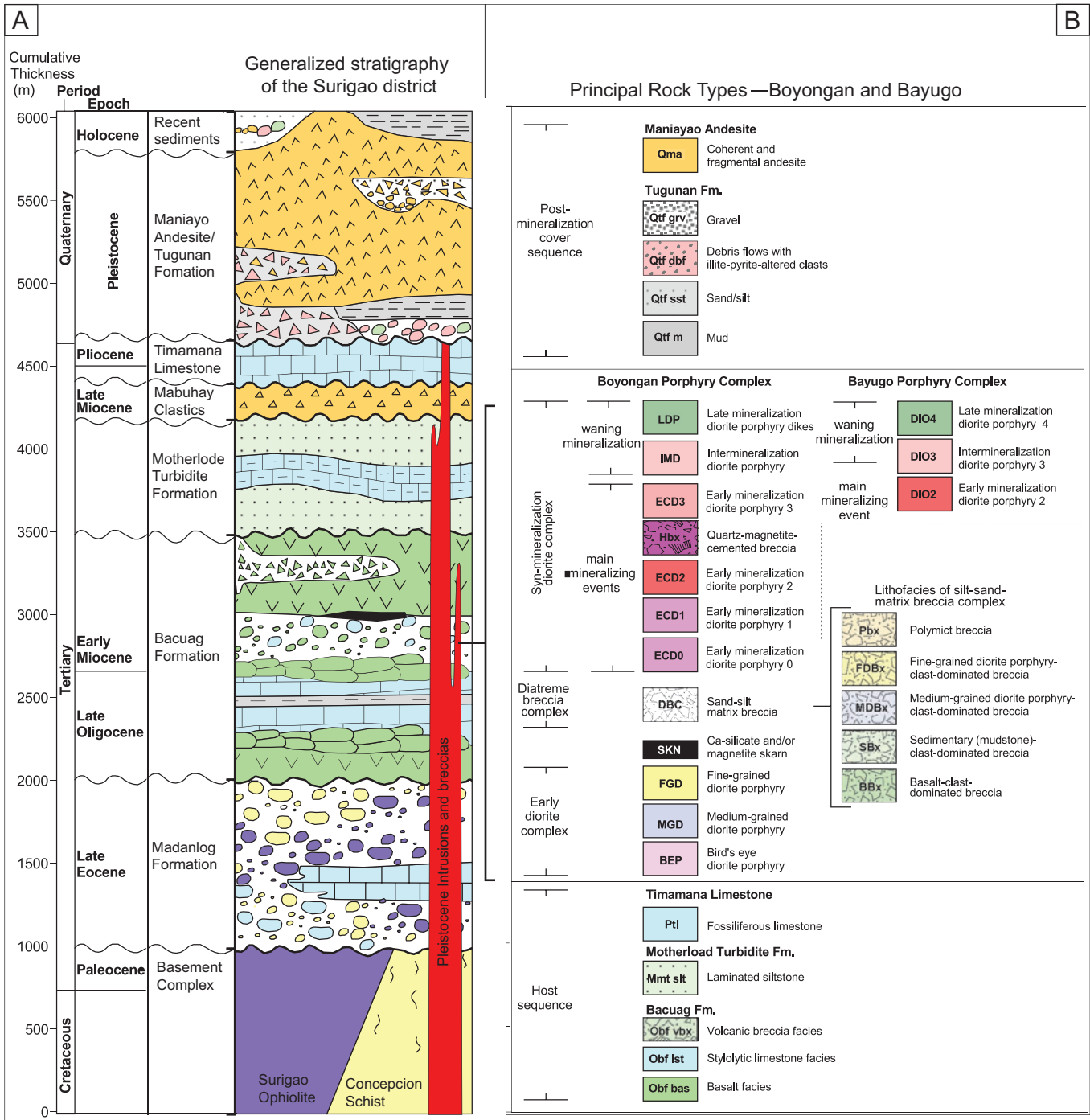


Fig. 3. (A) Generalized stratigraphy of the Surigao district, compiled from L. Santos-Ynigo (unpub. report, 1944), United Nations Development Program (1987), and Mitchell and Leach (1991). Stratigraphic thicknesses are variable, and those portrayed are approximations of the maximum thickness. (B) Legend for rock types represented in geologic maps and cross sections in Figures 5, 6, 11, 12, 20, 21, and 23, and Appendix 1 (Figs. A4–A6, A13–A18, A23, A34, A26–A28).

consist of well-rounded clasts of basement complex, while the limestones reportedly contain an Eocene-aged faunal assemblage (L. Santos-Yñigo, unpub. report, 1944).

Bacuag Formation

The Bacuag Formation is a heterolithic sequence of interstratified basaltic volcanics, limestones, and coarse clastic

rocks and includes the San Isidro Formation, Siana Formation, and Bacuag series of L. Santos-Yñigo (unpub. report, 1944). The Bacuag Formation underlies most of the Diwata Range and occurs as isolated outcrops in the Surigao lowlands and the Western Range (Fig. 1). Drilling by Anglo American revealed that the Bacuag Formation also underlies the region northeast of Lake Mainit, forming the principal stratigraphic

host to the intrusions of the Boyongan and Bayugo porphyry deposits.

Stratigraphic relationships between subunits of the Bacuag Formation are not well understood, since many contacts are unexposed or faulted. Figure 3 presents a tentative stratigraphic sequence for the Bacuag Formation, based largely on the compilation of United Nations Development Program (1987). The basal section (formerly the San Isidro Formation of L. Santos-Yñigo, unpub. report, 1944) contains amygdaloidal basalts and andesites, which have undergone widespread epidote-prehnite-albite alteration and locally intense brecciation. Also low in the sequence, massive to amygdaloidal, locally augite-phyric pillow basalts are interstratified with gray limestones and calcirudites (Siana beds) and carbonaceous shales. These rocks are best exposed in the environs of the Siana mine open pit, 7 km south-southwest of Boyongan (Fig. 4). Higher in the sequence, aphyric to feldspar-phyric basalts (App. 1, Fig. A1A) are locally interstratified with gray, stylolitic, locally coralline limestones (App. 1, Fig. A1B), coal-bearing sandstones, and limestone- and basalt-clast conglomerates (App. 1, Fig. A1C, D). Massive basalt intercalated with basaltic breccias, which contain chaotic, angular clasts in a green-brown fine-grained matrix, characterizes the highest stratigraphic intersections of the Bacuag Formation in the vicinity of the Boyongan and Bayugo porphyry deposits (App. 1, Fig. A1C).

Bacuag Formation fossiliferous limestones from Masapelid Island and elsewhere in eastern Surigao contain upper Oligocene to lower Miocene faunal assemblages (United Nations Development Program, 1987). Whole-rock K-Ar age determinations of 23 ± 1.1 (United Nations Development Program, 1987), 17.16 ± 0.36 , and 13.25 ± 0.62 Ma (Sajona et al., 1997) from basaltic rocks support an upper Oligocene-middle Miocene age for the Bacuag Formation.

Motherlode Turbidite Formation

The Motherlode Turbidite Formation, a gently folded sequence of silty mudstones, wackes, and basalt-dominated turbiditic sequences, underlies much of the northeastern Surigao peninsula (Fig. 4). A basal unconformity separates the Motherlode Turbidite Formation and the underlying Bacuag Formation in the Libas River valley, 1 km southwest of the Motherlode mine (United Nations Development Program, 1987). In the vicinity of the Boyongan and Bayugo deposits, dark, finely laminated, silty mudstones containing thin calcisiltite beds (App. 1, Fig. A2A) dominate the drill intersections of the Motherlode Turbidite Formation northeast of the Maniayao Volcanic Complex (Fig. 4).

The Motherlode Turbidite Formation contains a thick marl sequence variably termed the Taganaan Marl Member (United Nations Development Program, 1987) or the Libas marl (Mitchell and Leach, 1991). Foraminifera from this marl indicate a lower to middle Miocene age (United Nations Development Program, 1987). These data, in conjunction with K-Ar dating of basalts from the underlying Bacuag Formation, suggest a post-13.25 Ma age for the formation as a whole.

Mabuhay Clastics Formation

Andesitic clastic and volcanoclastic rocks and uncommon andesite flows crop out in northeastern Surigao and on Masapelid

Island. These rocks constitute the Mabuhay Clastics Formation, the most important host sequence for epithermal veins recognized to date in the Surigao district. Altered exposures in and around the workings of the Placer, Motherlode, Mapaso, and Siana mines (Fig. 4) have provided the basis for many of the lithologic descriptions of this unit (United Nations Development Program, 1987; Mitchell and Leach, 1991). In the Placer mine, polymictic (hornblende-phyric andesite, andesite porphyry, dacite, limestone, and siltstone) conglomerates are interbedded with immature cross-stratified wackes and grits. These are interstratified with the massive "Briggs pyroclastics" (United Nations Development Program, 1987), breccias consisting of medium-grained (generally <5 cm), chaotic, angular, unsorted, dominantly andesitic clasts in a fine-grained clastic matrix. Near the Motherlode mine, a coarse-grained polymictic basal conglomerate (Kambilid boulder bed) unconformably overlies the Motherlode Turbidite Formation.

Evidence for the Mabuhay Clastics Formation is equivocal in the vicinity of the Boyongan and Bayugo porphyry deposits. Drilling on the north and east margins of Boyongan intersected massive basalt interstratified with basaltic breccias containing chaotically distributed, angular clasts in a green-brown, fine-grained matrix (App. 1, Fig. A1D). Anglo American geologists originally interpreted this facies as a pyroclastic component of the Mabuhay Clastics Formation (Ignacio, 2005). However, the monomictic character and basaltic composition of the breccias, their intimate relationship with massive basalts, and the absence of underlying Motherlode Formation clastic rocks suggest that the breccias are a fragmental facies within the upper Bacuag Formation.

A post-lower to middle Miocene and pre-early upper Pliocene depositional age is inferred for the Mabuhay Clastics Formation, because limestone clasts from Mabuhay conglomerates near the Placer mine contain lower to middle Miocene fauna (United Nations Development Program, 1987). At the Pamenco quarry 2 km west of the Motherlode mine, a hornblende diorite hypabyssal plug dated at 3.23 ± 0.20 Ma (hornblende, Ar-Ar) has intruded the Mabuhay Clastics Formation (Camacho, 2001; P. Waters and R. Gonzales, unpub. report, 2003). Mitchell and Leach (1991) inferred a middle to early upper Miocene age for the Mabuhay Clastics Formation, based on a correlation with a similar clastic andesitic sequence that underlies an upper Miocene sequence at Tambis in central eastern Mindanao. This inference is consistent with the existing age constraints for the Mabuhay Clastics Formation in Surigao.

Timamana limestone

The Timamana limestone is a massive, cream-white, fossiliferous limestone forming prominent cliffs in the northern Diwata Range east and northeast of Lake Mainit (Fig. 1). In this region, limestone exposures unconformably overlie the Bacuag Formation, capping peaks exceeding 900 m a.s.l. In smaller exposures west of the Mapaso mine (Fig. 4), a similar limestone unconformably overlies the Motherlode Formation.

Deposition of the Timamana limestone is inferred to have occurred immediately prior to the mineralizing events in the Surigao district. Due to a lack of exposure, contact relationships with the Mabuhay Clastics Formation are not

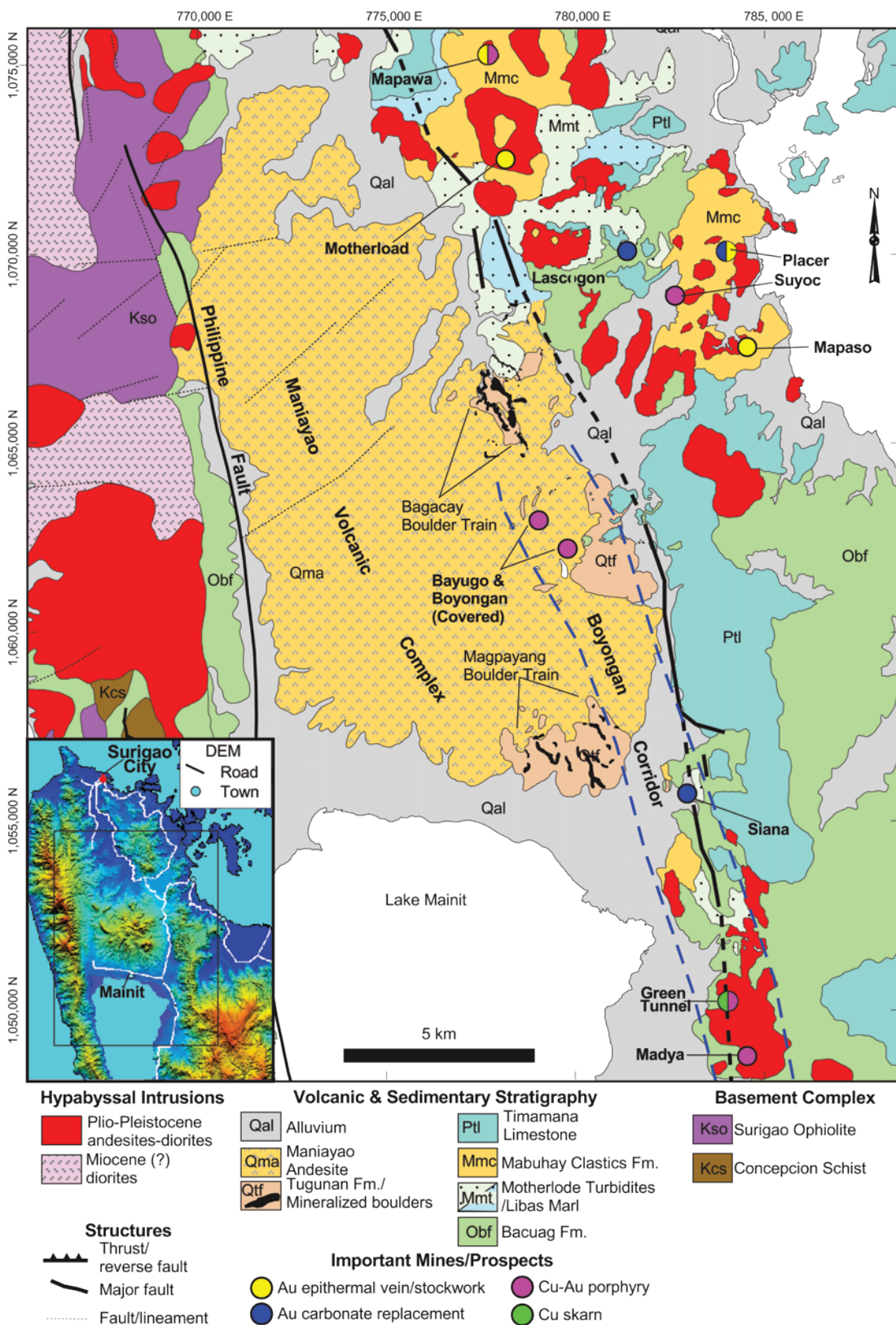


Fig. 4. Generalized geology of the northeast Surigao peninsula, showing locations of important mines and prospects. Compiled from mapping of L. Santos-Ynigo (unpub. report, 1944) for the Philippine Bureau of Mines and Geosciences (Bureau of Mines and Geosciences, 1983), mapping of United Nations Development Program (1987), and from unpublished mapping by Anglo American Exploration (Philippines) Inc. Map Projection: UTM zone 51N, datum: Clark 1864 (Luzon exclusive of Palawan). Abbreviations: DEM = digital elevation model.

understood, and age constraints for the Timamana limestone are commensurately poor. Micropaleontological analysis of a sample of fossiliferous Timamana limestone (Braxton, 2007) revealed an assemblage of large foraminifera containing *Alveolinella quoyii*, *Amphistegina* sp., *Operculina* sp., and *Marginopora* sp. The sample lacked *Lepidocyclus* sp., which became extinct during the late Miocene. Based on this assemblage and the lack of Pleistocene to Recent foraminifera such as *Baculogypsina* sp. and *Calcarina* sp., an age of latest late Miocene-Pliocene was estimated. Consequently, the Timamana limestone is inferred to postdate the middle to early upper Miocene Mabuhay Clastics Formation.

Tugunan Formation

The Tugunan Formation and Maniayao andesites form an extensive sequence of Quaternary clastic, volcanoclastic, and volcanic debris covering much of the central lowlands between the Diwata and Western ranges (Figs. 1, 4). These formations were deposited in the actively extending Mainit graben (L. Santos-Yñigo, unpub. report, 1944). Anglo American scout drilling over a 4- × 10-km region around Boyongan and Bayugo enabled definition of four lithofacies (App. 1, Fig. A3): illite-altered debris flow facies, fluvial facies, lacustrine facies, and volcanic facies.

Illite-pyrite-altered debris flow facies: Coarse-grained sequences of unstratified, chaotic, generally matrix-supported debris flows containing subrounded illite + pyrite-altered clasts of intrusions and associated pre-Quaternary host rocks occur close to Boyongan and Bayugo (App. 1, Fig. A3C). Clasts are generally supported in a white clay-rich (illite ± smectite ± chlorite ± kaolinite ± pyrophyllite), pyritized matrix. Drilling intersections locally exceed 100 m in apparent thickness (e.g., diamond drill hole JSD09). The clast types, clay alteration, and spatial distribution are consistent with derivation from an incompetent clay-dominated lithocap that is inferred to have overlain and/or occurred adjacent to the Boyongan/Bayugo mineralized complex. The thick sequences of mass-wasting deposits attest to catastrophic slope failures in environments of high relief. Generation of such relief probably reflects rapid surface displacement along normal faults associated with the Mainit graben, although surface inflation related to shallow magma movement beneath the Maniayao volcanic complex may also have played a role.

Fluvial facies: The Tugunan Formation fluvial facies includes poorly consolidated to unconsolidated gravels, sands, and silts (App. 1, Fig. A3D, E). The gravels commonly occur as 5- to 10-m-thick lenses within massive sands and silty sands and are well rounded, moderately well sorted, and clast supported with a sandy matrix. Clasts of pre-Quaternary rock units dominate the gravel composition near the base of the Tugunan Formation, including mineralized and/or altered intrusive rocks most likely derived from the Boyongan and Bayugo deposits. Andesite clasts occur at higher stratigraphic intervals and are the dominant clast type in the uppermost gravels.

Sands and silts are most abundant east of Boyongan and Bayugo, and gravel accumulations are greatest to the northwest and the south of the deposits (App. 1, Fig. A3D, E). In addition to bedding structures, the clast types, rounding, and distribution relative to inferred principal source areas

(Boyongan, Bayugo, and Maniayao) are consistent with transport and deposition within a fluvial setting.

Wood and leaf fragments commonly occur within the fluvial facies (App. 1, Fig. A2C), particularly near the pre-Quaternary unconformity. To constrain the timing of burial at Boyongan, Anglo American geologists collected three samples of this material from the unconformity for radioisotopic ¹⁴C dating. A sample of leaves collected from an elevation of 4 m below sea level (b.s.l.) gave a ¹⁴C age of 30,080 ± 1,270 before present (BP). Two samples of wood collected from higher elevations on the unconformity (73 and 130 m) returned ages of 1,640 ± 80 and 1,760 ± 80 BP, respectively (Braxton et al., 2012). The dating showed that the final stages of burial of the Boyongan and Bayugo deposits occurred in the latest Pleistocene to Holocene.

Lacustrine facies: The lacustrine facies contains silty carbonaceous, locally bioturbated muds characteristic of a low-energy depositional setting. The muds vary from well laminated to massive and commonly contain shells of gastropods (high and low spire) and bivalves (App. 1, Fig. A2D). The muds thicken southward toward Lake Mainit (App. 1, Fig. A3F), but in the vicinity of Bayugo local thick accumulations suggest isolated, structurally controlled basins.

Because of the region's low elevation and proximity to the ocean, deposition in an estuarine environment is a possibility for some of these fine-grained sediments. However, Braxton's (2007) examination of four samples of Tugunan Formation silty mud revealed no marine microfauna.

Maniayao andesite: Clastic and coherent andesitic rocks (App. 1, Fig. A2D) of the Maniayao andesite form the prominent volcanic landforms in the Maniayao volcanic complex north of Lake Mainit (Fig. 4). Although exposures are poor, several positive topographic features within the Maniayao complex (refer to digital terrain model in Fig. 1B) suggest that there are multiple vent locations or subvolcanic plugs. The most prominent structure is the large (2 km) circular depression near the center of the complex, cored by a rounded hill. These two features appear to be an eruptive crater and resurgent dome, respectively, and based on their high degree of preservation, United Nations Development Program (1987) estimated an age not exceeding 0.1 Ma. A broad apron of volcanoclastic material surrounds the volcanic hills, covering much of the area between Lake Mainit and the Surigao lowlands (Fig. 1). Extensive drilling by Anglo American on the east margin of the Maniayao complex revealed that the volcanic package thickens to over 700 m westward (App. 1, Fig. A3B).

Recent fluvio-lacustrine sediments

Unconsolidated gravel, sand, silt, and mud cover much of the low-lying areas of the Surigao peninsula (Figs. 1B, 4). In the Bagacay and Magpayang areas (Figs. 2B, 4), clasts of quartz-vein-stockworked diorite porphyry are a common component of the gravels. Reworking of Tugunan Formation debris flows and conglomerates by active streams may explain this distribution.

The recent sediments are similar in composition and depositional patterns to the fluvial and lacustrine facies of the Tugunan Formation. These similarities reflect the general continuity of sediment provenance, transport, and depositional

environments operating since the onset of extension in the Surigao peninsula.

Surigao District Metallogeny

Until the discovery of the Boyongan porphyry Cu-Au deposit in 2000, the Surigao district was known primarily for epithermal Au, though workers in the 1980s (e.g., Sillitoe and Gappe, 1984) highlighted the Surigao district as prospective for porphyry Cu deposits. Mechanized mining began in the 1930s and, following a hiatus during World War II, has continued intermittently to the present day. Although all mines were initially worked as underground operations, the Siana, Placer, and Motherlode mines developed small open pits in the 1980s (Mitchell and Leach, 1991). At the time of writing, the Siana and Placer Au mines make up the active production from the Surigao. Estimates of historic Au production from the district exceed 2 Moz (Red 5, 2005; Conde, 2014).

Three principal styles of hydrothermal deposits occur in the Surigao district: vein-hosted epithermal Au, sediment-hosted/carbonate replacement Au, and porphyry Cu-Au (Table 1). In most deposits, altered diorite porphyry intrusions are spatially associated with metal accumulation.

Epithermal gold in the Surigao district

Epithermal Au deposits include the Placer, Motherlode, Mapawa, and Mapaso deposits, all located in eastern Surigao (Fig. 4). In these systems, Au occurs principally as electrum and Au tellurides associated with comb quartz, pyrite, and minor base metals in veins and restricted stockworks. The

mineralized structures have pervasive pyrite-illite \pm kaolinite alteration envelopes associated with varying degrees of silicification. Gold mineralization and alteration was focused in the Mabuhay Clastics Formation and in diorite porphyry intrusions. In the vicinity of the Motherlode (Mabuhay) mine, veins extend below the Mabuhay Clastics Formation into the underlying Motherlode Turbidite Formation.

Sediment-hosted Au mineral occurrences are present in the Lascogon, Napo, and Danao prospects (Maglambayan et al., 2005) and in the Reno pit of the Placer mine (Mitchell and Leach, 1991; P. Waters and R. Gonzales, unpub. report, 2003). In these systems, Au occurs in black jasperoids that replaced decalcified marls. The Au is associated with disseminated pyrite and local stibnite vug fill. Base metal sulfides are rare or absent.

In contrast to the Lascogon, Napo, Danao, and Placer mineral occurrences, ore at the Siana sediment-hosted Au deposit (Fig. 4) occurs in association with massive sulfide bodies hosted by locally brecciated limestone. Pyrite is the dominant phase in the massive sulfides, occurring with subordinate sphalerite, galena, and minor chalcopyrite. Gold also occurs as finely disseminated electrum associated with the breccia matrix and limestone clasts. Coarse-grained feldspar porphyry dikes intruded the basalt and limestone host rock and are exposed on the north side of the open pit. Shallow illite-pyrite alteration affected the feldspar porphyry and the basalts, while magnetite \pm chalcopyrite veinlets occur in the basalt at depth. These features suggest that Siana may be associated with a porphyry Cu-Au system.

Table 1. Important Gold and Copper Mines and Prospects in the Surigao District

Name	Mineral inventory ¹				Contained metal			Status	Easting ²	Northing ²	References ³
	Size (Mt)	Cu (%)	Au (g/t)	Ag (g/t)	Cu (Mt)	Au (Moz)	Ag (Moz)				
Porphyry copper-gold											
Asiga River	26	0.36			0.09			Prospect	788859	1025741	1, 2, 3
Maraat								Prospect	792474	1030000	3
Suyoc	5	1	3		0.05	0.5		Inactive mine	782701	1068911	1, 3
Boyongan	299	0.51	0.70		1.52	6.7		Mineral deposit	779796	1062198	4
Bayugo	132	0.67	0.67		0.88	2.8		Mineral deposit	779010	1063049	4
Madya								Prospect	784526	1048796	5
Skarn-porphyry copper-gold											
Green Tunnel								Prospect	783886	1050085	1
Epithermal gold											
Mapawa	8.8		1.02	2.85		0.3	0.8	Inactive mine	777723	1075304	1, 3
Mapaso								Inactive mine	784545	1067553	1, 3
Motherlode	4		5			0.6		Inactive mine	778148	1072501	1, 3
Placer	11		2.3			0.8		Active mine	784114	1069698	1, 3
Sediment-hosted/carbonate replacement gold											
Siana	11.2		5.4			1.9		Active mine	782950	1055712	5, 6, 7, 8
Lascogon								Prospect	781363	1070063	9
Napo								Prospect	780573	1073114	9
Danao								Prospect	780725	1071188	9

¹ Prospects: geologic resource; mines: past production as of 2016

² UTM Zone 51N; datum: Luzon 1911 (exclusive of Palawan)

³ References: (1) P. Waters and R. Gonzales, unpub. report, 2003; (2) Sillitoe and Gappe, 1984; (3) Mitchell and Leach, 1991; (4) Philex, 2011; (5) Red 5, 2005; (6) Red 5, 2012; (7) Red 5, 2015; (8) Red 5, 2016; (9) Maglambayan et al., 2005

Copper-gold porphyries in the Surigao district

Until the discovery of Boyongan and Bayugo, the only porphyry systems recognized in the Surigao peninsula were the Asiga River-Maraat prospects (Sillitoe and Gappe, 1984; Mitchell and Leach, 1991), located approximately 35 km southeast of Boyongan (Fig. 1). Since 1999, grassroots exploration and reevaluation of known epithermal districts led to the recognition of several additional porphyry Cu-Au systems (Table 1; Fig. 4).

The Asiga River and Maraas prospects are associated with a large composite diorite complex displaying a prominent north-east alignment in the Eastern Cordillera (Fig. 1). At least five zones of porphyry-style alteration are present here. Copper occurs as chalcopyrite, bornite, and covellite associated primarily with zones of K silicate alteration and peripheral magnetite skarn (P. Waters and R. Gonzales, unpub. report, 2003).

At Suyoc (Fig. 4), diamond drilling by Manila Mining Corporation revealed dense magnetite-quartz-vein stockworks containing late chalcopyrite and pyrite, centered on a small diorite porphyry stock. A pervasive intermediate argillic assemblage overprinted K silicate alteration associated with the stockwork. A possible late- to postmineralization diatreme breccia may have removed a portion of the Suyoc deposit (P. Waters and R. Gonzales, unpub. report, 2003).

Recent drilling at the nearby Placer deposit (Fig. 4) revealed deep (>400 m) porphyry-style Cu-Au intercepts beneath the Ntina pit (Conde, 2014). Here hydrothermal biotite, K-feldspar, and magnetite affect diorite stocks that intruded the Mabuhay Clastics Formation. Copper and Au are associated with chalcopyrite-bornite-chalcocite-pyrite-bearing assemblages in quartz-anhydrite stockworks that are spatially associated with the diorite intrusions. Similar to Suyoc, there is evidence of postporphyry diatreme formation at Placer in the form of Cu-bearing clasts of microdiorite porphyry described from polymictic breccias in the Ntina pit (Conde, 2014).

At the nearby Mapawa mineral deposit (Fig. 4), P. Waters and R. Gonzales (unpub. report, 2003) described a similar diorite porphyry stock with magnetite-quartz vein stockworks and K silicate alteration overprinted by pervasive intermediate argillic alteration. These authors interpreted the auriferous quartz-pyrite structures with broad argillized halos (United Nations Development Program, 1987) superimposed on the diorite porphyry to represent telescoping of epithermal mineralization onto the porphyry system.

South of Suyoc, a NNW-trending belt of porphyry and porphyry-skarn occurrences contains the most significant porphyry Cu-Au mineral deposits yet identified in the Surigao district (Fig. 4). Copper-gold occurrences along what has become known as the "Boyongan corridor" include the Boyongan and Bayugo mineral deposits, the Madya porphyry Cu-Au prospect, and the Green Tunnel Cu skarn/porphyry prospect. The Siana sediment-hosted Au deposit, itself displaying a possible porphyry association, also lies along the Boyongan corridor (Fig. 4).

Boyongan and Bayugo Mineral Deposits Intrusive History

The Boyongan and Bayugo Cu-Au mineral deposits formed in spatial relationship to a composite diorite porphyry complex.

At Boyongan, emplacement of a large silt-sand matrix breccia body shattered the earliest-formed diorite intrusions, setting the stage for emplacement of a series of early-, inter-, and late-mineralization diorite porphyry stocks associated with elevated Cu-Au grades. The diatreme breccia complex is absent at Bayugo, where a sequence of early-, inter-, and late-mineralization diorite porphyry stocks similar to those at Boyongan intruded the early diorite complex. Quartz-magnetite cemented breccias with associated K-feldspar alteration developed in association with the early- and intermineralization intrusions at Bayugo and Boyongan and are most significant in Boyongan's eastern high-grade zone.

Postmineralization volcanism and sedimentation buried the intrusions and host rocks of the Boyongan and Bayugo deposits (Fig. 5A). Drilling beneath this cover has revealed that Boyongan and Bayugo are centered on a complex of composite diorite stocks and diatreme breccias emplaced into volcanic and sedimentary rocks of the Bacuag and Motherlode Turbidite Formations (Figs. 3, 5B).

The intrusions share a common phenocryst assemblage containing plagioclase and hornblende, locally with minor (<2 vol %) biotite and/or clinopyroxene. They lack igneous quartz. The diorite complex contains at least 12 discrete diorite phases, distinguished on the basis of texture and timing relationships to veining, alteration, and brecciation. Figure 6 as well as Appendix 1, Figures A4 through A6 present geologic cross sections showing the geometry and spatial distribution of these intrusions. Table 2 lists the texturally and compositionally distinctive features of each intrusive phase in the complex and provides a centralized reference for the nomenclature employed in this study. Figure 7 emphasizes the changes in quartz vein abundance and Au grade that highlight intrusive contacts.

Mineralizing and brecciation events serve to subdivide diorite emplacement into temporally distinct episodes. (1) Initial magmatism formed an early diorite complex consisting of at least three intrusive phases: bird's-eye diorite porphyry, medium-grained diorite porphyry, and fine-grained diorite porphyry. These intrusive events predated Cu-Au mineralization. (2) At Boyongan, a large, premineralization silt-sand matrix breccia complex partially fragmented the early diorite complex and surrounding wall rock. (3) A series of early-mineralization diorite porphyry stocks (ECD0-ECD3) then intruded the silt-sand matrix breccia complex at Boyongan. These intrusions bear a spatial relationship to elevated Cu-Au grades and quartz-vein stockworks. Quartz-magnetite cemented breccias formed in spatial and temporal relation to the early-mineralization diorite series intrusions. At Bayugo, the early-mineralization diorite porphyry 2 (DIO2), intruded the medium-grained diorite porphyry and is the intrusive phase associated with quartz-vein stockworks and elevated Cu-Au grades. However, the absence of crosscutting relationships with the silt-sand matrix breccia precludes more precise age constraints of the Bayugo intrusions relative to breccia formation. (4) A series of moderately-altered intermineralization and late-mineralization diorite porphyry stocks and dikes cuts the early-mineralization diorite porphyry stocks. At Boyongan, these are the intermineralization diorite porphyry stock and the late-mineralization diorite porphyry dikes. At Bayugo, diorite porphyries 3 and 4 (DIO3 and DIO4)

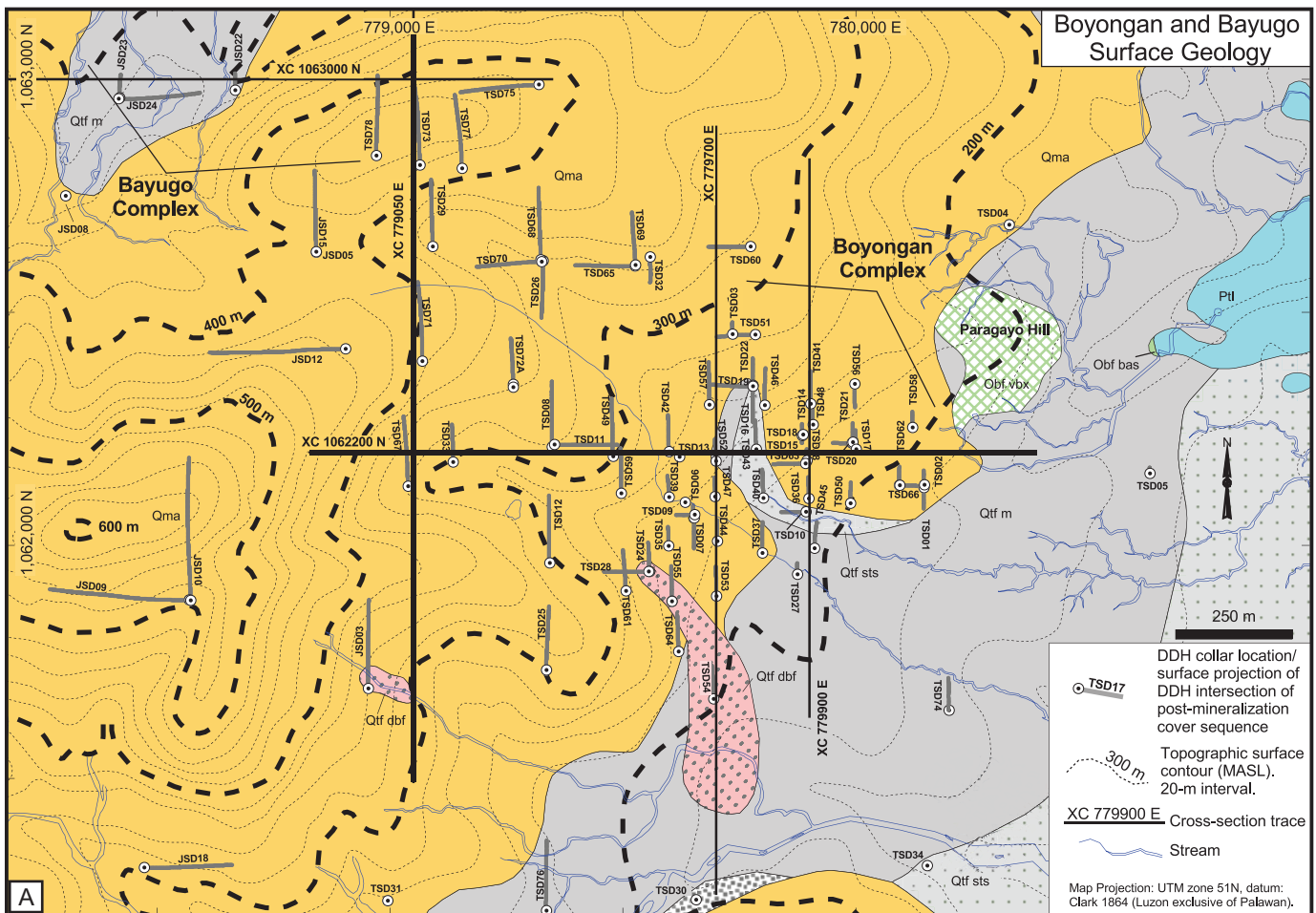


Fig. 5. (A) Surface geology, topography, and diamond drill locations for Boyongan and Bayugo deposits. The geologic map is based on the authors' reinterpretation of unpublished mapping by Anglo American Exploration (Philippines) Inc., incorporating drilling results for material encountered in the first meter (Anglo American, 2004). Maniayao andesitic volcanic rocks cover the western side of the prospects and underlie a prominent ridge in the vicinity of Bayugo. Mud, silt, sand, and gravel of the Tugunan Formation fluviolacustrine facies cover much of the eastern sector and occupy a small basin overlying Bayugo in the northwest. Southwest of Boyongan are isolated exposures of illite-pyrite-altered debris flows intercalated within the fluviolacustrine facies. Restricted exposures of Bacuag Formation volcanic breccia facies (Paragayo Hill) and Timamana limestone crop out where the Tugunan Formation thins to the east.

represent intermineralization and late-mineralization intrusive events, respectively.

Early diorite complex

Three texturally distinctive diorite porphyry stocks characterize the earliest phases of magmatism in the Boyongan-Bayugo complex. They all intruded prior to the emplacement of the silt-sand matrix breccia complex and include the bird's-eye diorite porphyry, medium-grained diorite porphyry, and fine-grained diorite porphyry. The low quartz vein abundances and absence of vein-quartz xenoliths in these intrusions (Table 2) are consistent with their emplacement prior to the main mineralizing events at Boyongan and Bayugo.

Bird's-eye diorite porphyry: The bird's-eye porphyry is a coarse-grained, plagioclase- and hornblende-phyric diorite stock named for its distinctive feldspar megacrysts resembling bird eyes (Table 2; App. 1, Fig. A7A). Diamond drill hole TSD67 intersected approximately 580 vertical meters of the bird's-eye porphyry on the western edge of the Boyongan

complex (Figs. 5B, 6). Definition of the bird's-eye porphyry stock geometry is poor, as increasing cover thickness to the west and south has discouraged additional drilling. In the vicinity of Bayugo, diamond drill hole JSD15 stopped after intercepting 129 m of bird's-eye porphyry (App. 1, Fig. A6). Although contact relationships with other intrusions are not exposed, clasts of the bird's-eye porphyry in the silt-sand matrix breccia complex (described below) indicate that the bird's-eye porphyry belongs to the early diorite complex.

Medium-grained diorite porphyry: The medium-grained diorite porphyry is a crowded, plagioclase- and hornblende-phyric diorite intrusion locally containing minor biotite (Table 2; App. 1, Fig. A7B). This phase forms a large irregular stock near the approximate center of the Boyongan intrusive complex (Fig. 5B), where the largest contiguous body measures 1,200 × 400 m in plan. The medium-grained diorite porphyry texture is seriate and finer grained (MGD-s in Table 2; App. 1, Fig. A7C) near its intrusive contacts with the basalt host rock, such as on the northeast side of the Boyongan complex

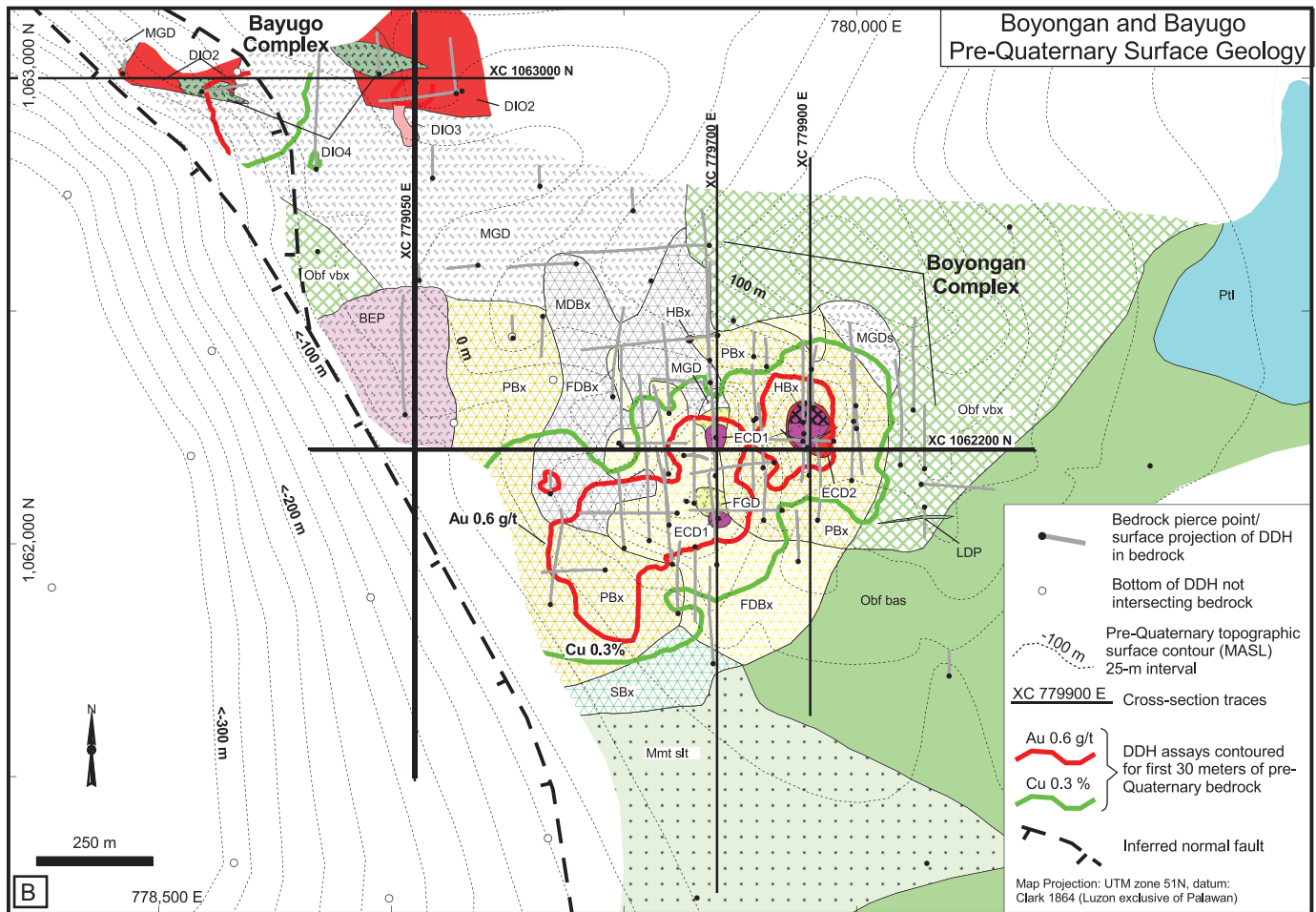


Fig. 5. (Cont.) (B) Pre-Quaternary geology, topography, and diamond drill locations for Boyongan and Bayugo deposits. The relationships depicted are based on the authors' interpretation of logging along sections indicated and on reinterpretation of drilling data in Anglo American (2004). An early diorite complex has intruded the Bacuag and Motherlode Formations, consisting of bird's-eye diorite porphyry (BEP), medium-grained diorite porphyry (MGD), and fine-grained diorite porphyry (FGD) phases. A large silt-sand matrix breccia complex shattered much of the early diorite complex and incorporated clasts of early diorite intrusions and wall-rock fragments. Breccia zones defined by the dominant clast type subdivide the breccia complex into wall-rock-dominated (SBx), intrusion-dominated (MDBx and FDBx), and polymict (PBx) facies. At Boyongan, Au and Cu are associated with small early-mineralization diorite porphyry stocks (ECD1 and ECD2) emplaced within the silt-sand matrix breccia complex. These intrusive centers are marked by two prominent topographic highs on the paleosurface. At Bayugo, early-mineralization diorite porphyry (DIO2) stocks are associated with Cu and Au. An intermineralization diorite porphyry stock (DIO3) truncated the DIO2 stocks at Bayugo. Late-mineralization diorite porphyry dikes at Boyongan (LDP) and Bayugo (DIO4) are the youngest observed intrusive phases. The elevation of the pre-Quaternary surface drops away abruptly on the west side of the deposits, inferred to be controlled by normal faulting. Figure 3 provides an explanation of rock types for all deposit-scale geologic sections and plans in this paper. Cross section locations (1,062,200 N and 779,050 E) for Figures 6, 11, 12, 20, 21, and 23 shown in bold to distinguish them from locations for cross sections 1,063,000 N, 779,700 E, and 779,900 E in Appendix 1 (Figs. A4–A6, A13–A18, A23, A24, A26–A28).

(Fig. 5B). The younger diorite intrusions of Bayugo bound the medium-grained diorite porphyry stock to the north, while the Boyongan silt-sand matrix breccia complex forms the southern limit (Fig. 5B). Clasts of the medium-grained diorite porphyry in the silt-sand matrix breccia complex indicate that emplacement of the medium-grained diorite porphyry predated breccia formation.

Fine-grained diorite porphyry: The fine-grained diorite porphyry is a plagioclase-phyric diorite with fine (<1 mm) plagioclase phenocrysts, which locally display a strong alignment suggestive of flow banding (App. 1, Fig. A7D). Replacement by hydrothermal biotite and/or chlorite of the fine mafic

phenocrysts (possibly hornblende) has obscured their original character. The fine-grained diorite porphyry occurs primarily as fragments and large blocks within the silt-sand matrix breccia complex (Fig. 5B). Xenoliths of medium-grained diorite porphyry within the fine-grained diorite porphyry in diamond drill hole TSD52 (188–220 m) demonstrate that the fine-grained diorite porphyry is the younger of these two intrusive phases.

Boyongan early-, inter-, and late-mineralization intrusions

Boyongan early-mineralization diorite porphyries (ECD0–ECD3): At Boyongan, Cu-Au grades are highest in and

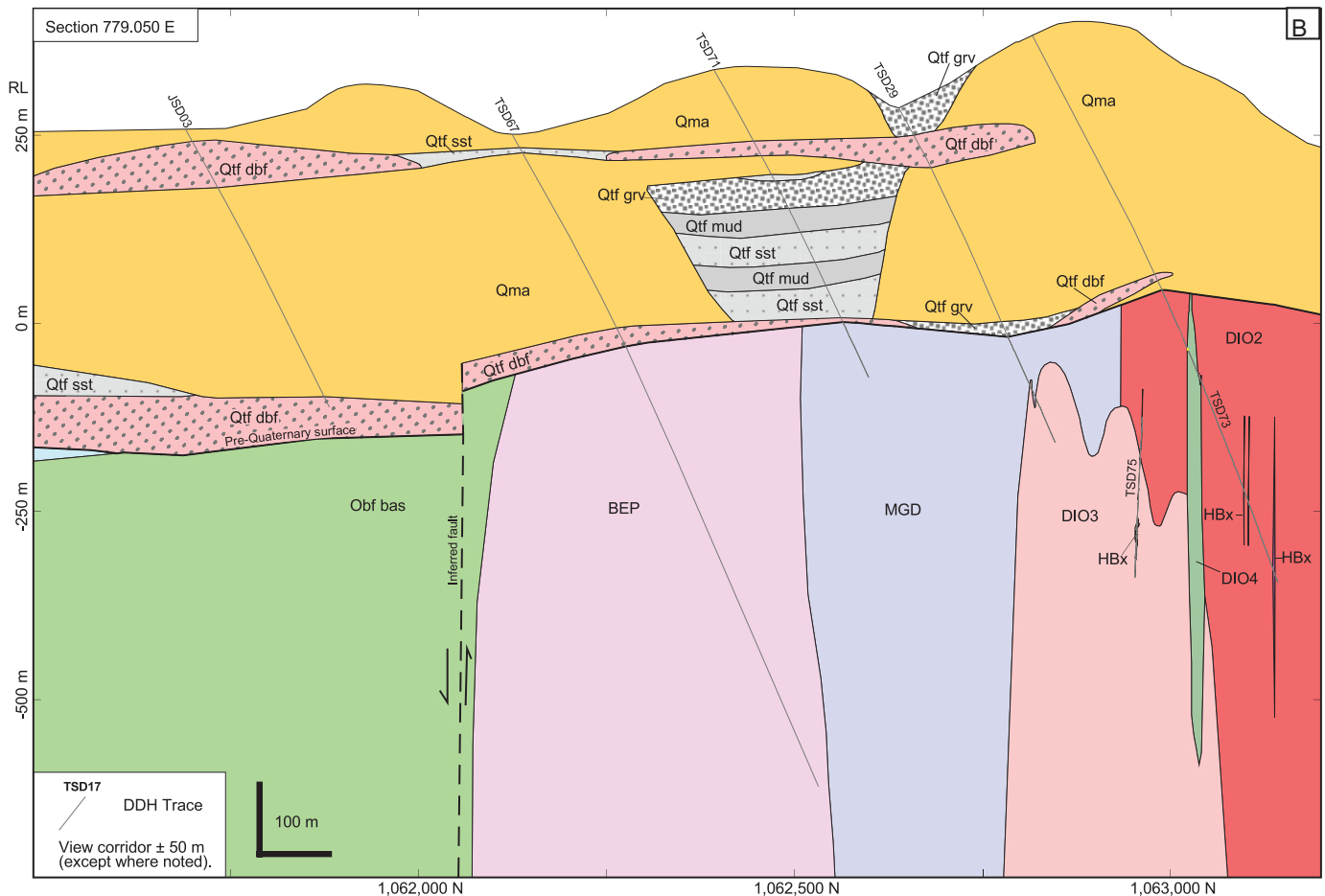


Fig. 6. (Cont.) (B) Interpretive geologic cross section through eastern Bayugo looking west along 779,050 E. The relationships depicted are based on logging by the authors and on reinterpretation of geologic data in Anglo American (2004). Stocks of the early diorite complex (BEP and MGD) intruded the Bacuag Formation. Gold and Cu are associated with an early-mineralization diorite porphyry (DIO2) that intruded the early diorite complex medium-grained diorite porphyry stock. Intermineralization and late-mineralization diorite porphyry stocks (DIO3 and DIO4, respectively) intruded the DIO2 stock. Drilling has shown that the elevation of the pre-Quaternary surface drops away abruptly to the south, inferred to be controlled by normal faulting. Interstratified debris flows and fluviolacustrine sediments cover the pre-Quaternary unconformity and are overlain by a sequence of intercalated andesitic volcanic rocks and debris flows. Abrupt lateral facies changes (e.g., dominantly volcanics in TSD67 and dominantly sediments in adjacent TSD71) emphasize the complex depositional environment during burial. See Figure 5 for the cross section location and Figure 3 for an explanation of rock types.

host rocks were cut by a lower-intensity quartz-vein stockwork (averaging 15% quartz; Table 2) lacking the distinctive ribbon-textured veins (Fig. 7B). The ECD1 stock is the most significant intrusion in the western high-grade zone in terms of volume and spatial relationship to elevated Cu-Au grades.

At least three early-mineralization diorite porphyry intrusions (ECD1, ECD2, and ECD3; Table 2) occur in the eastern high-grade zone (Fig. 6A; App. 1, Figs. A5A, A8C-F). The earliest recognized phase (ECD1) has a crowded texture similar to the ECD1 intrusion logged in the western high-grade zone. In the eastern high-grade zone, the ECD1 phase displays an intense quartz-stockwork and occurs as roof pendants and stope blocks in the cupola and on the margin of the younger ECD2 stock. The ECD2 stock also has a crowded texture and is volumetrically the most significant intrusion in the eastern high-grade zone. Both ECD1 and ECD2 host significant quartz-vein stockworks (averaging 42% and 14% quartz, respectively; Table 2). The latest recognized phase of

early-mineralization diorite porphyry (ECD3) occurs as narrow dikes of diorite porphyry that intruded the ECD2 stock at depth (Fig. 6A; App. 1, Fig. A5). These ECD3 dikes are also cut by a quartz-vein stockwork (averaging 16% vein quartz; Table 2).

Boyongan intermineralization diorite porphyry: A larger (>250-m diam) crowded plagioclase- and hornblende-phyric diorite stock truncated the early-mineralization diorite series at depth. This stock represents the deepest intrusion encountered thus far in the Boyongan intrusive complex (App. 1, Fig. A9A). Quartz veining and Cu-Au mineralization also affected this intrusion, albeit with a lower grade and abundance of quartz veining (averaging 2% vein quartz; Table 2) than the series. Therefore, this intrusive phase is termed an intermineralization diorite porphyry stock (Fig. 6A; Table 2; App. 1, Figs. A4, A5). Internal fine-grained contacts are present locally and may suggest more than one phase of magma emplacement. However, textural similarity between discrete

Table 2. Distinctive Features of Intrusive Phases at Boyongan and Bayugo

Intrusive phase	Texture	Minerals ¹	Phenocrysts					Groundmass (μm)	Accessory minerals	Quartz veining (vol %) ²	Vein-quartz xenoliths	Cu (%)	Au (g/t)
			Total abundance (%)	Mafics (%)	Plagioclase (mm)	Hornblende (mm)	Grain Size						
Early diorite complex													
BEP	Birds-eye porphyry	pg, hb	50-60	10-20	3-7	0.2-1.5	2-20	mt, zir	0.6%	Absent	0.1%	0.2	
MGD	Medium-grained diorite	pg, hb, (bio)	75-80	8-10	1-5	0.5-3	10	mt, ap, zir	0.9%	Absent	0.3%	0.3	
MGD-s	Medium-grained diorite-seriate variant	pg, hb, (cpx)	85-90	9	0.5-2	0.2-2	40-50		0.9%	Absent	0.2%	0.4	
FGD	Fine-grained diorite	pg, hb? ² ->2bio	40-45	5	0.1-0.7	0.05-0.5	2-10		2%	Absent	0.7%	1.4	
Boyongan: Early-mineralization intrusions													
ECD0	Early-mineral coarse-grained diorite: 0	pg, hb	75-80	10	0.8-1.2	0.4-0.8	10-30	mt	23%	Absent	0.5%	0.5	
ECD1	Early-mineral coarse-grained diorite: 1	pg, hb	70-80	5-10	1.5-2	0.5-1	10-15	mt	42% ³	Absent ³	3.2% ⁴	12.2 ³	
ECD2	Early-mineral coarse-grained diorite: 2	pg, hb	70-80	5-8	0.5-3	0.5-1.2	10-60	mt	15% ⁴	Present ⁴	0.4% ⁴	0.99 ⁴	
ECD3	Early-mineral coarse-grained diorite: 3	pg, hb, (cpx)	60-65	8	1.5-3	0.2-0.5	15-20	mt, ilm	16%	Common	0.2%	0.1	
Boyongan: Inter- and late-mineralization intrusions													
IMD	Intermineral diorite	pg, hb, (bio, cpx)	65-70	10-15	1.5-2.5	0.2-0.2	20-25	mt, ilm, ap, zir	2%	Common	0.1%	0.2	
LDP	Late-mineral diorite	pg, hb	45-75	8-10	0.3-3	0.2-1.2	15-30	mt, ilm, ap, zir	0.6%	Common	0.4%	0.4	
Bayugo: Early-mineralization intrusion													
DIO2	Early-mineral diorite: 2	pg, hb, (bio, cpx)	70-85	10-15	1.6-3.6	1.2-1.6	10-20	mt, zir	8%	Common ⁵	0.6%	0.8	
Bayugo: Inter- and late-mineralization intrusions													
DIO3	Intermineral diorite: 3	pg, hb, (bio, cpx)	70-80	12	2.5-4	0.5-1.4	15-25	mt, ap, zir	8%	Common	0.21%	0.37	
DIO4	Late-mineral diorite: 4	pg, hb, (cpx)	80-85	8	1-2	0.2-1.6	100-250	mt, ap, zir	4%	Common	0.4%	0.31	

Abbreviations: 2bio = secondary (hydrothermal) biotite, ap = apatite, bio = biotite, cpx = clinopyroxene, hb = hornblende, ilm = ilmenite, mt = magnetite, pg = plagioclase, zir = zircon

¹Accounting for 15% or more of the phenocryst population by volume; low-abundance phenocrysts (5-15%) are indicated parenthetically

²References: Sillitoe and Gappe, 1984; Mitchell and Leach, 1991; P. Waters and R. Gonzales, unpub. report, 2003; Maglambayan et al., 2005; Red 5, 2005, 2012, 2015, 2016; Philex, 2011

³Eastern high-grade zone

⁴Western high-grade zone

⁵Absent from earliest phases of the DIO2, common in later DIO2 phases (indicated by presence of internal fine-grained margins)

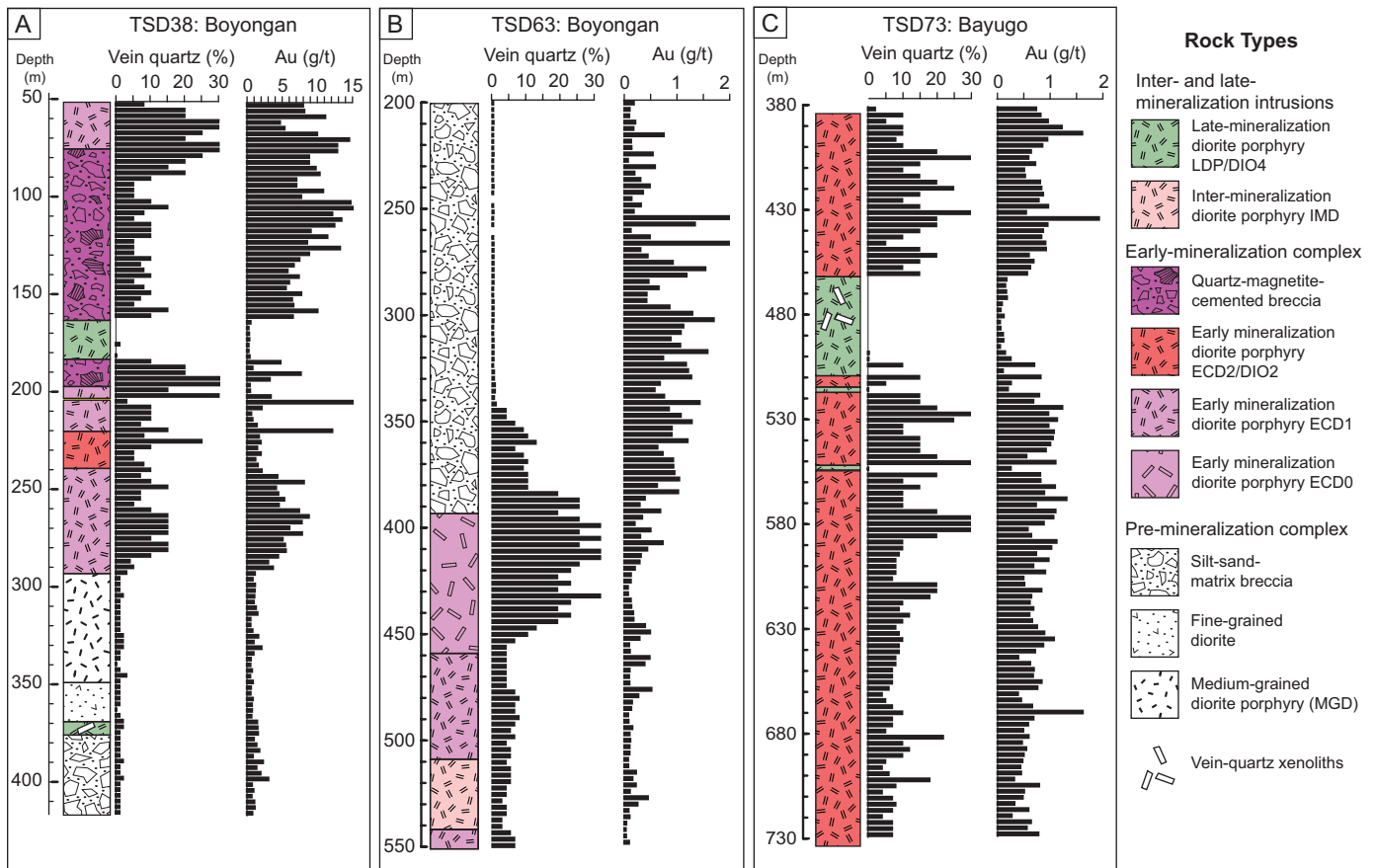


Fig. 7. Simplified geologic logs from Boyongan (A, B) and Bayugo (C) showing the relationships between various intrusive phases, quartz vein intensity, and Au concentration, based on logging by the authors and supplemented by geologic and assay data in Anglo American (2004). (A) Boyongan: interval through the shallow eastern high-grade zone emphasizing the high quartz vein abundance and Au association with the ECD-series intrusions and hydrothermally cemented breccia and antithetic relationship with the late-mineralization diorite porphyry dikes. (B) Boyongan: interval through the western high-grade zone. Quartz vein abundance distinguishes ECD0 from ECD1, while variations in texture and low quartz vein abundance distinguish the intermineralization diorite porphyry and late-mineralization diorite porphyry intrusions. The diminishing abundance of vein quartz affecting the silt-sand matrix breccia with distance from the intrusive contact with early-mineralization ECD0 is evidence for atypically premineralization paragenetic position for the diatreme breccia complex at Boyongan. (C) Interval through eastern Bayugo emphasizing the association of high quartz vein abundance and elevated Au concentrations with the DIO2 intrusion and inverse relationship with the DIO4 intrusion.

intermineralization diorite porphyry intrusions away from these contacts precluded the mapping of individual phases.

Boyongan late-mineralization diorite porphyry dikes: The latest phase of magmatism in the Boyongan intrusive complex produced narrow (<1–15 m) late-mineral plagioclase- and hornblende-phyric diorite dikes (Fig. 6A; Table 2; App. 1, Figs. A4, A5). These dikes are subvertical, and correlation between various diamond drill holes suggests that they are east trending. The greater abundance of groundmass, lower intensity of quartz veining (averaging 0.6% vein quartz; Table 2), flow-banded contacts, and clear crosscutting relationships (Fig. 7A) distinguish the late-mineralization diorite porphyry from earlier intrusions at Boyongan (App. 1, Fig. A9B).

Bayugo early-, inter-, and late mineralization intrusions

The bird's-eye porphyry and medium-grained diorite porphyry phases of the early diorite complex extend northwest from Boyongan to Bayugo, where they host several diorite porphyry intrusions associated with elevated Cu-Au grades.

Younger magmatic events at Bayugo are distinguished from the bird's-eye porphyry and the medium-grained diorite porphyry by their texture and their spatial and temporal relationships to quartz veining (Fig. 7C). Logging by the authors and Anglo American geologists enabled definition of three principal intrusive phases emplaced in the early diorite complex (Figs. 5B, 6B; App. 1, Fig. A6).

Bayugo early-mineralization diorite porphyry 2 (DIO2): A crowded plagioclase- and hornblende-phyric diorite (DIO2; Table 2; App. 1, Fig. A10A) intruded the medium-grained diorite porphyry at Bayugo (Figs. 5B, 6B; App. 1, Fig. A6). Drilling to date suggests that the DIO2 porphyry formed two discrete stocks. The western stock (open to the north) measures 250 m east to west, and the eastern stock (open to the north and east) exceeds 200 m in diameter (Fig. 5B). A locally intense quartz-vein stockwork (averaging 8% vein quartz; Table 2) associated with elevated Cu-Au grades affected the DIO2 intrusions. Internal chilled margins document multiple intrusive phases within the DIO2 stocks, the younger of which

commonly contain vein-quartz xenoliths (App. 1, Fig. A10B). The spatial association with quartz veining and the absence of vein-quartz xenoliths in the oldest intrusive phases suggests that the DIO2 stocks are the oldest phases of magmatism genetically associated with Cu-Au mineralization at Bayugo.

Bayugo intermineralization diorite porphyry 3 (DIO3): Drilling in the east side of Bayugo intersected a crowded plagioclase- and hornblende-phyric diorite stock that has intruded the medium-grained diorite porphyry and DIO2 stocks (Fig. 6B; App. 1, Fig. A6). This intrusion (DIO3; Table 2; App. 1, Fig. A10C) has generally larger plagioclase phenocrysts and a more crowded texture than the earlier medium-grained diorite porphyry and DIO2 stocks and displays a quartz stockwork broadly similar in intensity (averaging 8% vein quartz; Table 2) to that affecting the DIO2 stock.

Bayugo late-mineralization diorite porphyry 4 (DIO4): Texturally distinctive seriate to crowded plagioclase- and hornblende-phyric diorite bodies (DIO4; Table 2) intruded the medium-grained diorite porphyry and DIO2 stocks at Bayugo. This intrusive stage was affected by low-intensity quartz veining (averaging 4% vein quartz; Table 2) and contains abundant vein-quartz xenoliths (App. 1, Fig. A10D). Drilling has not exposed contact relationships between DIO4 and DIO3 (Fig. 6B; App. 1, Fig. A6). However, lower quartz vein density and abundance of vein-quartz xenoliths in DIO4 suggest that this phase was emplaced after the intense veining that affected DIO3.

Boyongan Silt-Sand Matrix Breccia Complex

Brecciation of a large portion of the early diorite complex (bird's-eye porphyry, medium-grained diorite porphyry, and fine-grained diorite porphyry) and surrounding host rock occurred prior to the emplacement of the early-mineralization diorite series at Boyongan. Description of breccia characteristics requires some definition of terminology, and that employed hereunder follows the general approach presented by Davies (2002). That author proposed a descriptive scheme for breccias in terms of alteration, internal organization (clast morphology, abundance, distribution, sorting, and stratification), components (clast, matrix, cement, and composition), grain size, and overall geometry. Infill refers to interclast material and is subdivided into cement (igneous or hydrothermal minerals interpreted to have precipitated in situ) and matrix (fragmental material in the sand [63 μm to 2 mm], silt [4–63 μm], and clay [$<4 \mu\text{m}$] grain sizes). Clasts are defined as fragments exceeding 2 mm in their largest dimension.

The breccia complex at Boyongan is a polyphase, silt-sand matrix breccia pipe of generally cylindrical shape. As exposed at the pre-Quaternary surface (Fig. 5B), the breccia complex footprint describes a roughly circular feature with a diameter exceeding 900 m. Stocks of bird's-eye porphyry and medium-grained diorite porphyry bound the breccia complex on the north and northwest margins, respectively, and basalts and basalt-dominated volcanic breccias of the Bacuag Formation form the eastern margin. Detailed drill definition of the breccia margins is lacking on the southern margin, although breccia clast types and projections from drilling farther south suggest that the bounding units are basalts and limestones of the Bacuag Formation and siltstones of the overlying Motherlode Formation. The western margin of the breccia complex

is poorly defined owing to thickening cover (>400 m) toward the west.

The breccia complex varies between matrix supported and clast supported and generally lacks stratification or other internal organization. Fine (<0.5 mm) sand- and silt-sized fragments comprise the breccia matrix, and alteration and weathering have largely obscured its nature. Petrographic observations in this study indicate that the infill is largely fragmental in character, consisting of finely comminuted rock fragments. The fragmental texture does not preclude a tuffaceous igneous component to the matrix, although no clearly juvenile material (e.g., fluted or curved glass shards or fragments suggestive of devitrified glass, igneous cement) was identified in hand specimen or thin section.

Logging shows that most of the facies within the breccia complex contain two or more clast types. Anglo American geologists defined five breccia facies distinguished on the basis of the volumetrically dominant clast type (Figs. 5B, 6A; App. 1, Figs. A4, A5): (1) basalt-dominated breccia (Fig. 8A, B), (2) mudstone-dominated breccia (Fig. 8C, D), (3) medium-grained diorite porphyry-dominated breccia (Fig. 9A), (4) fine-grained diorite porphyry-dominated breccia (Fig. 9B), and (5) polymict breccia (Fig. 9C).

Transitions between breccia facies are generally gradational, reflecting changes in the proportion of clast types. Locally narrow (2–10 cm) breccia dikelets crosscut earlier breccia bodies, documenting a second phase of brecciation (Fig. 9B–D). Vein-quartz clasts, a common feature in subsequent intrusions and breccias, are absent from the silt-sand matrix breccia complex. Their absence is consistent with the interpretation that brecciation predated mineralization.

Basalt clast-rich breccia

Basalt clast-rich breccia is abundant at depth, where the breccia complex contacts Bacuag Formation basalts (Fig. 6A; App. 1, Figs. A4, A5). This facies is generally clast-supported (70–90% clasts) and contains angular subrounded clasts of dark aphanitic basaltic fragments in a melanocratic fragmental silt-sand-sized matrix. Locally the basalt clast-rich breccia facies contains clasts of white porous quartz and massive magnetite similar to skarn alteration within the Bacuag Formation (Fig. 8B).

The textural and compositional complexity locally exhibited by the basalt clast-rich breccia (e.g., TSD52, 750–936.5 m) may partially reflect the heterogeneous provenance of breccia clasts derived from the Bacuag Formation. Logging of the Bacuag Formation outside the breccia complex revealed discrete sequences of basalt interbedded with limestone, carbonaceous/coal-bearing shale, and polyolithic conglomerate.

Sedimentary clast-rich breccia

Breccia with abundant mudstone clasts was intersected in diamond drill hole TSD54 (148.75–256 m) on the southern portion of the breccia complex (Fig. 5B; App. 1, Fig. A4). This breccia facies is clast supported, with approximately 20% matrix material. Over 90% of the clasts in the upper breccia sequence (148.75–219.2 m) consist of fine, green-gray mudstone, together with angular clasts of basalt and diorite porphyry. The matrix in this interval is mud sized and gray-green in color. Some fragments within this sequence resemble accretionary lapilli: concentrically zoned 0.5- to 2.0-mm spheroids

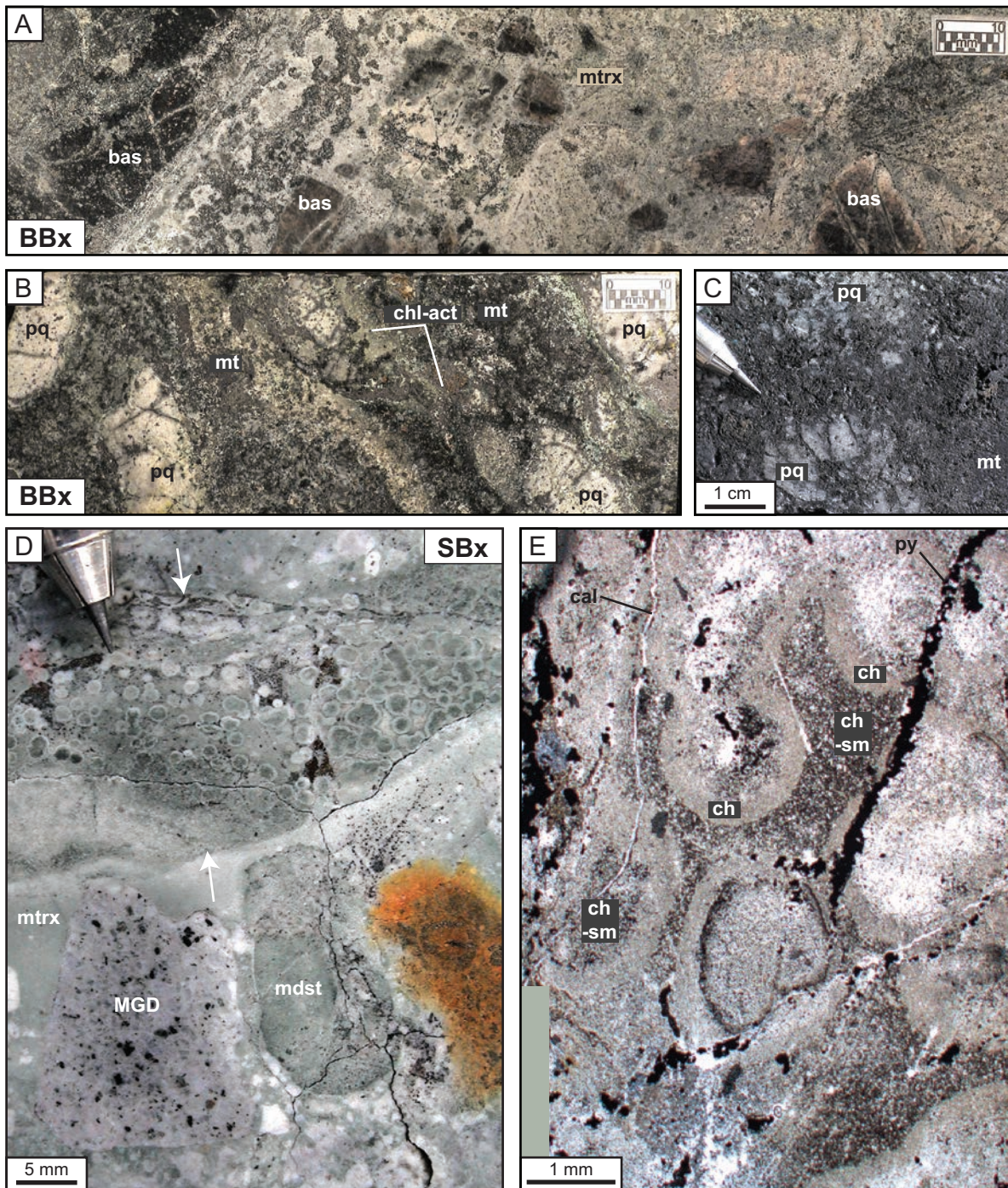


Fig. 8. Wall-rock-dominated facies of the Boyongan diatreme breccia complex. (A) Basalt-dominated breccia facies (BBx) showing chaotic, unstratified, unsorted, silt-sand matrix breccia containing subrounded clasts of fine-grained dark, locally feldspar-phyric basalt (bas). Clasts and matrix (mtrx) display intense, pervasive chlorite replacement. Sample: 819463. Diamond drill hole TSD52, 790.8 m. (B) Basalt-dominated breccia facies (BBx) showing silt-sand matrix breccia containing clasts of basalt (bas), magnetite (mt), and white, porous quartz (pq). Matrix is composed of silt-sized domains of chlorite-actinolite (chl-act) and illite. Sample: 819464. Diamond drill hole TSD52, 773.18 m. (C) Magnetite (mt) skarn with white, porous quartz (pq) fragments; possible source of magnetite and quartz in (B). Sample: 819470. Diamond drill hole TSD52, 680.3 m. (D) Mudstone-dominated breccia facies (SBx) demonstrating two distinct subfacies: The lower portion contains rounded clasts of medium-grained diorite (MGD) and mudstone (mdst) in a greenish muddy matrix (mtrx). The upper interval (arrows) contains zoned spheroids with slightly darker green aphanitic cores and gray aphanitic rims similar to accretionary lapilli. Sample: 819591. Diamond drill hole TSD54, 208.48 m. (E) Photomicrograph of upper zone in (C), showing concentric zoned lapilli with coarser-grained cores containing chlorite (ch) and dark clots of smectite (sm), lighter rims of micron-scale chlorite, and dark chlorite-smectite interstitial material. The breccia contains abundant disseminated and veinlet pyrite (py) and is cut by fine calcite (cal) veinlets. Plane-polarized light.

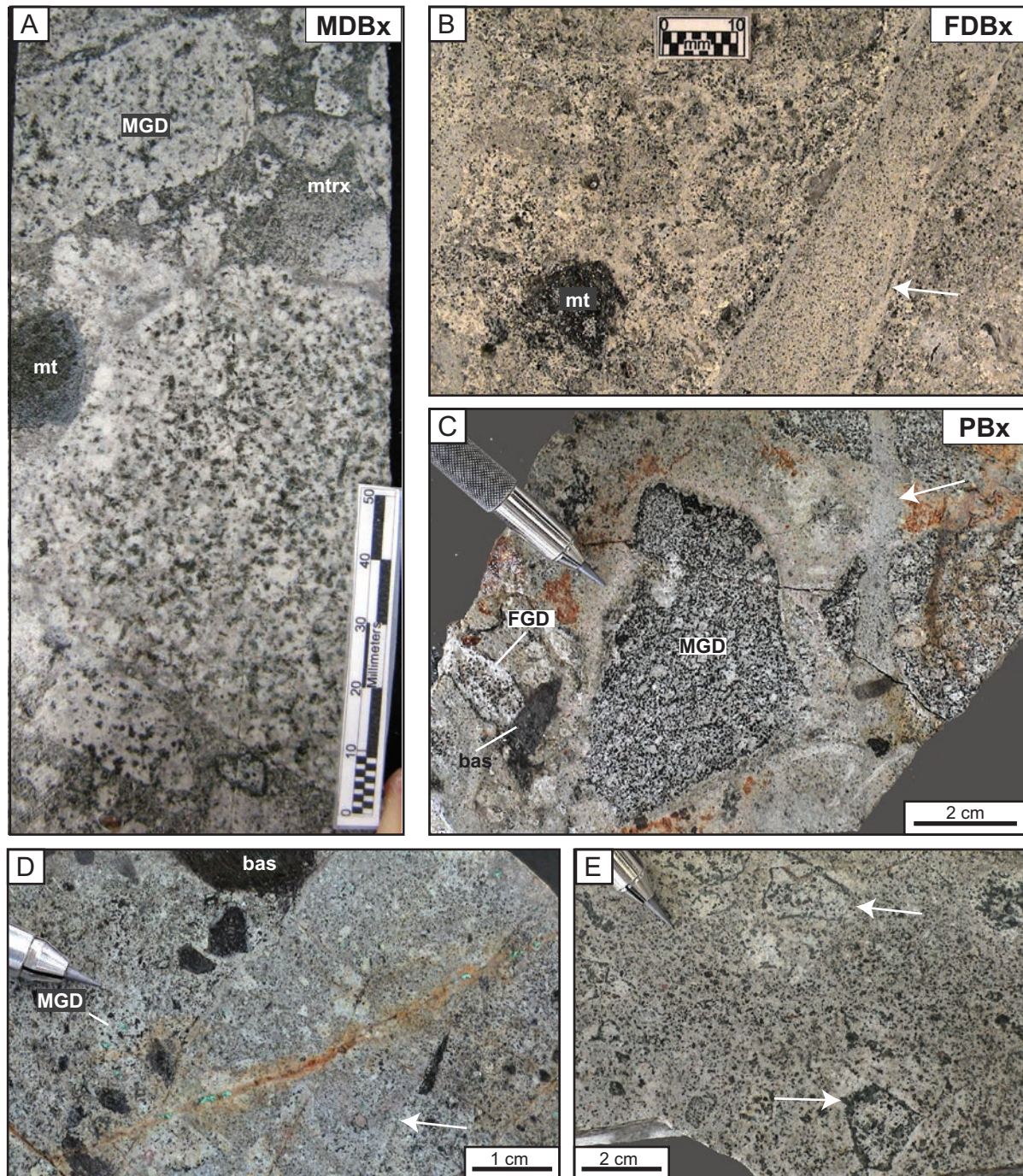


Fig. 9. Intrusive-dominated facies and polymict facies of the Boyongan diatreme breccia complex. (A) Medium-grained diorite clast-rich breccia (MDBx) facies showing chaotic, unstratified, unsorted, silt-sand matrix (mtrx) breccia, containing subrounded clasts of medium-grained diorite (MGD) porphyry and occasional clasts of massive magnetite (mt). Diamond drill hole TSD87A, 537 m. (B) Fine-grained diorite clast-rich breccia (FDBx) facies showing chaotic, unstratified, unsorted, silt-sand matrix (mtrx) breccia containing subrounded clasts of fine-grained diorite porphyry and occasional clasts of massive magnetite (mt). The breccia was affected by a second phase of fragmentation dominated by silt-sand dikelet (arrow). Sample: 819475. Diamond drill hole TSD52, 468.56 m. (C) Polymict breccia (PBx) facies showing chaotic, unstratified, unsorted, silt-sand matrix breccia containing subrounded clasts of medium-grained diorite porphyry, fine-grained diorite (FGD) porphyry, and basalt (bas). The arrow indicates a silt-sand dikelet resembling that shown in (B). Sample: 819370. Diamond drill hole TSD45, 178.62 m. (D) Silt-sand matrix breccia containing angular clasts of medium-grained diorite porphyry and basalt cut by monomictic silt-sand matrix breccia (arrow) containing angular clasts of fine-grained diorite porphyry. A quartz vein with a central seam containing malachite and goethite has cut both breccia events, demonstrating the premineral or early-mineral timing of the silt-sand matrix breccia. Sample: 814761. Diamond drill hole TSD63, 198.08 m. (E) Biotite reaction rims (arrows) on angular medium-grained diorite porphyry clasts in silt-sand matrix breccia. Sample: 819373. Diamond drill hole TSD45, 232.05 m.

with slightly darker green aphanitic cores and gray aphanitic rims (Fig. 8C, D). These lapilli are well sorted and display systematic grading over 2- to 3-cm intervals toward the base of the upper sequence (205–219.2 m). In the lower sequence (219.2–256 m) clasts are fragments of fine-grained, bleached, yellow-white angular garnet-epidote-calcite skarn in a silt-sized yellow-white matrix of garnet fragments. In this interval, a cement of pyrite, magnetite, sphalerite, and calcite occupies clast interstices, locally reaching 20% of the rock. This interval represents the only convincing example of cement present in the dominantly fragmental infill of the breccia complex.

A likely source for the aphanitic green-gray clasts and matrix in the upper breccia sequence is the mudstone-rich Motherlode Formation. This formation overlies the Bacuag Formation and was intersected in diamond drill holes TSD30 (Fig. 5B) and TSD34 approximately 0.5 km to the south and southeast of TSD54. The skarn rock fragments in the deeper breccia sequence are likely derived from limestone within the Bacuag Formation. Their presence as fragments in the breccia emphasize that at least some skarn formation occurred prior to brecciation.

The presence of accretionary lapilli provides insight into the conditions of formation of the breccia complex. In subaerial volcanic environments, accretionary lapilli can form when ash plumes interact with a moisture-rich environment in which the fine-grained airborne ash can agglomerate around a nucleus of a water droplet or solid particle (Cas and Wright, 1987). The accretionary lapilli at Boyongan may reflect fluidization at the breccia complex margins during fragmentation, forming by agglomeration in a subsurface vapor stream containing a suspension of very fine grained particles. Several researchers (Walker, 1971; Cas and Wright, 1987; McPhie et al., 1993; Wormald et al., 1993; Carman, 1994) have described similar accretionary textures that evidently formed in subvolcanic pipes and breccias.

Medium-grained diorite clast-rich breccia

Clasts of medium-grained diorite porphyry are the most abundant in this facies (Fig. 9A), with clasts of fine-grained diorite locally forming a significant subpopulation. Clasts of basalt and bird's-eye diorite porphyry are common but make up generally less than 5% of the clast population. Basalt is also present as xenoliths in larger clasts of medium-grained diorite porphyry, and it is likely that many of the basalt clasts in the medium-grained diorite clast-rich breccia facies were derived from xenoliths. Clast-matrix proportions in the medium-grained diorite clast-rich breccia vary between 50% in matrix-supported intervals to 90% in clast-supported zones. The matrix is sand-silt sized and leucocratic. The medium-grained diorite clast-rich breccia occupies the north-central portion of the breccia complex and is bounded on the north by its contact with the medium-grained diorite porphyry stock (Figs. 5B, 6A; App. 1, Figs. A4, A5). Diamond drilling indicates that the medium-grained diorite clast-rich breccia extends into the breccia complex approximately 500 m south from this contact, grading into a fine-grained diorite clast-rich breccia facies.

Fine-grained diorite clast-rich breccia

Breccia rich in fine-grained diorite clasts occurs in the central, southeastern, and northeastern regions of the breccia complex

(Fig. 5B). This facies grades laterally into polymict breccia to the east and west and into medium-grained diorite clast-rich breccia facies to the northwest. The most abundant clast type within the fine-grained diorite clast-rich breccia facies is fine-grained diorite (Fig. 9B), with clasts of medium-grained diorite porphyry representing a significant clast subpopulation. The breccia matrix is silt-sand sized and leucocratic. The similarity in color and texture between the fine-grained diorite porphyry and the fragmental breccia matrix made accurate estimates of clast-matrix ratios difficult during core logging, particularly in intervals of intense weathering and/or strongly broken core.

Polymict breccia

Although virtually all facies in the breccia complex contain two or more clast types (and are therefore polymict in the strict sense), one type is generally volumetrically dominant. The polymict breccia facies defined herein contains clasts of basalt and early diorite complex intrusions (Fig. 9C, D) in roughly equal proportions. Marginal and deeper phases of the polymict breccia facies contain more basalt clasts, while the clast proportion of medium- and fine-grained diorite increases relative to basalt toward the center of the breccia complex. The matrix is sand-silt sized and leucocratic, and clast-matrix proportions in the polymict breccia facies vary between 50% in matrix-supported intervals to 90% in clast-supported zones.

This facies forms two distinct zones on the west and east sides of the breccia complex. The eastern polymict breccia zone flares upward to the north and south, overlying the fine-grained diorite clast-rich breccia facies on the breccia complex margins (App. 1, Fig. A5). The western zone of polymict breccia lies between intrusive rock-dominated breccia facies to the east (medium-grained diorite clast-rich breccia and fine-grained diorite clast-rich breccia) and the bird's-eye diorite porphyry stock to the northwest. Contact relationships are poorly defined in the western zone of polymict breccia, and it is unclear if this breccia body has upward-flaring contacts similar to those present in the eastern zone.

Boyongan silt-sand matrix breccia complex—interpretation

The Boyongan silt-sand matrix breccia complex displays mappable breccia facies characterized by the dominant clast type. The composition and position of these facies reflects the proximity of the brecciated units to breccia clast source regions. Breccia facies dominated by wall-rock clasts (basalt clast-rich breccia and sedimentary clast-rich breccia) occupy the margins of the breccia complex, while breccia facies dominated by intrusive clasts (medium-grained diorite clast-rich breccia and fine-grained diorite clast-rich breccia) make up the breccia complex core. The polymict breccia facies displays the greatest diversity of clast types and represents a transitional facies between wall-rock dominated and intrusive dominated breccia facies. This pattern suggests a prebreccia configuration of medium-grained and fine-grained diorite porphyry stocks elongate along a north to northwest trend (Fig. 5B).

Most characteristics of the Boyongan silt-sand matrix breccia complex are typical of diatremes associated with Philippine porphyry deposits. Diatreme breccias occur in spatial association with at least nine Philippine porphyry deposits (Far Southeast, Guinaoang, Santo Niño, Santo Tomas II,

Ampucao, Dizon, Pisumpan, Salatan, and Amacan), and their presence underscores the shallow subvolcanic environment of porphyry formation (Sillitoe and Gappe, 1984; Hedenquist et al., 1998). These diatremes contain angular subrounded, heterolithic, sand- to boulder-sized clasts. In some districts the infill consists of a silt-sand matrix (e.g., Santo Niño, Santo Tomas II, Salatan, and Boyongan), while in others the infill contains a mixture of fragmental matrix with a juvenile crystal-rich tuffaceous component (e.g., Guinaoang, Dizon, and Pisumpan). Wall-rock fragments make up the bulk of clasts, although locally fragments of carbonized wood (Dizon and Santo Niño: Sillitoe and Gappe, 1984) and occasionally logs (Balatoc: Sawkins et al., 1979) are present.

In the Boyongan diatreme breccia complex, the distribution of clast rock types, the dominantly angular clast morphology, and the generally clast-supported nature of the breccia complex all suggest that milling, clast transportation, and gas streaming were only of local significance (e.g., the apparent accretionary lapilli of the sedimentary clast-rich breccia). The absence of quartz-stockworked clasts and vein-quartz clasts demonstrates a premineralization relationship to Cu-Au mineralization. In this respect, the timing relationship between porphyry emplacement and breccia formation at Boyongan differs from all other Philippine porphyry districts. Crosscutting relationships and the presence of mineralized diatreme clasts show that most Philippine diatremes postdate porphyry emplacement, and in many cases (i.e., Guinaoang, Santo Niño, Dizon, Pisumpan, and Salatan) diatreme emplacement destroyed part of the original orebody (Sillitoe and Gappe, 1984). With evidence for diatreme formation before porphyry mineralization, Boyongan shares paragenetic characteristics with the Grasberg Cu-Au porphyry in Indonesia and the Galore Creek porphyry in British Columbia, Canada (Sillitoe, 2010, and references therein).

Although the lack of vein-quartz clasts suggests that the formation of the diatreme breccia complex predated the main mineralizing events at Boyongan, there is evidence of local hydrothermal alteration prior to and during diatreme formation. Clasts of massive magnetite and/or garnet are present locally in the basalt clast-rich breccia, sedimentary clast-rich breccia, medium-grained diorite clast-rich breccia, and fine-grained diorite clast-rich breccia facies (Fig. 9A, B), suggesting derivation from previously altered rocks. Some diorite clasts in the medium-grained diorite clast-rich breccia and fine-grained diorite clast-rich breccia facies display biotite-altered rims (Fig. 9E), suggesting some synfragmentation hydrothermal alteration.

Despite their common association with Philippine porphyry deposits, these diatreme rock types in the Philippines were long considered volcano-sedimentary diamictites (e.g., Bryner, 1970; Mitchell and Balce, 1990), and only familiarity with diatreme lithofacies coupled with detailed three-dimensional definition by mining and/or drilling led to the recognition of these features as discordant intrusive breccia complexes (Malihan, 1982; Sillitoe and Gappe, 1984; Sillitoe and Angeles, 1985). This spatial definition revealed that diatremes are typically steep-sided, commonly upward-flaring bodies exceeding 1 km in maximum horizontal dimension. Exploratory drilling for geothermal power in the Balatoc diatreme (Baguio district) defined a vertical extent exceeding 2.5 km (M. de Guzman,

unpub. report, 1986). Diatreme contacts with wall rock are typically sharp with variable wall-rock fracturing. Distinct facies defined by clast type, shape, and internal organization and by infill abundance and composition reflect clast provenance from various stratigraphic levels and varying degrees of fluidization during diatreme emplacement. The presence of wood and the recognition of base surge deposits led Sillitoe and Gappe (1984) to conclude that many diatreme breccia pipes in the Philippines breached the surface during their formation.

Hydrothermally Cemented Breccias

Intermineralization hydrothermally cemented breccias

A second significant phase of brecciation developed in association with the early-mineralization diorite porphyries, following the formation of the diatreme breccia complex. During the emplacement of these Boyongan early-mineralization diorite series intrusions, volumetrically significant quartz-magnetite cemented breccias formed in Boyongan's eastern high-grade zone (Figs. 5B, 6A; App. 1, Fig. A5). The presence of hydrothermal quartz and/or magnetite cement in the infill distinguishes these breccias from the silt-sand matrix breccias of the diatreme breccia complex. These characteristics resemble those described for magmatic-hydrothermal breccias by Sillitoe (1985). Figure 10 illustrates the convention employed in distinguishing clasts, matrix, and hydrothermal cement.

The largest hydrothermally cemented breccia body developed in the cupola of the ECD2 stock in the eastern high-grade zone. This breccia body is roughly cylindrical, measures 90 m in diameter, and has a minimum vertical extent of 150 m (App. 1, Fig. A5). Contacts with the wall rock are subvertical and sharp, with narrow (1–2 m) cracked margins. The breccia is texturally massive, unsorted, clast supported, and contains dominantly subangular fragments derived from quartz veins, ECD1, ECD2, and the diatreme breccia complex (App. 1, Fig. A11A, B). Most clasts range in size from 2 to 64 mm, with generally less than 10% of clasts coarser than 64 mm. However, characterization of breccias exclusively in drill core probably precluded identification of boulder-sized clasts. The infill, varying between 20 and 30% of the rock, consists of a matrix of silt-sized fragments cemented by quartz and subordinate supergene hematite after magnetite (Fig. 10).

In the eastern high-grade zone below –300 m relative level (RL), a quartz-magnetite cemented breccia body is present along the margin of the ECD2 stock (App. 1, Fig. A5). This breccia contains fragments of vein quartz, ECD2, and basalt in varying proportions, and the matrix and clast grain size distribution is similar to that of the shallow breccia body. The deeper breccia is generally clast supported, although narrow (0.1–1 m) intervals of infill-supported breccia occur (App. 1, Fig. A11D, E). Clasts are dominantly subangular, although marginal facies commonly show a higher degree of rounding (App. 1, Fig. A11F). In the deeper breccia, broad (>50 m) zones of low-density magnetite-quartz cemented crackle breccia occur in the ECD2 stock above the deep breccia body. TSD14 intersected a quartz-magnetite cemented breccia to the north of the ECD2 stock (App. 1, Fig. A5). This clast-supported breccia contains moderately rounded fragments of fine-grained diorite porphyry and basalt with minor open-space interstices (App. 1, Fig. A11C).

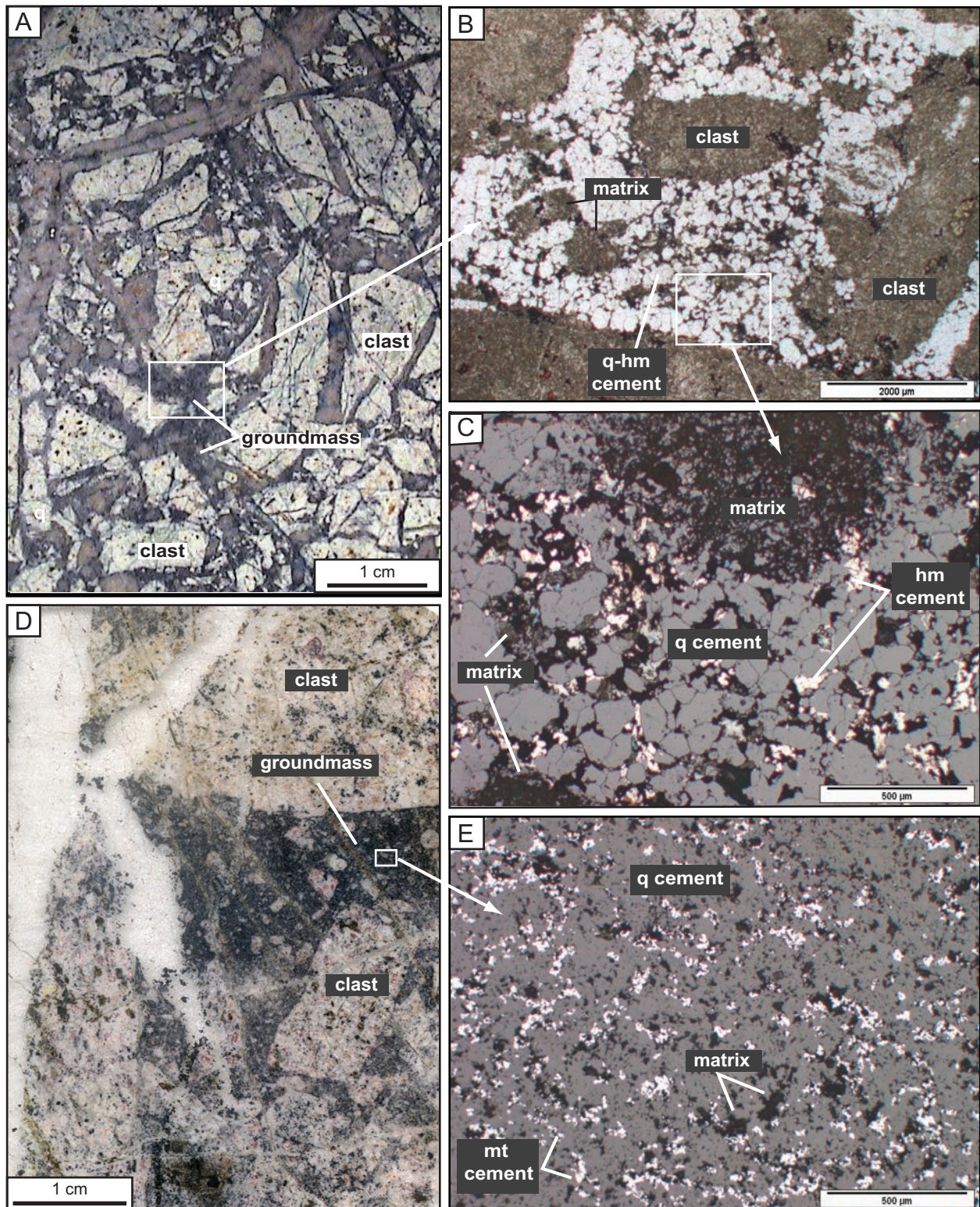


Fig. 10. Character of clastic and chemical components of infill in hydrothermally cemented breccias. (A) Chaotic, angular, clast-supported, unsorted, ECD1 and vein-quartz clast-bearing, quartz-magnetite (now supergene hematite) cemented breccia. (B-C) Photomicrographs of (A) showing infill of fragmental material (matrix) and hydrothermal cement (quartz and magnetite). (A-C) from sample 819360. Diamond drill hole TSD38, 84.2 m. (D) Chaotic, angular, clast-supported, unsorted, ECD2 and vein-quartz clast-bearing, quartz-magnetite cemented breccia. (E) Photomicrograph of (D) showing infill of silt-sized fragmental material (matrix) and hydrothermal cement (quartz and magnetite). (D-E) from sample 819321. Diamond drill hole TSD18, 541.35 m. Abbreviations: hm = hematite, mt = magnetite, q = quartz.

Outside the eastern high-grade zone, drilling intersected narrow (0.1–15 m) intervals of similar quartz-magnetite and magnetite cemented breccias within the medium-grained diorite porphyry and the diatreme breccia complex in the western high-grade zone as well as within diorites DIO2 and DIO3 at Bayugo (Fig. 6B).

Hydrothermal K-feldspar occurs in association with the quartz-magnetite and magnetite cemented breccias. K-feldspar occurs as halos on the breccia margins and on the edges of larger clasts. K-feldspar also replaced the smaller clasts and sand- and silt-sized matrix material (other than vein-quartz fragments) in the quartz-magnetite and magnetite cemented breccias (App. 1, Fig. A11A, C), locally giving the impression of K-feldspar cement.

In a review of breccia characteristics from 48 Philippine porphyry deposits, Sillitoe and Gappe (1984) described intermineralization breccias as a common but volumetrically small component of most Philippine porphyry deposits. Such breccias occur as irregular to steep-sided pipes, similar to those defined in the eastern high-grade zone of Boyongan. The breccias described by Sillitoe and Gappe (1984) display an extreme range of clast size, from grit to boulder, and contain angular to rounded, locally polyolithic clasts. The silt-sand-sized matrix of these breccias varies between a few percent to more than 50% by volume. Breccia cement consists of chlorite ± quartz ± calcite, with pyrite + chalcopyrite ± bornite ± molybdenite occurring as interstitial sulfides. The gangue alteration assemblage described by Sillitoe and Gappe (1984) differs from the magnetite-quartz-K-feldspar association at Boyongan and Bayugo, suggesting that breccias associated with K silicate alteration are relatively uncommon in Philippine porphyry Cu-Au deposits.

Copper-Gold Mineralization and Hydrothermal Alteration

This section focuses on documenting the characteristics and paragenesis of Cu-Au mineralization and hydrothermal alteration assemblages and on interpreting their relationships to the discrete intrusive events outlined above.

Methods employed

Petrography: Graphic logging along four principal cross sections through Boyongan and Bayugo provided the samples and context for subsequent studies of alteration and mineralization assemblages. Petrographic observations on 209 polished thin sections and 27 polished blocks focused on characterizing the primary, alteration, and vein mineral assemblages. As a compliment to observations made during logging and petrographic observations, 65 polished slabs were prepared to determine the macroscopic relationships between veins and alteration assemblages. Petrographic descriptions of 25 additional samples by P. White (unpub. report, 2000) supplemented the work by the authors.

K-feldspar staining: Hydrothermal K-feldspar is an important component of the K silicate alteration assemblage at Boyongan and Bayugo. However, hypogene variations in color and the subsequent modification by supergene processes rendered consistent recognition of K-feldspar difficult during core logging. Systematic staining of rock slabs was therefore undertaken to identify K-feldspar and to characterize its textural

relationships to the various vein types. Staining of slabs up to 20 cm in length revealed larger-scale textural relationships and provided a more representative estimate of K-feldspar abundance than by relying on thin sections alone. After first etching with hydrofluoric acid, the authors stained 280 samples with $\text{Na}_3\text{Co}(\text{NO}_2)_6$, including 102 polished thin-section offcuts and 261 sawn slabs, following the methodology described by Norman (1974). The staining was conducted on samples collected from four principal cross sections through Boyongan and Bayugo and enabled estimation of K-feldspar vol % in photographs of each sample, using the image analysis software eCognition® (App. 1, Fig. A12). Appendix 2 presents the process of image analysis and quantification of K-feldspar abundance.

Clay mineral studies: Clay minerals are important components of many alteration assemblages in porphyry deposits (Meyer and Hemley, 1967). Logging at Boyongan has revealed abundant and widespread clay minerals, but deep oxidation and weathering have partially masked the nature of hypogene clay alteration assemblages (Ignacio, 2005). The authors conducted a systematic study of clay minerals to help distinguish hypogene and supergene assemblages, allowing the definition of hypogene clay mineral alteration zonation. This study employed a combination of X-ray diffraction (XRD), short-wavelength infrared spectroscopy (SWIR), electron microprobe analyses, and petrography to identify the clay species present, determine the relative abundance of different clay components, and ultimately distinguish hypogene from supergene clay mineral assemblages.

For XRD analyses, the authors prepared clay mineral-sized separates (App. 3) from 178 samples along three principal cross sections through the Boyongan deposit. XRD scans, conducted at the University of Utah's Department of Geology and Geophysics (in collaboration with Professor Erich Petersen), enabled identification of the clay mineral species present in each separate. The authors then employed the software program Newmod™ (Reynolds and Reynolds, 1996) to quantify the relative abundance of each clay mineral species in each separate (App. 3, Table A2). To broaden the sampling distribution, the study also incorporated the results of XRD analyses of 42 sample separates conducted by P. White (unpub. reports, 2000, 2001).

Copper-gold distribution

Elevated Cu and Au grades at Boyongan and Bayugo primarily coincide with quartz-vein stockworks in and around the early- and intermineralization (Boyongan early-mineralization diorite, DIO2, intermineralization diorite porphyry, and DIO3) diorite intrusions. Drilling has been most comprehensive at Boyongan, where mineralization formed two steep-sided ellipsoidal bodies respectively termed the eastern and western high-grade zones (Fig. 11; App. 1, Figs. A13, A14). Geochemical assays for Au >1 g/t in the western high-grade zone define a body with a pronounced north-south elongation measuring approximately 300 m vertically, 400 m north to south, and 150 m east to west. In the eastern high-grade zone Au assays >1 g/t define a more pipe-like body measuring approximately 300 m vertically, 150 m north to south, and 180 m east to west. Grades in the eastern high-grade zone reach exceptionally high levels: a 105-m intercept in TSD38 averaged 3.3% Cu and 9.5 g/t Au (Fig. 7). At Bayugo, preliminary drilling results

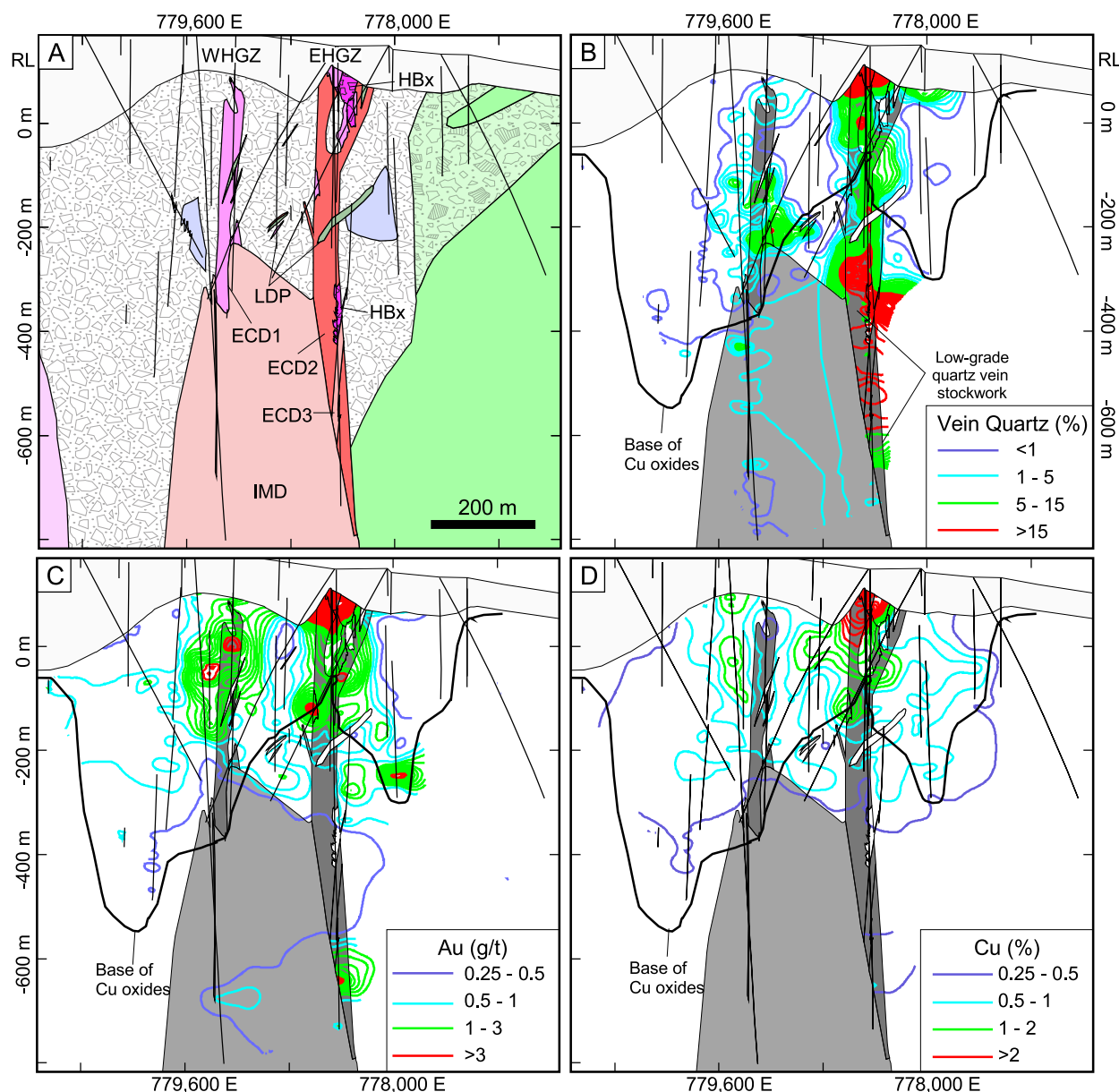


Fig. 11. Interpretive cross section along 1,062,200 N through Boyongan eastern and western high-grade zones showing relationships between quartz vein abundance and grade distribution for Au and Cu. (A) Generalized geology. Refer to Figure 3 for an explanation of rock types, Figure 5B for section location, and Figure 6A for detailed geologic information. (B) Contours of quartz vein abundance based on logging by Anglo American geologists. (C) Contours of Au assays. (D) Contours of Cu assays. Vein quartz abundance, Cu grades, and Au grades are highest in and around the cupolas of the early-mineralization diorite stocks in the eastern and western high-grade zones. The base of Cu oxides provides a reference for the lower limit of significant supergene modification of the hypogene system. Quartz vein abundance and assay data are from Anglo American (2004). Abbreviations: WHGZ = western high-grade zone; EHGZ = eastern high-grade zone.

have defined two Cu-Au mineralized zones spatially associated with the DIO2 and DIO3 stocks (Fig. 12; App. 1, Fig. A15). Within these zones, Au assays >0.5 g/t define two mineralized bodies with minimum dimensions exceeding 150 m in width and 200 m in vertical extent.

Sulfide zonation

Distinct hypogene sulfide zonation patterns characterize Boyongan and Bayugo. Because sulfate minerals are rare to absent in the explored regions of Boyongan and Bayugo, assays of

total sulfur from diamond drilling provide a means of quantifying the sulfide distribution. Hypogene Cu-bearing sulfides are concentrated in and around the early- and intermineralization diorite stocks (early-mineralization diorite series and intermineralization diorite porphyry at Boyongan; DIO2 and DIO3 at Bayugo), and a distinct pyrite halo rings these intrusions at Boyongan near the edge of the diatreme breccia complex (Fig. 13; App. 1, Figs. A16, A17).

Hypogene copper-sulfide zonation: At Boyongan, bornite and chalcopyrite are the principal hypogene Cu-bearing

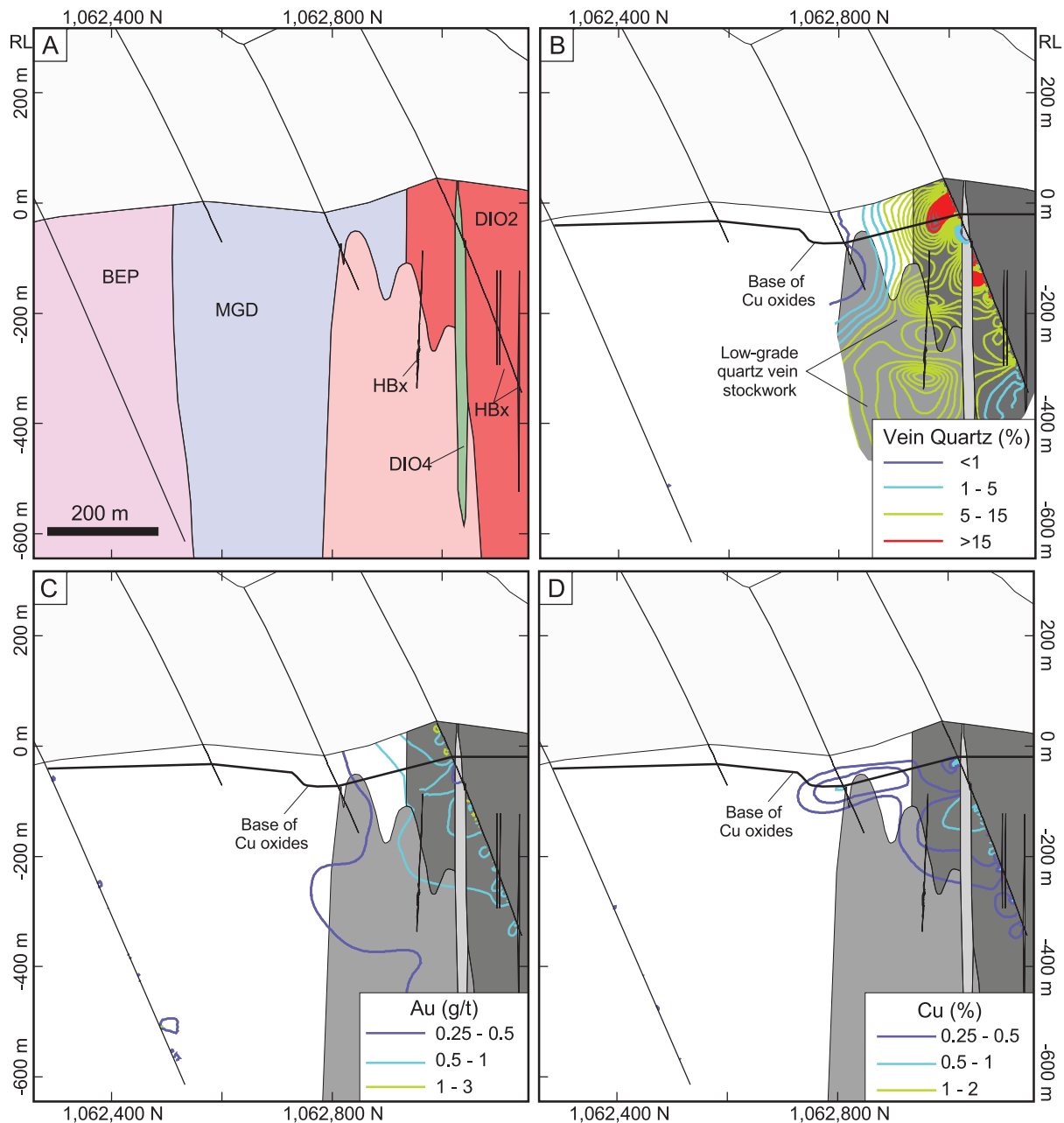


Fig. 12. Interpretive cross section along 779,050 E through Bayugo showing relationships between quartz vein abundance and grade distribution for Au and Cu. (A) Generalized geology. Refer to Figure 3 for an explanation of rock types, Figure 5B for section location, and to Figure 6A for detailed geologic information. (B) Contours of quartz vein abundance based on logging by Anglo American geologists. (C) Contours of Au assays. (D) Contours of Cu assays. Vein quartz abundance, Cu grades, and Au grades are highest in and around the cupola of the DIO2 stock. Lower-grade quartz vein stockworks have affected the DIO3 stock, while the DIO4 intrusion has truncated older quartz vein stockworks. The base of Cu oxides provides a reference for the lower limit of significant supergene modification of the hypogene system. Quartz vein abundance and assay data are from Anglo American (2004).

sulfides and are present in and around the early-mineralization diorite stock in the eastern high-grade zone. Bornite is largely absent in the later intermineralization diorite porphyry stock and late-mineralization diorite porphyry dikes, where chalcopyrite is the only significant hypogene Cu-sulfide phase (Fig. 13A; App. 1, Fig. A17). In Boyongan's western high-grade zone, near-complete sulfide oxidation in the high-grade zone precludes a detailed analysis of hypogene sulfide mineralogy

(App. 1, Fig. A16). At Bayugo, chalcopyrite is the dominant hypogene Cu-bearing sulfide, with virtually no bornite identified to date. Overall sulfide contents are low at Bayugo, with chalcopyrite generally <2% in the DIO2 stock (Fig. 13C, D).

Pyrite halo: At Boyongan a peripheral zone of elevated pyrite content (pyrite halo) lies between 250 and 500 m from the edges of the early- and intermineralization diorite stocks and is at least 250 m wide. Sulfide abundance in this zone

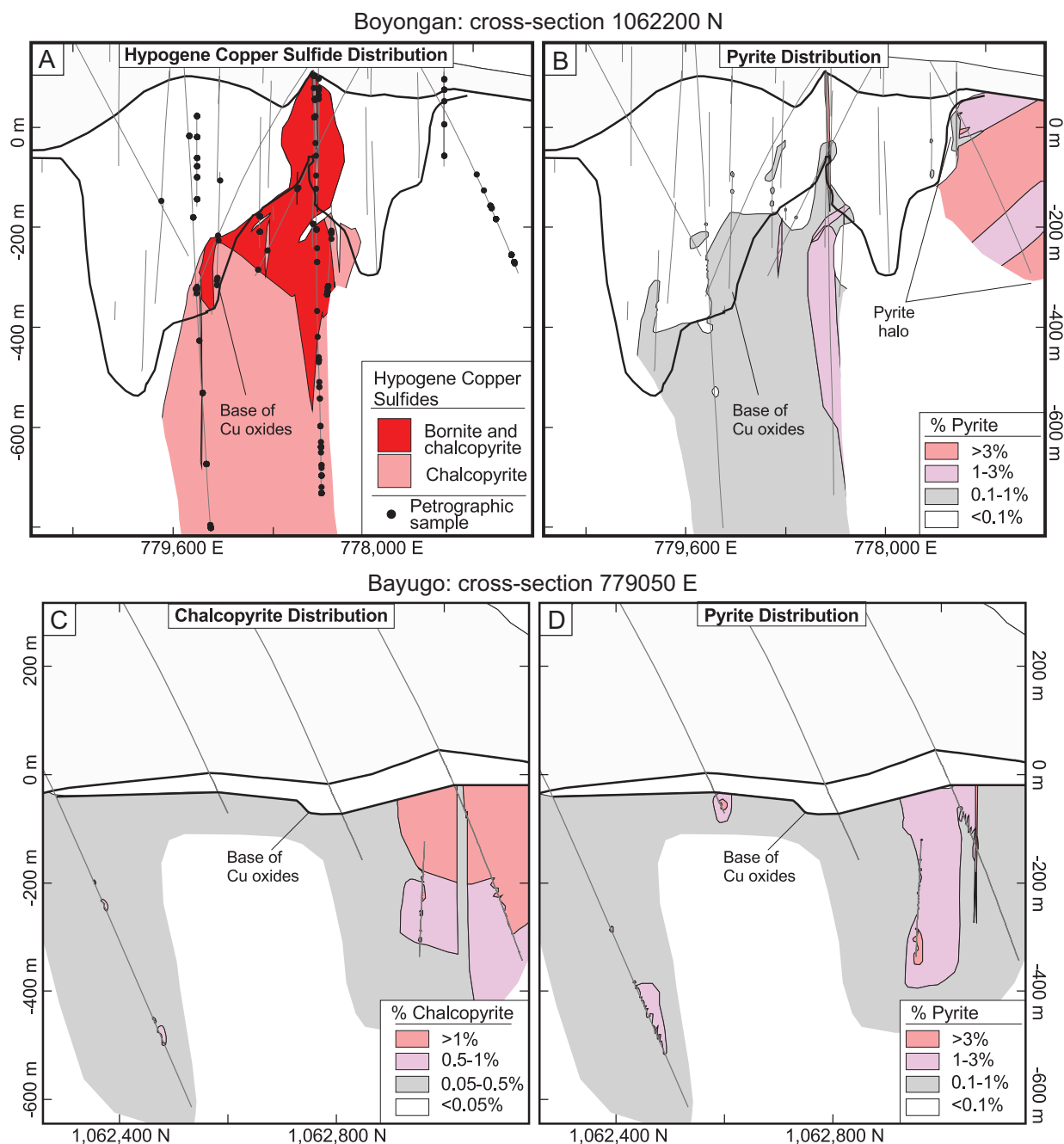


Fig. 13. Interpretive cross sections showing hypogene sulfide zonation from Boyongan (A and B, along 1,062,200 N) and Bayugo (C and D, along 779,050 E). Refer to Figure 5B for section location and to Figure 6 for detailed geologic information. (A, C) Distribution of hypogene Cu sulfides based on petrography and logging. Oxidation and leaching have removed much of the sulfur above the base of Cu oxides. At Boyongan (A), bornite and chalcopyrite are present in and around the early-mineralization diorite intrusions, while only chalcopyrite is present in the deeper intermineralization diorite porphyry intrusion and wall rocks. Near-total sulfide oxidation in the shallow portions of the western high-grade zone precludes a more complete analysis of the hypogene Cu sulfide distribution in that area. At Bayugo (C) chalcopyrite distribution is greatest in and around the DIO2 and DIO3 stocks, while bornite is virtually absent from Bayugo, enabling calculation of chalcopyrite abundance based on assay data (Anglo American, 2004). (B, D) At Boyongan (B) pyrite distribution in the intrusive/breccia complex is dominantly below 1%. Pyrite contents in the pyritic halo generally exceed 1% and reach 10% in the Bacuag Formation volcanic breccia facies on the eastern margin. At Bayugo (D) pyrite above 1% is concentrated irregularly around the DIO2 and DIO3 stocks, while bornite is virtually absent from Bayugo, enabling calculation of chalcopyrite abundance based on assay data (Anglo American, 2004). The pyrite content from Boyongan (A) was estimated from logging (Anglo American, 2004) in the bornite/chalcopyrite zone and/or above the base of Cu oxides or where total sulfur assays were not available (i.e., TSD13 and TSD18). Elsewhere, the pyrite content was calculated from total sulfur and Cu assays (Anglo American, 2004) after subtracting total sulfur to account for Cu as chalcopyrite. (C, D) Interpretive sections from Bayugo showing hypogene sulfide zonation along 779,050 E.

varies with host lithology. Pyrite concentrations in the basaltic facies of the Bacuag Formation range between 1 and 3% and generally exceed 3% in the volcanic breccia facies (Fig. 13D; App. 1, Fig. A16B, D). At Bayugo the paucity of detailed drilling at the time of the study limited the definition of sulfide zonation in this area. However, the zone exceeding 1% pyrite in the medium-grained diorite porphyry and DIO3 stocks to the south of the DIO2 stock (Fig. 13D) may be part of a pyrite halo.

Hydrothermal alteration and vein assemblages

Four distinct alteration and vein assemblages are present in and around the Boyongan and Bayugo deposits. These are termed the calc-silicate, K silicate, illite-smectite-chlorite, and illite-pyrite assemblages. A fifth type, the quartz-alunite-clay assemblage, is locally preserved in altered diorite clasts in the Tugunan Formation debris flows and conglomerates.

Calc-silicate (skarn) assemblage: Assemblages of calc-silicate minerals \pm magnetite occur as small (<1–20 m thick) zones within or adjacent to the Bacuag and Motherlode Formations (App. 1, Figs. A4, A5). Two distinct alteration assemblages are present (App. 1, Fig. A18). Skarns on the southern margin of the Boyongan complex contain an assemblage of fine-grained, massive garnet + clinopyroxene \pm epidote that has locally been brecciated and cemented by magnetite, calcite, sphalerite, and chalcopyrite (App. 1, Fig. A19A–C). The garnet is fine grained, pale yellow-green, and Ca, Al, and Fe rich, with average compositions of $\text{Ca}_{3.1}\text{Mg}_{0.1}(\text{Al}_{1.1}\text{Fe}_{0.9}\text{Mn}_{0.1}\text{Ti}_{0.1})(\text{SiO}_4)_3$ (App. 4, Table A1). Minor bismuth tellurides such as tetradyrite ($\text{Bi}_2\text{Te}_2\text{S}_{0.8}\text{Se}_{0.4}$) locally occur with magnetite (App. 4, Table A2).

Deep skarns on the northeast margin of the Boyongan intrusive complex lack garnet and consist of magnetite + actinolite + epidote + calcite \pm pyrite \pm chalcopyrite \pm chlorite (App. 1, Fig. A19D–O). Massive magnetite \pm pyrite occurs in intervals up to 3 m thick, bounded by zones of intense actinolite-chlorite alteration. The magnetite occurs primarily as bladed musketoite, a pseudomorph of specular hematite. Texturally distinctive, white, porous quartz (App. 1, Fig. A19F) commonly occurs intergrown with magnetite. In the basalt adjacent the massive skarns, albite flooding and replacement of calcic plagioclase occurs locally.

Calc-silicate-altered zones are not a significant host to Cu or Au at Boyongan. Despite the presence of chalcopyrite, Cu grades rarely exceed 0.25%, and Au concentrations are generally much less than 0.5 g/t (Fig. 11; App. 1, Fig. A13). The massive character of these zones suggests pervasive replacement of reactive sequences such as limestone, calcareous conglomerate, and basalt within the host stratigraphy.

Clasts containing massive magnetite, actinolite, albite, and porous quartz in the diatreme breccia complex (Figs. 8B, 9B) suggest that some calc-silicate alteration predated this breccia event, although selective alteration of calcareous clasts within the breccia complex is an alternative explanation. The proximity of the medium-grained diorite porphyry stock to the deep magnetite-actinolite skarns in the Bacuag Formation (App. 1, Fig. A18) is consistent with the former assertion. However, drilling also intersected a small skarn body in contact with the intermineralization diorite porphyry intrusion (App. 1, Fig. A14), suggesting multiple calc-silicate alteration events.

The association of actinolite + magnetite \pm albite in some Boyongan skarns reflects similarities to early formed Ca-Na silicate alteration assemblages recently identified in a number of porphyry deposits (e.g., Arancibia and Clark, 1996; Cannell et al., 2005). These authors described Ca-Na silicate alteration as an assemblage of Ca- and/or Ca-Na amphibole (actinolite/hornblende) with Na feldspar (albite-oligoclase) \pm magnetite. Those studies showed that amphibole and magnetite typically occur as irregular veinlets (locally together), with Na feldspar occurring in halos to these veins as a selectively pervasive (Titley, 1982) replacement of feldspar. Sillitoe (2000) noted that the Ca-Na silicate assemblage generally lacks sulfide phases and often occurs in the deep portions of porphyry stocks and adjacent wall rocks, where it may transition into early K silicate alteration assemblages. Despite the presence of actinolite + magnetite \pm albite zones at Boyongan, the replacement textures and mineralogy are typical of many skarn deposits, suggesting that the Boyongan calc-silicate alteration involved contact metasomatism and subsequent retrograde hydrothermal alteration.

K silicate assemblage and associated copper-gold mineralization

Hydrothermal biotite and K-feldspar \pm magnetite \pm quartz define the K silicate alteration assemblage at Boyongan and Bayugo. Biotite occurs as a selectively pervasive replacement of preexisting ferromagnesian silicates (App. 1, Fig. A20) as well as in veinlets and selvages to quartz veins. Hydrothermal K-feldspar occurs as a texturally destructive pervasive replacement of silicates (other than quartz), commonly occurring as halos to quartz veins or quartz-cemented breccias (App. 1, Fig. A21). Hydrothermal magnetite occurs as irregular blebs, disseminations, veinlets, as breccia cement, and with quartz veins. Bornite and chalcopyrite (with minor pyrite and molybdenite) are the principal sulfides associated with the K silicate assemblage and account for most hypogene Cu (and Au) introduced at Boyongan. At Bayugo, chalcopyrite is the dominant hypogene Cu-bearing sulfide and bornite is rare to absent.

Crosscutting relationships reveal a characteristic progression of veining related to K silicate alteration at Boyongan and Bayugo. On the basis of vein composition and texture, the authors define five discrete stages of K silicate-related veining and alteration (App. 1, Table A1).

Stage 0: unidirectional solidification textures: The earliest-formed hydrothermal features are comb-textured quartz bands interlayered with igneous material (Fig. 14A). Bands consist of domains of optically continuous quartz and are 3 mm to 5 cm wide. Within these bands, euhedral quartz terminations generally point in the same direction. Logging at Boyongan identified these features in the ECD1 and late-mineralization diorite porphyry diorite phases. Numerous workers have described similar comb quartz or unidirectional solidification textures from intrusive carapaces of various porphyry Cu and porphyry molybdenum deposits (Shannon et al., 1982; Kirkham and Sinclair, 1988; Atkinson and Ware, 2002; Harris et al., 2005), where the euhedral quartz generally points inward from the intrusive contact. The orientation of euhedral quartz is consistent with growth into open space within the margin of a crystallizing intrusion. The rhythmic

interlayering with porphyritic diorite suggests that each unidirectional solidification texture band was underplated by successive aliquots of magma as the intrusion crystallized.

Stage 1: magnetite and biotite veins: Thin, discontinuous veinlets of magnetite or biotite with K-feldspar alteration halos and little or no quartz define the earliest demonstrably subsolidus stage of veining. The stage 1 magnetite veins resemble the "M" veinlets described by Clark and Arancibia (1995), although the former lack actinolite and have K-feldspar alteration halos (Fig. 14B). Stage 1 biotite occurs as thin discontinuous wispy veinlets with K-feldspar alteration halos and are similar to the streaky biotite veinlets of Sillitoe (2000).

Stage 2: quartz veins with magnetite or biotite: Quartz reappears as an important component in stage 2, where it occurs with subsidiary magnetite or biotite. Stage 2 quartz has a sugary texture, reflecting the presence of anhedral quartz grains varying in size between 50 μm and 1 mm. There are three styles of stage 2 infill: breccia cement, miarolitic cavities, and veins (App. 1, Table A1). As breccias, the dominant cement is quartz, with disseminated magnetite and intense K-feldspar alteration of clast margins. The quartz-magnetite cemented breccias in the eastern high-grade zone of Boyongan (see intermineralization hydrothermally cemented breccias described above) are an expression of stage 2 (Fig. 10; App. 1, Fig. A11). Miarolitic cavities filled by euhedral quartz and biotite with K-feldspar alteration halos (Fig. 14D) represent another expression of stage 2. At Boyongan, miarolitic features were identified only in the upper portions of the intermineralization diorite porphyry stock. As veins, stage 2 quartz contains disseminated and/or selvage biotite or magnetite. These veins generally lack internal texture, although occasionally display concordant magnetite banding. Veins are variable in width (1–90 mm), irregular in form (Fig. 14C), and commonly display intense K-feldspar alteration halos.

Stage 3: quartz veins lacking magnetite and biotite: A lack of biotite and magnetite distinguishes stage 3 quartz veins from earlier vein stages. Stage 3 consists of irregular sugary texture to the quartz in stage 2 (Fig. 14B, C). Stage 3 quartz veins commonly contain a concordant central seam, expressed by distinctive cavities lined by coarser-grained euhedral quartz (Fig. 14F). This texture is similar to that observed for "B" quartz veins from the El Salvador deposit, described by Gustafson and Hunt (1975). In some stage 3 veins, regular fluctuations in quartz grain size have created texturally distinctive concordant banding (e.g., ribbon veins; Figs. 14E, G, 15A, B). K-feldspar alteration halos are commonly weaker and more diffusely developed in stage 3 than around earlier vein stages.

Stage 3 represents the volumetrically most significant vein stage, making up most of the quartz stockworks depicted in Figures 11 and 12 and in Appendix 1, Figures A13 through A15. Much of the Cu and Au at Boyongan and Bayugo is spatially associated with stage 3 stockworks. Bornite (at Boyongan) and/or chalcopyrite are common in stage 3 veins, occurring as disseminations, in the central seam, or concentrated along the banding (Fig. 15A, B). In stage 3, native Au occurs as <10- μm blebs within chalcopyrite and bornite and uncommonly as very fine free grains in quartz. Copper-bearing sulfides also commonly occur in stage 3 veins as discordant

hairline veinlets (Fig. 14B). These features clearly postdate stage 3 vein formation and may represent a transition into stage 4 sulfide-dominated veins.

Stage 4: copper sulfide veins: Stage 4 sulfide veins with moderate to intense K-feldspar alteration halos make up the final stage in the K silicate alteration cycle and are distinguished from earlier stages by the paucity of associated quartz and from all previous stages by the predominance of Cu-bearing sulfides. In the shallow portion of the eastern high-grade zone at Boyongan, stage 4 consists of irregular bornite-chalcopyrite veinlets and breccia cement, which contribute significantly to Cu and Au grades (Figs. 14G, H, 15A). In the deeper, lower-grade portions of the eastern high-grade zone, stage 4 consists of thin chalcopyrite-pyrite veinlets with minor bornite. In stage 4, native Au occurs exclusively as 5- to 100- μm blebs within bornite (Fig. 15C, D). Microprobe analyses indicate that native Au from stage 4 at Boyongan is of high fineness, with an average stoichiometry of $\text{Au}_{0.94}\text{Ag}_{0.03}\text{Cu}_{0.03}$ (App. 4, Table A2). At Bayugo, stage 4 veins consist primarily of chalcopyrite with minor pyrite, but native Au has not been identified therein.

Cyclicality of magmatism, K silicate alteration, and copper-gold mineralization

The K silicate alteration progression outlined above is similar to that described from other porphyry deposits (e.g., El Salvador: Gustafson and Hunt, 1975). Observation of vein crosscutting relationships within a given intrusion reveals that a similar progression of veining and alteration affects each of the early-, inter-, and late-mineralization intrusions (Figs. 16, 17, 18; App. 1, Table A1, Fig. A22). One might conclude from these relationships that all intrusive events occurred before any veining events and that the observed paragenesis of five stages represents the overall evolution of conditions within the magmatic-hydrothermal system.

The challenges to this simple hypothesis are fourfold:

1. The presence of vein-quartz xenoliths from vein stages 2 and/or 3 in the ECD2, ECD3, intermineralization diorite porphyry, late-mineralization diorite porphyry, DIO2, DIO3, and DIO4 intrusions (Table 2; Figs. 16B, F, 17A, 18A, D; App. 1, Fig. A10B, D) is evidence that stage 2 and 3 quartz veins existed prior to the emplacement of each of these intrusions.
2. Each of the Boyongan early-mineralization diorite, intermineralization diorite porphyry, late-mineralization diorite porphyry, and diorite porphyry intrusions was cut by vein stages that predate the quartz vein stages (stage 1 veins). In all intrusions, stage 1 veins were subsequently cut by quartz vein stages 2 and 3 and (in some cases) Cu-bearing sulfide vein stage 4.
3. An abrupt change in quartz vein abundance and/or grade characterizes the intrusive contacts between many discrete intrusions (Fig. 7).
4. Certain recognizable vein stages (e.g., the distinctive ribbon stage 2 and 3 quartz veins; Fig. 14E) are absent from the demonstrably younger intermineralization diorite porphyry and late-mineralization diorite porphyry intrusions. These same distinctive vein types are recognizable as vein-quartz xenoliths in younger intrusions (e.g., Fig. 17A).

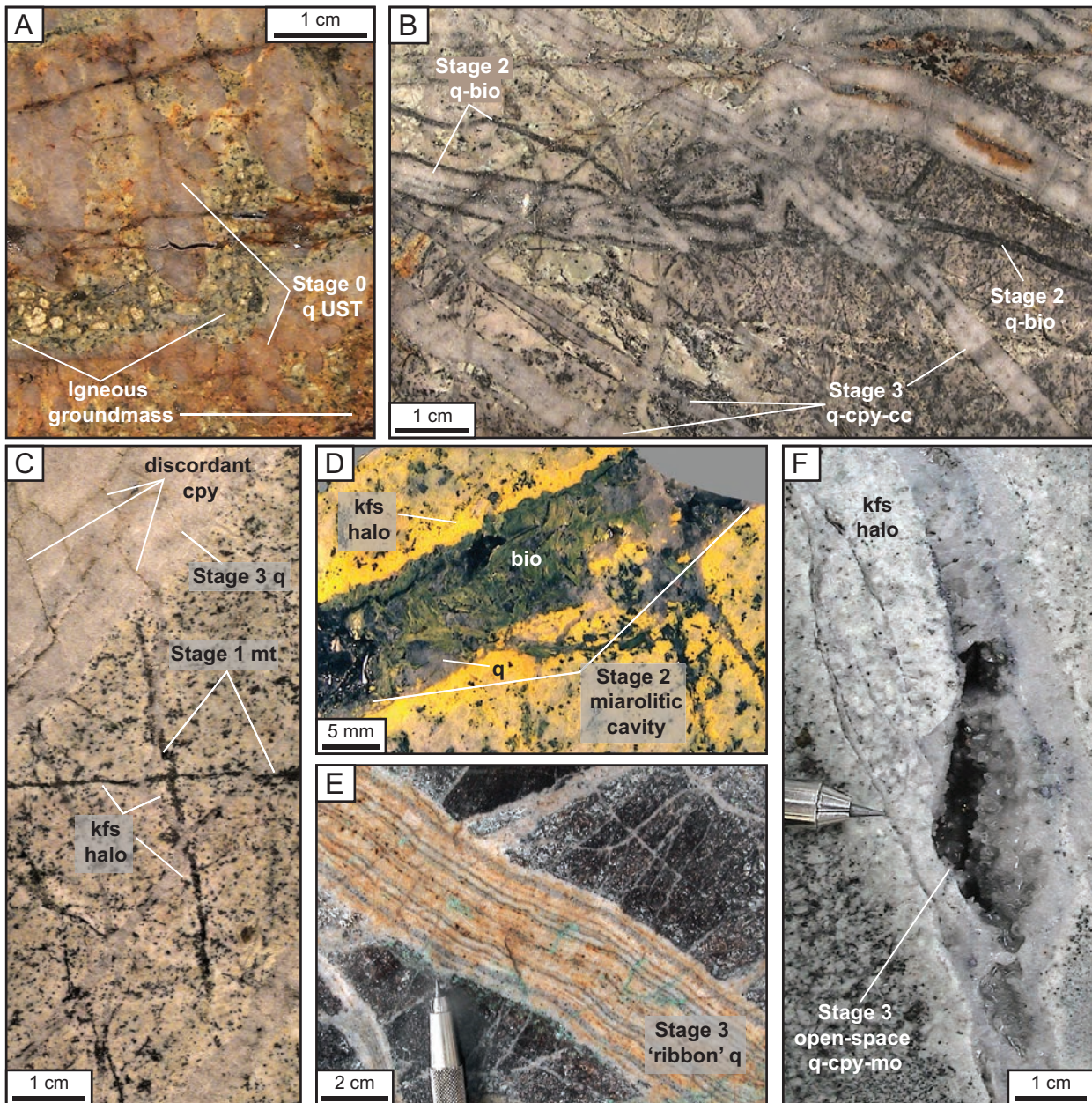


Fig. 14. Examples of vein styles associated with K silicate alteration. (A) Interval of late-mineralization diorite porphyry dike containing stage 0 comb quartz (unidirectional solidification texture) interlayered with porphyritic diorite. Sample: 819336. Diamond drill hole TSD18, 203.85 m. (B) Intensely K-feldspar-altered interval cut by stage 2 quartz veinlets with biotite selvages and by stage 3 quartz veins with discordant chalcopyrite stringers (now partially replaced by chalcocite). Sample: 819439. Diamond drill hole TSD44, 285.85 m. (C) Interval of intensely K-feldspar altered ECD2 cut by stage 1 magnetite veinlets. Magnetite veinlets have been cut by stage 3 quartz veins that contain discordant chalcopyrite veinlets. Sample: 819312. Diamond drill hole TSD18, 769.5 m. (D) Interval of intermineralization diorite porphyry containing stage 2 miarolitic cavity filled with quartz and biotite and flanked by an intense K-feldspar alteration halo (yellow staining). Sample: 819431. Diamond drill hole TSD44, 520.1 m. (E) Finely banded stage 3 ribbon quartz with banding defined by variations in quartz grain size. Ribbon veins commonly contain fine concordant Cu sulfides and represent a significant stage of Cu-Au introduction. Sample: 819362. Diamond drill hole TSD38, 59.65 m. (F) Interval of medium-grained diorite porphyry cut by stage 3 open-space quartz vein lined by euhedral quartz. Molybdenite and chalcopyrite have intergrown with and filled interstices of euhedral quartz. This mineral assemblage and open-space texture define one of the latest stages of porphyry-style quartz veining recognized at Boyongan. Sample: 819474. Diamond drill hole TSD52, 548.1 m. (G) Brecciated interval with clasts of stage 3 ribbon vein quartz (containing concordant bornite-chalcopyrite) cemented by stage 4 bornite-chalcopyrite (now partially chalcocite). Sample contains abundant fracture-hosted supergene Cu carbonates (malachite and azurite). Sample: 819358. Diamond drill hole TSD38, 104.76 m. (H) Interval of medium-grained diorite porphyry cut by stage 4 chalcopyrite-bornite vein with intense K-feldspar alteration halo. Sample: 819477. Diamond drill hole TSD52, 440.35 m. Abbreviations: az = azurite, bio = biotite, bn = bornite, cc = chalcocite, cpy = chalcopyrite, kfs = K-feldspar, mal = malachite, mo = molybdenite, mt = magnetite, q = quartz, UST = unidirectional solidification texture.

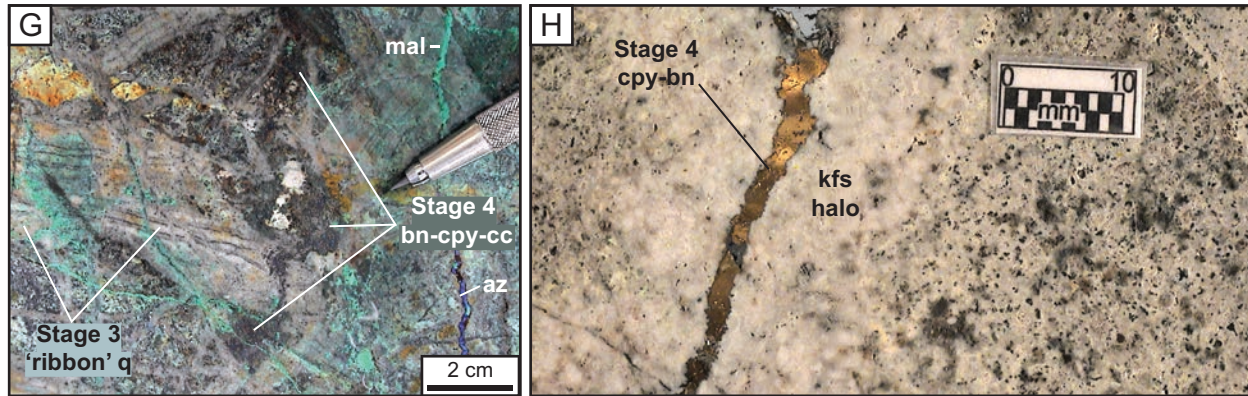


Fig. 14. (Cont.)

The five apparent stages of K silicate-related veining and alteration described for Boyongan are considered to be a deceptively simple paragenesis. The above observations show that a similar progression of K silicate alteration and mineralization has been repeated with successive intrusions, making for numerous discrete but mineralogically and texturally similar vein and breccia events. Figure 19 summarizes the observed paragenesis of veining and alteration in the context of the intrusive events at Boyongan. The spatial coincidence of multiple overprinting fertile magmatic-hydrothermal cycles may help to explain the development of spectacular Cu (>3%) and Au (>9 g/t) grades in the eastern high-grade zone.

Boyongan and Bayugo are not unique in their cyclical relationships between intrusive and vein-forming events. Investigations at Bingham Canyon, USA (Redmond et al., 2001, 2004; Redmond and Einaudi, 2001, 2010), Bajo de la Alumbrera, Argentina (Proffett, 2003), and Ridgeway, Australia (Wilson et al., 2003) have also documented similar intimate relationships between multiple intrusive events and veining cycles.

K silicate alteration zonation

Because of the paragenetic association of Cu and Au with K silicate alteration, this study sought to develop various indices of K silicate alteration intensity to refine patterns of alteration zonation around the Boyongan and Bayugo deposits. These indices include (1) the percent of primary mafic phenocrysts selectively replaced by hydrothermal biotite, (2) the distribution of hydrothermal biotite occurring in veins or as vein selvages (vein stages 1 and 2), (3) the distribution of hydrothermal magnetite occurring in veins or as vein selvages (vein stages 1 and 2), and (4) the intensity of K-feldspar replacement of silicates other than quartz.

Hydrothermal biotite: Hydrothermal biotite occurs as a selectively pervasive replacement of primary mafic phenocrysts as well as in K silicate vein stages 1 and 2. Hydrothermal biotite is Mg and F rich, and limited electron microprobe analyses (App. 4, Table A1) suggest an average stoichiometry of $K_{0.8}Mg_{2.2}Fe_{0.6}AlSi_{2.9}Ti_{0.1}O_{10}(OH)_{0.5}F_{0.5}$.

In thin section, primary mafic phenocrysts replaced by biotite are recognizable by their primary subhedral morphology (App. 1, Fig. A20). The percentage of primary mafic phenocrysts replaced by biotite provides a means of quantifying

the intensity of this style of alteration. Petrographic studies were used to categorize each sample as having weak (<25%), moderate (25–75%), or intense (>75%) biotite replacement of primary mafic phenocrysts. Subsequent chloritization of mafic phases can mask the original nature and extent of biotite alteration. At Boyongan and Bayugo, chloritization of mafic silicates is commonly incomplete, leaving remnants of primary igneous mafic minerals or hydrothermal biotite in most chloritized sites. During the petrographic analysis, mafic phenocryst sites completely altered to mixtures of hydrothermal biotite and chlorite were assumed to have been purely hydrothermal biotite prior to chloritization. At Boyongan, selectively pervasive biotitization is most intense in and around the early-mineralization diorite series intrusions and is considerably diminished in the intermineralization diorite porphyry and late-mineralization diorite porphyry intrusions (Fig. 20C; App. 1, Figs. A23C, A24C). At Bayugo, selectively pervasive biotite replacement was intense, exceeding 75% in all of the porphyry intrusions (bird's-eye porphyry, medium-grained diorite porphyry, and DIO series) investigated (Fig. 21B).

Another useful index of biotite alteration has been the observed distribution of hydrothermal biotite occurring in veins (i.e., stages 1 and 2) as identified by the authors during drill core logging. At Boyongan, vein-related biotite defines a narrow zone around the early-mineralization diorite, intermineralization diorite porphyry, and late-mineralization diorite porphyry intrusions (Fig. 20D; App. 1, Figs. A23D, A24D), reflecting the spatial distribution of vein assemblages described above. Vein-related biotite at Bayugo is uncommon (App. 1, Table A1), as stage 1 and 2 veins are dominated by magnetite.

Hydrothermal magnetite: Hydrothermal magnetite related to K silicate alteration occurs in stage 1 and stage 2 veins and breccias. In the shallow weathered zones, magnetite is partially to completely replaced by earthy hematite (App. 1, Fig. A11), although its association with stages 1 and 2 makes recognition of its hypogene character during logging relatively easy. At Boyongan, magnetite from stages 1 and 2 occurs within an envelope around the late-mineralization diorite porphyry and early-mineralization diorite series intrusions (Fig. 20C; App. 1, Figs. A23C, A24C). Vein-related magnetite in the intermineralization diorite porphyry stock is uncommon. At Bayugo, magnetite-bearing stage 1 and 2 veins are associated with the

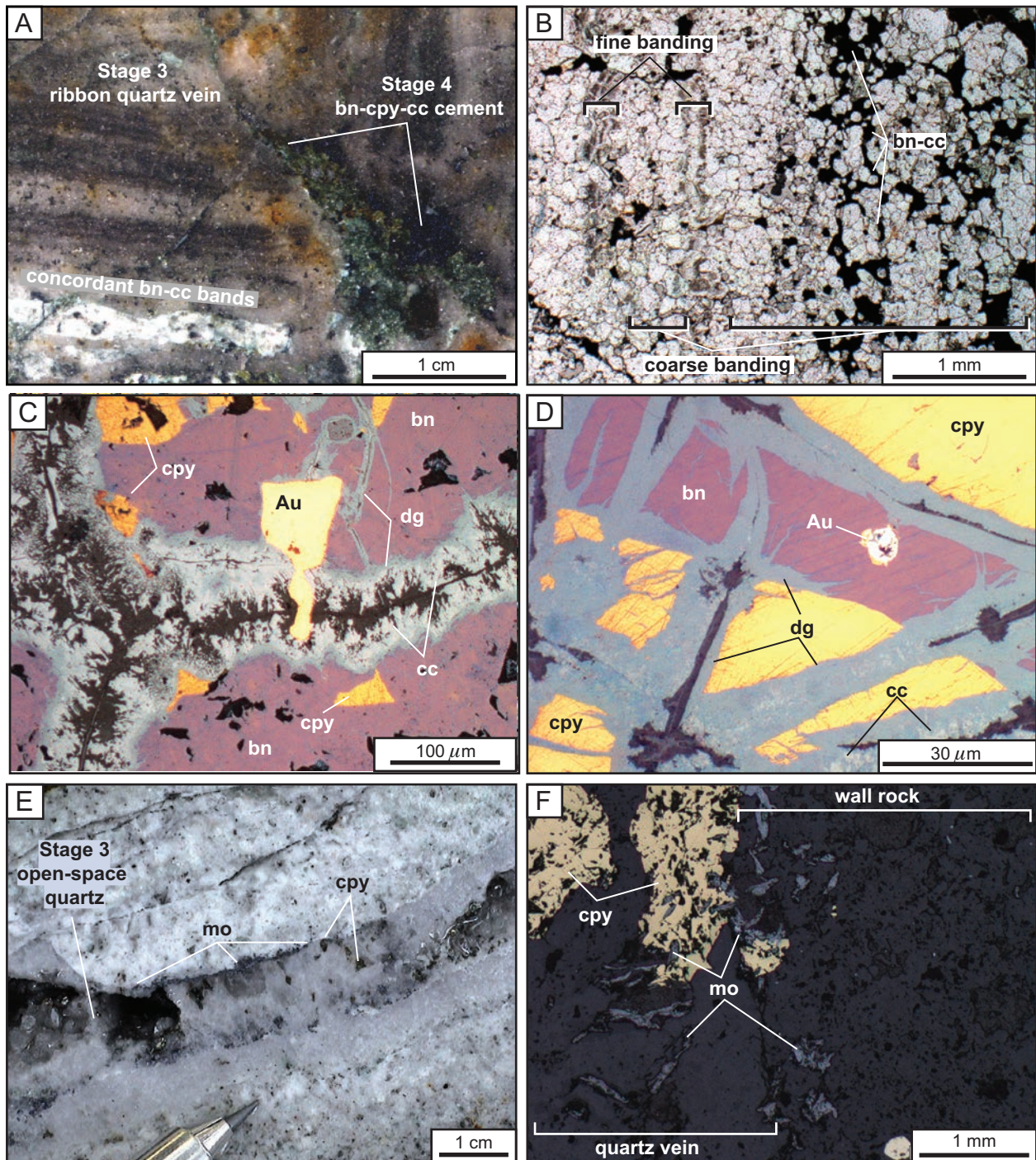


Fig. 15. Character of hypogene Cu sulfide, Au, and molybdenite mineralization at Boyongan. Supergene digenite and chalcocite have replaced the hypogene Cu sulfides along fractures in some samples. (A) Finely banded stage 3 ribbon quartz vein containing concordant bornite (now partially chalcocite) brecciated and cemented by stage 4 bornite and chalcopyrite. Sample: 819357. Diamond drill hole TSD38, 105.16 m. (B) Stage 3 ribbon vein in transmitted light photomicrograph showing banding defined by variations in size of quartz domains. Bornite (now partially replaced by supergene chalcocite) occupies quartz interstices in coarser-grained domains highlighting concordant banding. Sample: 819358. Diamond drill hole TSD38, 104.76 m. (C, D) Bornite and chalcopyrite in stage 4 breccia cement containing blebs of high-fineness Au. Sample in (C): 819358. Diamond drill hole TSD38, 104.76 m. Sample in (D): 819349. Diamond drill hole TSD38, 290.23 m. (E) Stage 3 open-space quartz vein with disseminated molybdenite and chalcopyrite occurring near the quartz vein margins. Sample: 819474. Diamond drill hole TSD52, 548.1 m. (F) Reflected-light photomicrograph of (E) showing relationships of sulfide minerals to quartz vein. Abbreviations: Au = native gold, bn = bornite, cc = chalcocite, cpy = chalcopyrite, dg = digenite, mo = molybdenite.

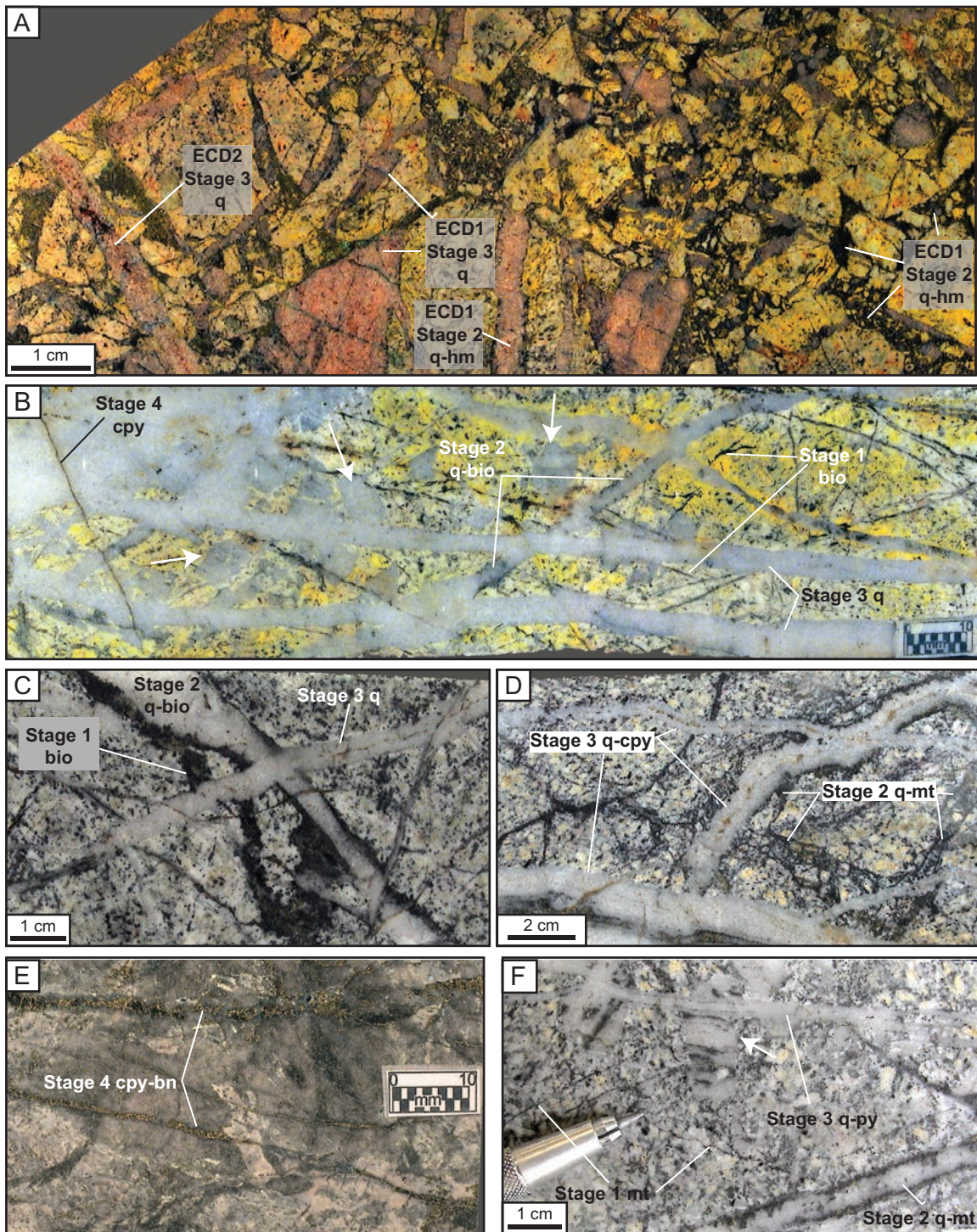


Fig. 16. K silicate vein stages that have cut the early mineralization diorite porphyries ECD1, ECD2, and ECD3 from the eastern high-grade zone at Boyongan. (A) Quartz-magnetite (now supergene hematite) cemented breccia containing veined clasts of ECD1. Prebreccia veins represent vein stages 2 and 3 associated with the ECD1 cycle. The breccia cement represents stage 2 associated with the ECD2 cycle. Quartz veins with central seams cut the breccia and represent ECD2 stage 3. Sample: 819360. Diamond drill hole TSD38, 84.2 m. (B) ECD2 containing stage 3 vein-quartz xenoliths (arrows) associated with ECD1 and cut by vein stages 1, 2, 3, and 4. Sample: 819315. Diamond drill hole TSD18, 681.65 m. (C) ECD2 cut by vein stages 1, 2, and 3. Sample: 819312. Diamond drill hole TSD18, 769.5 m. (D) ECD2 cut by stages 2 (quartz-magnetite breccia cement) and 3. Sample: 819326. Diamond drill hole TSD18, 413.58 m. (E) Brecciated and K-feldspar-altered ECD1 cut by chalcopyrite-bornite veins thought to be associated with stage 4 of ECD2. Sample: 819492. Diamond drill hole TSD20, 306.6 m. (F) ECD3 containing vein-quartz xenoliths (arrows) associated with ECD2 (stage 2) and cut by vein stages 1, 2, and 3. Sample: 819314. Diamond drill hole TSD18, 691.5 m. Slabs in (A) and (B) stained to reveal K-feldspar (yellow). Abbreviations: bio = biotite, bn = bornite, cpy = chalcopyrite, hm = hematite, mt = magnetite, py = pyrite, q = quartz.

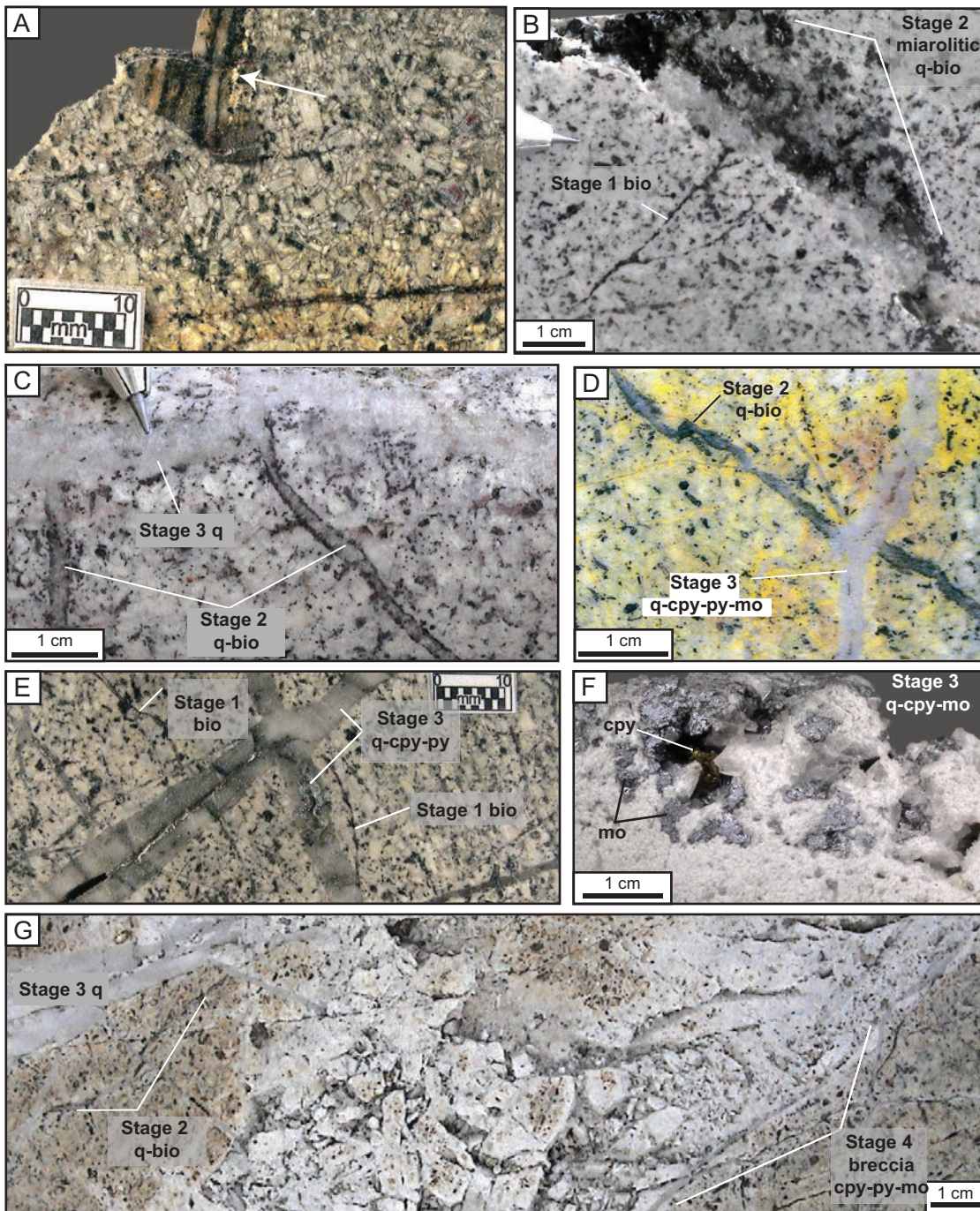


Fig. 17. K silicate vein stages that have cut the intermineralization diorite porphyry stock. (A) Interval of intermineralization diorite porphyry (IMD) containing a xenolith of distinctive ribbon quartz-magnetite vein similar to ECD0 vein stage 2 (App. 1, Fig. A22) Sample: 815176. Diamond drill hole TSD23, 561.58 m. (B) Interval of intermineralization diorite porphyry cut by stage 1 (biotite veinlets) and stage 2 (euhedral quartz and biotite filling miarolitic cavities) Sample: 819431. Diamond drill hole TSD44, 520.1 m. (C) Intermineralization diorite porphyry cut by stage 2 (quartz-biotite veins) and stage 3 (quartz veins). Sample: 819420. Diamond drill hole TSD13, 617.88 m. (D) Intermineralization diorite porphyry cut by stage 2 (quartz-biotite veins) and stage 3 (quartz veins with central sulfide seam). Slab stained to reveal K-feldspar (yellow). Sample: 819301. Diamond drill hole TSD18, 907.11 m. (E) Interval of intermineralization diorite porphyry cut by stage 1 (biotite veinlets) and stage 3 (quartz veins with disseminated or central-seam chalcopyrite and pyrite). Sample: 819433. Diamond drill hole TSD44, 452.52 m. (F) Stage 3 vein from intermineralization diorite porphyry stock consisting of euhedral quartz, with interstitial chalcopyrite and molybdenite occurring in open spaces. Sample: 819306. Diamond drill hole TSD18, 848.12 m. (G) Interval of intermineralization diorite porphyry cut by stage 2 (quartz-biotite veinlets) and stage 3 (quartz veins). Brecciation (stage 4) has followed stage 3: K-feldspar alteration has bleached the clasts, and chalcopyrite, pyrite, and molybdenite have occupied the interstitial void space. Sample: 814752. Diamond drill hole TSD63, 527.98 m. Abbreviations: bio = biotite, cpy = chalcopyrite, mo = molybdenite, py = pyrite, q = quartz.

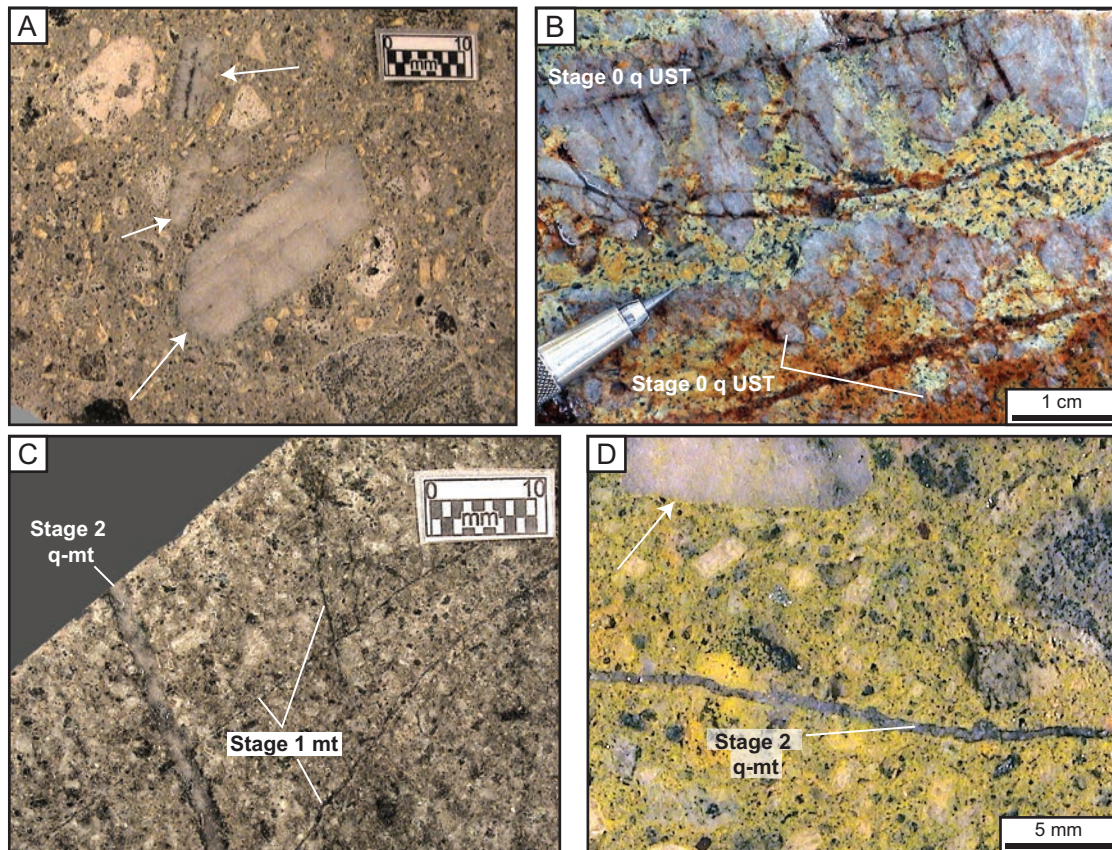


Fig. 18. K silicate vein stages that occur within the late mineralization diorite porphyry (LDP) dikes at Boyongan. (A) Interval of late-mineralization diorite porphyry containing various xenoliths including vein-quartz fragments (arrows) derived from earlier veining events. Sample: 819345. Diamond drill hole TSD38, 373.75 m. (B) Comb quartz unidirectional solidification textures (stage 0 UST) interlayered with late-mineralization diorite porphyry diorite porphyry. Fractures cutting the USTs contain native Cu, reflecting the sample's origin in the weathered zone. Sample: 819336. Diamond drill hole TSD18, 203.85 m. (C) Interval of late-mineralization diorite porphyry cut by stage 1 (magnetite veinlets) and stage 2 (quartz-magnetite) veinlet. Sample: 815147. Diamond drill hole TSD52, 911.85 m. (D) Interval of late-mineralization diorite porphyry containing various xenoliths including vein-quartz clasts (arrows) derived from earlier veining events. Sample cut by stage 2 (quartz-magnetite) veinlet. Sample stained to reveal weak K-feldspar halo (yellow). Sample: 819345. Diamond drill hole TSD38, 373.75 m. Abbreviations: mt = magnetite, q = quartz, UST = unidirectional solidification texture.

DIO2 and DIO3 stocks and sporadically within the bird's-eye porphyry stock to the south (Fig. 21C).

Hydrothermal K-feldspar: Hydrothermal K-feldspar occurs in association with vein stages 1 to 4 as variably white or pale-pink alteration halos. Where K-feldspar halos are wide and/or veining is intense, K-feldspar alteration halos have coalesced, leading to a flooding or pervasive replacement of the aluminosilicate phases in the rock (App. 1, Fig. A21).

In the weathered portions of the deposits, white K-feldspar alteration halos are easily mistaken for sericite where the rock hardness had been reduced due to incipient replacement by supergene clay. The systematic staining of sawn slabs with $\text{Na}_3\text{Co}(\text{NO}_2)_6$ (App. 2) has therefore assisted in the discrimination between albite, illite, and K-feldspar (App. 1, Figs. A12, A21).

K-feldspar alteration only affected aluminosilicates, not quartz or opaque minerals. In quantifying the intensity of K-feldspar alteration it was necessary to consider only the reactive aluminosilicate component of the rock, which at Boyongan and Bayugo proved to be principally plagioclase

phenocrysts and groundmass. Petrographic studies of the basaltic host rocks and dioritic intrusions revealed no primary orthoclase, so all K-feldspar identified by staining can be attributed to hydrothermal alteration. The image analysis software eCognition® (Definiens, 2005) was used to discriminate K-feldspar, quartz, plagioclase, groundmass, and opaque phases in digital photographs of the stained slabs and to quantify the proportional surface area of each of these components. This procedure enabled quantification of the proportion of aluminosilicates in the sample that had been converted to K-feldspar, a measure independent of the amount of quartz or other inert phases in the slab (App. 1, Fig. A12).

The intensity of hydrothermal K-feldspar alteration as defined by this technique is greatest in and around the early-mineralization diorite and intermineralization diorite porphyry stocks at Boyongan (Fig. 20D; App. 1, Figs. A23D, A24D) and the DIO2 stock at Bayugo (Fig. 21D). In zones of intense stockwork veining, K-feldspar alteration intensity exceeds 25% by volume and drops below 10% in zones peripheral to the stockwork.

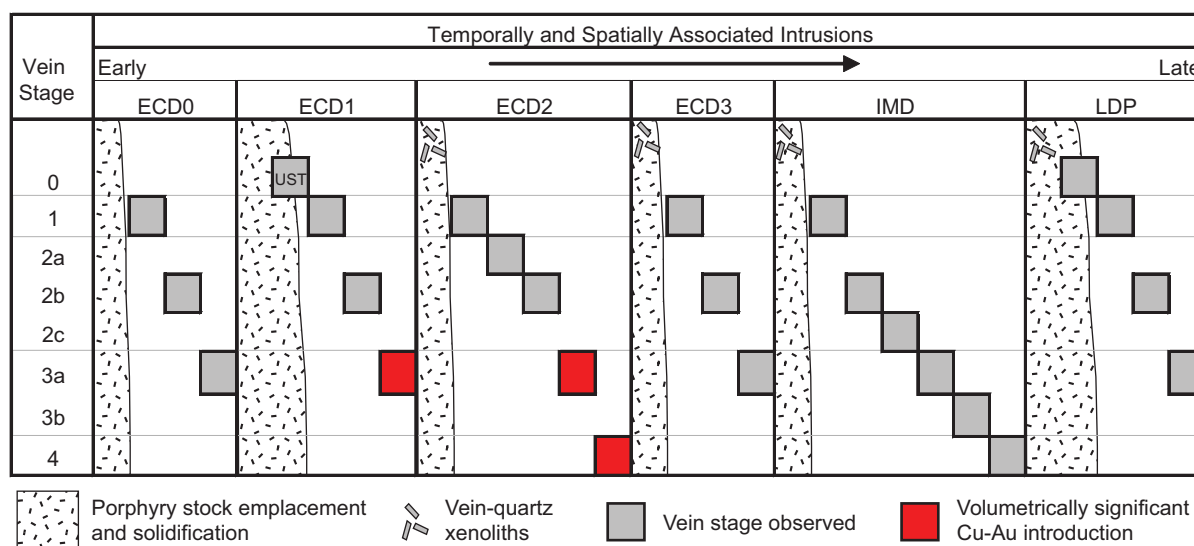


Fig. 19. Schematic summary of repeated cycles of K silicate-stage veining, alteration, and mineralization, punctuated by successive intrusive events. The diagram summarizes the vein stages observed to cut a given intrusion and emphasizes that mineralogically and texturally similar veining and alteration cycles are repeated with new intrusive events. Figures 16–18 document these crosscutting relationships in detail. The presence of vein-quartz xenoliths and abrupt changes in quartz vein abundance and grade at intrusive contacts support the model for magmatic-hydrothermal cycles. Abbreviations: UST = unidirectional solidification texture.

Clay mineralogy

The authors conducted detailed XRD and SWIR studies of the clay mineralogy at Boyongan in an effort to distinguish hypogene from supergene components in the weathering profile. This work revealed six principal clay species at Boyongan: kaolinite (118 samples), illite (197 samples), pyrophyllite (4 samples), smectite (112 samples), interstratified illite/smectite (11 samples), and chlorite (174 samples). These clay minerals form the principal components of the illite-smectite-chlorite, illite-pyrite, and kaolinite assemblages defined at Boyongan.

Clay distribution in the weathered zone

The XRD and SWIR analyses revealed that kaolinite, illite, smectite, and chlorite are the most common and widespread clay minerals at Boyongan. Kaolinite abundance is high in the weathered zone and diminishes rapidly below the zone of Cu oxides (a proxy for the base of oxidative weathering). Illite, smectite, and chlorite extend well below the base of oxidation, but of these three only illite persists into the uppermost portions of the supergene profile where weathering is most intense.

Ignacio (2005) also described kaolinite from the weathered zone at Boyongan based on SWIR investigations. He theorized that acid produced by supergene sulfide oxidation had reacted with feldspar to produce kaolinite. In the current study, the close spatial coincidence of the kaolinite zone and the Cu oxide zone is consistent with Ignacio's (2005) model of supergene kaolinite. The absence of smectite and chlorite and the persistence of illite in the strongly weathered zones probably reflect the differential stability of these minerals under low-pH (supergene) weathering conditions.

Illite-smectite-chlorite alteration assemblage

A widespread, low-intensity assemblage of phyllosilicates consisting of illite, smectite (\pm interstratified illite/smectite), and chlorite (Fig. 22A) overprinted the Ca-Na silicate and K silicate alteration assemblages at Boyongan. In this assemblage, illite occurs as a weak dusting of plagioclase (Fig. 22E), resulting in indistinct or blurred feldspar phenocrysts in hand sample. Smectite occurs as a selectively pervasive replacement of mafic minerals (Fig. 22C), plagioclase phenocrysts, and groundmass. Where abundant, smectite alteration is recognizable by characteristic arcuate shrinkage cracks (Fig. 22A) resulting from desiccation in the core tray. Chlorite occurs in two styles, depending on the character of the protolith. In the fine-grained basalt and sedimentary wall rocks, chlorite alteration is pervasive, imparting a dark-green tone to the chloritized groundmass. In porphyritic rocks, chlorite has selectively replaced primary and hydrothermal mafic minerals (Fig. 22F-H).

The petrographic and XRD studies have shown that the illite-smectite-chlorite assemblage is widespread throughout the Boyongan and Bayugo complex. Modeling with Newmod™ provides quantitative measures of the relative abundance of each clay mineral species in $<2\text{-}\mu\text{m}$ separates (Moore and Reynolds, 1989; Reynolds and Reynolds, 1996). Although this modeling does not necessarily reflect changes in the absolute abundance of clay minerals, it provides a measure of the relative alteration intensity for each clay mineral component in a given assemblage. The relative intensity of illite-smectite-chlorite alteration can be described by three alteration indices, incorporating the results of the petrographic studies and clay mineral modeling.

Illite alteration intensity: Modeling of the relative abundance of clay minerals with Newmod™ provides a means

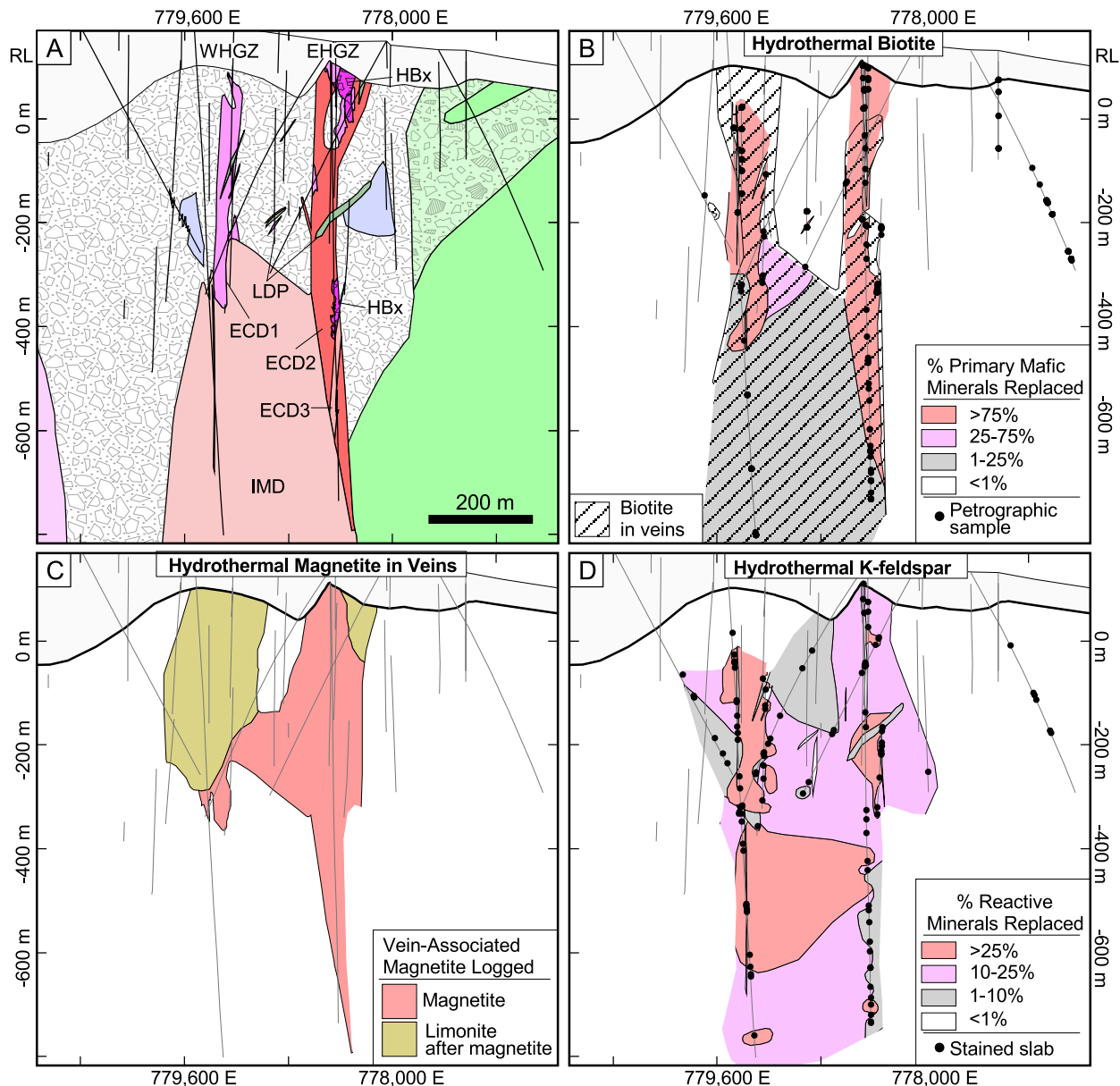


Fig. 20. Interpretive sections from Boyongan showing K silicate alteration zonation along 1,062,200 N. (A) Generalized geology and Cu-Au distribution. Refer to Figure 3 for an explanation of rock types, Figure 5B for section location, and Figure 6A for detailed geologic information. (B) Distribution of hydrothermal biotite. Solid colors denote the degree of selectively pervasive replacement of primary mafic phenocrysts by hydrothermal biotite. Broad ranges (i.e., <1%, 1–25%, 25–75%, and >75%) reflect general estimates based on visual inspection of biotite replacement in thin sections. Biotite replacement is most intense in ECD-series intrusions. Diagonal lines denote the distribution of hydrothermal biotite as veinlets and selvages to quartz veins, based on logging and petrographic descriptions by the authors. The spatial distribution of vein-associated biotite reflects proximity to intermineralization diorite porphyry and ECD-series intrusions. (C) Distribution of hydrothermal magnetite as veinlets and as selvages to quartz veins, based on logging and petrographic descriptions by the authors. Vein-related magnetite is primarily associated with the ECD-series intrusions, with only rare vein magnetite in the intermineralization diorite porphyry stock. (D) Replacement of aluminosilicate rock component by hydrothermal K-feldspar as revealed by systematic staining of sawn slabs for K-feldspar with $\text{Na}_3\text{Co}(\text{NO}_2)_6$ and supplemented by logging by the authors. K-feldspar alteration intensity is greatest in and around the intermineralization diorite porphyry and ECD-series intrusions.

to quantify the intensity of illite alteration at Boyongan. The metric employed uses the illite index, here defined as the mass percentage of illite among all hydrothermal clay minerals ($100 \times \text{illite} / [\text{illite} + \text{smectite} + \text{illite/smectite} + \text{chlorite}]$) determined by XRD. Kaolinite is therefore excluded from

the illite index, as its presence seems to reflect weathering, not hydrothermal processes. The illite index is lowest in the deeper parts of the intrusive/breccia complex at Boyongan and commonly exceeds 75% in the shallow weathered zone (Fig. 23B). This increase of the illite index in the weathered

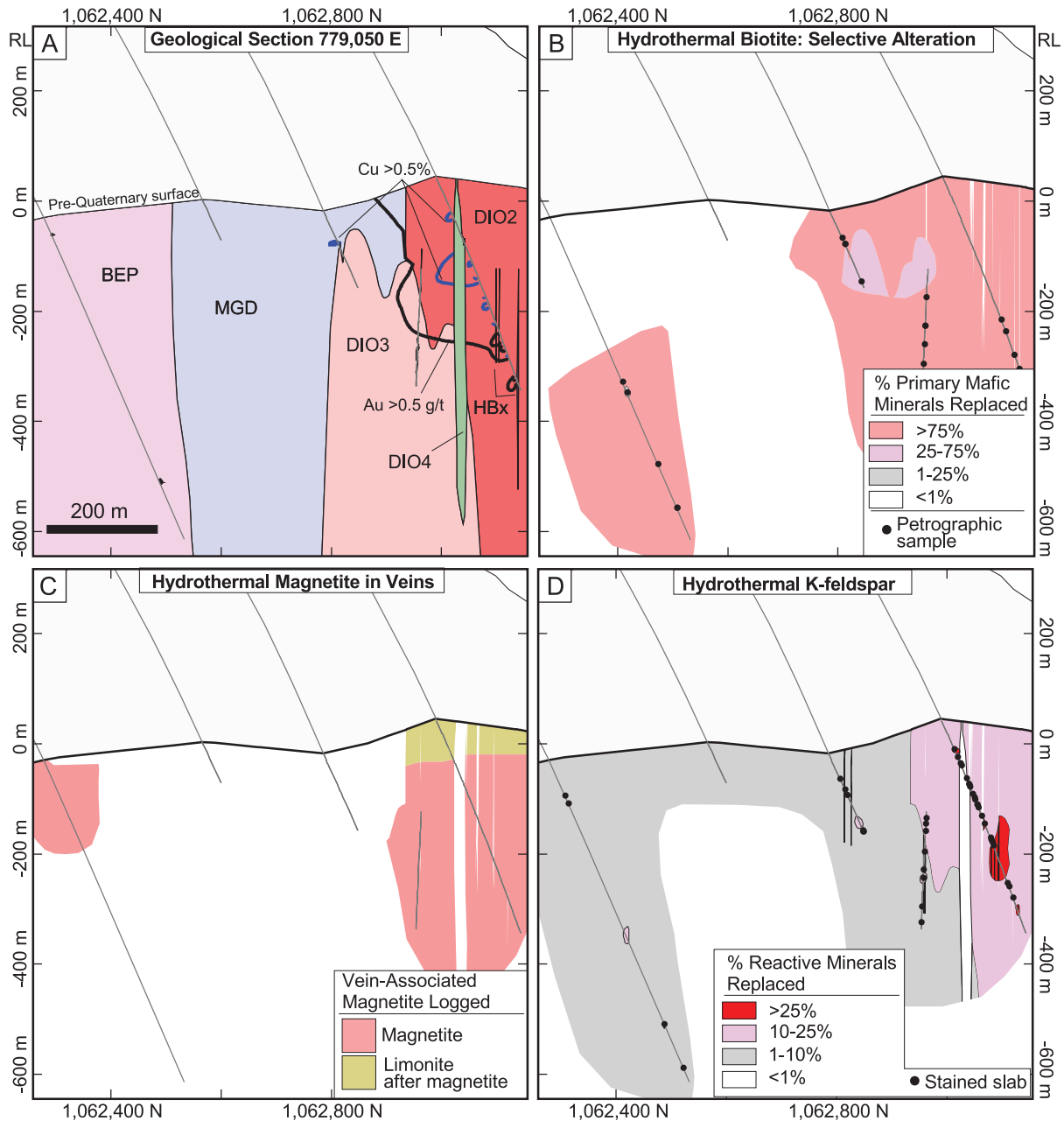


Fig. 21. Interpretive sections from Bayugo showing K silicate alteration zonation along 779,050 E. (A) Generalized geology and Cu-Au distribution. Refer to Figure 3 for an explanation of rock types, Figure 5B for section location, and Figure 6B for detailed geologic information. (B) Degree of selectively pervasive replacement of primary mafic phenocrysts by hydrothermal biotite, based on visual estimate in polished thin sections. Biotite replacement is intense in most porphyry intrusions evaluated. (C) Distribution of hydrothermal magnetite as veinlets and as selvages to quartz veins, based on logging and petrographic descriptions by the authors. Vein-related magnetite is primarily associated with the DIO2 and DIO3 stocks and to a lesser extent in the bird's-eye porphyry stock. (D) Replacement of reactive minerals (i.e., silicates other than quartz) by hydrothermal K-feldspar as revealed by systematic staining of sawn slabs for K-feldspar with $\text{Na}_3\text{Co}(\text{NO}_2)_6$. K-feldspar alteration intensity is greatest in and around the DIO2 stock.

zone may reflect greater stability of illite relative to chlorite and smectite in the low-pH weathering environment. Illite indices exceeding 95% are related to illite-pyrite alteration along structures that have cut the intrusive complex (Fig. 23B; App. 1, Figs. A26B, A27B).

Smectite alteration intensity: The smectite index is defined here as the mass percentage of smectite among all

hydrothermal clays (100*[smectite/[illite + smectite + illite/smectite + chlorite]]) as determined by XRD and quantified using Newmod™. Smectite is absent from the intensely weathered portions of Boyongan. As with the illite index, kaolinite is excluded in this analysis, because its presence is inferred to be related to weathering. Figure 23C and Appendix 1, Figures A26C and A27C summarize the intensity of

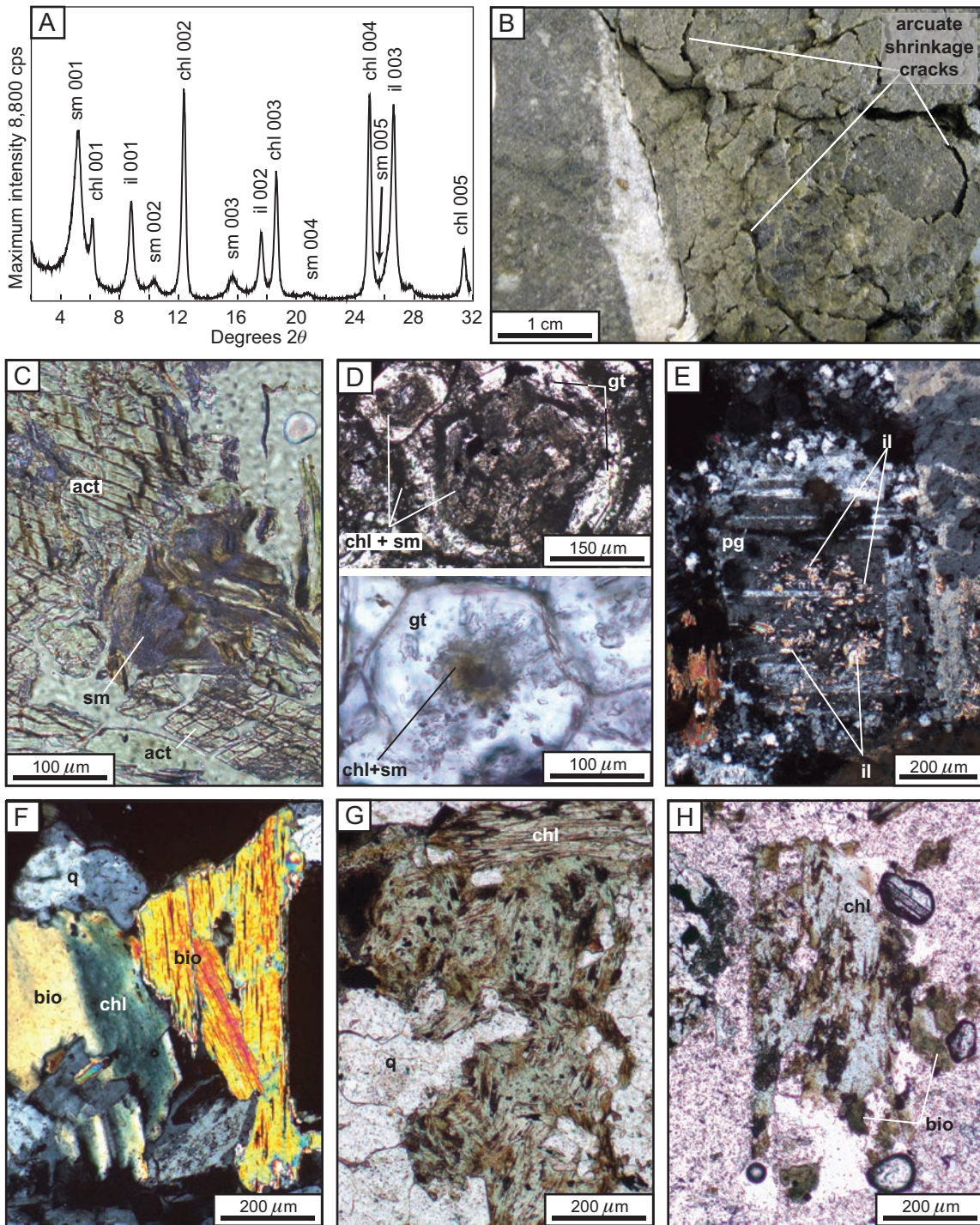


Fig. 22. Styles of illite-smectite-chlorite alteration at Boyongan. (A) XRD pattern of ethylene-glycol-solvated oriented clay separate showing typical illite-smectite-chlorite assemblage. Peak positions (e.g., 001) mark the diagnostic spectra for each clay mineral. Sample: 814781. Diamond drill hole TSD70, 261.83 m. (B) Smectite-rich interval of basalt with arcuate fractures reflecting shrinkage of expanding clays during core desiccation. Diamond drill hole TSD85, 601 m. (C) Plane-polarized photomicrograph showing smectite replacement of hydrothermal actinolite. Sample: 819407. Diamond drill hole TSD13, 523.8 m. (D) Plane-polarized photomicrographs showing selective smectite and chlorite replacement of garnet along growth zones. Sample: 819589. Diamond drill hole TSD54, 235.02 m. (E) Cross-polarized photomicrograph showing illite dusting in core of plagioclase phenocryst. Sample: 819420. Diamond drill hole TSD13, 617.88 m. (F) Cross-polarized photomicrograph depicting weak selective replacement of hydrothermal biotite by chlorite. Sample: 819486. Diamond drill hole TSD20, 485.62 m. (G) Plane-polarized photomicrograph showing intense selective replacement of hydrothermal biotite by chlorite. Sample: 819358. Diamond drill hole TSD38, 104.76 m. (H) Primary mafic phenocryst replaced by hydrothermal biotite and subsequently by chlorite (plane-polarized photomicrograph). Sample: 815090. Diamond drill hole TSD60, 948.6 m. Abbreviations: act = actinolite, bio = biotite, chl = chlorite, gt = garnet, il = illite, pg = plagioclase, q = quartz, sm = smectite.

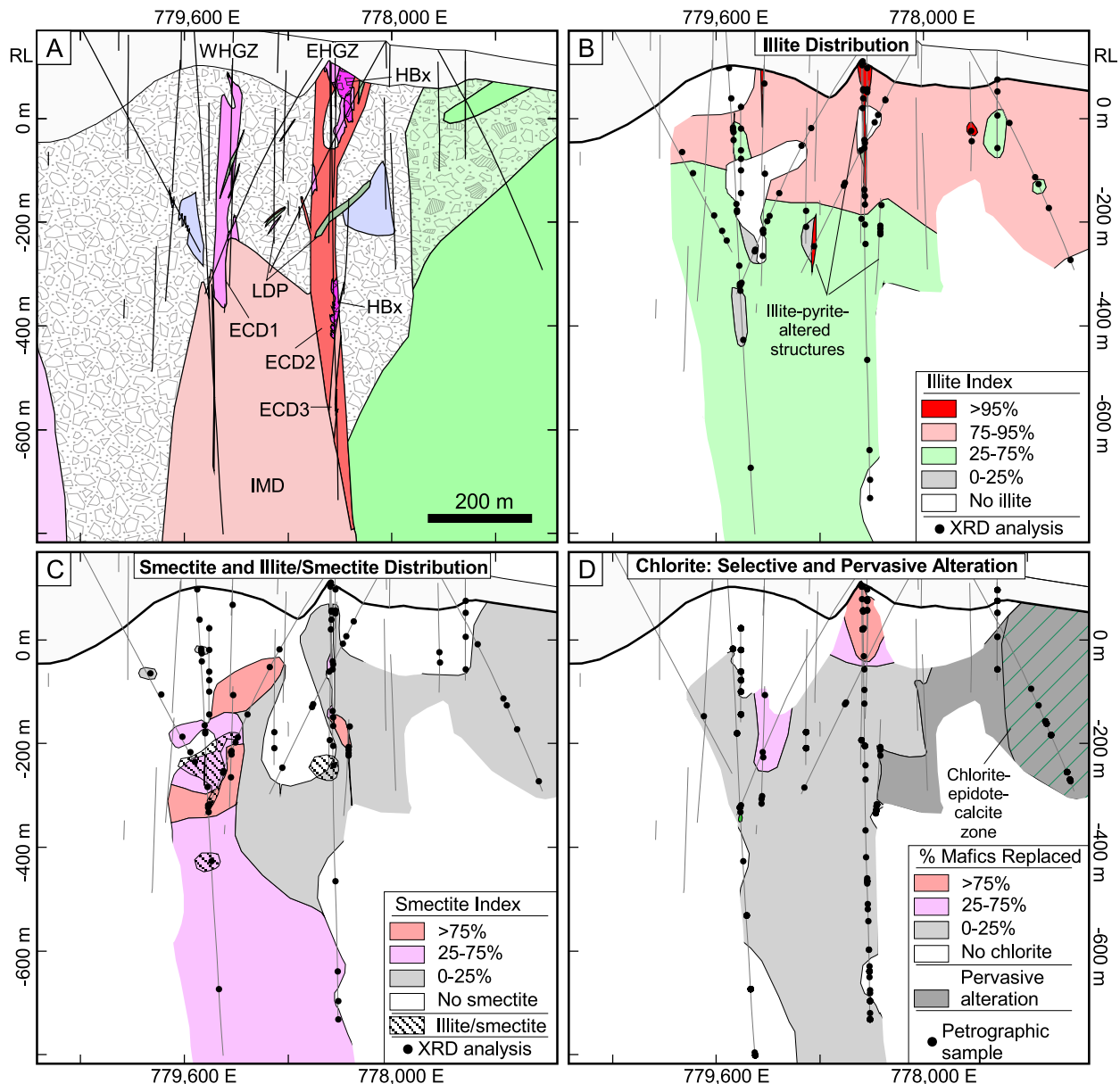


Fig. 23. Interpretive sections from Boyongan showing hydrothermal clay mineral alteration zonation along 1,062,200 N. (A) Generalized geology and Cu-Au distribution. Refer to Figure 3 for an explanation of rock types, Figure 5B for section location, and Figure 6A for detailed geologic information. (B) Illite index ($100^{\circ}\text{illite}/[\text{illite} + \text{smectite} + \text{illite/smectite} + \text{chlorite}]$) as determined by XRD and modeled using NewmodTM. The high proportion of illite in the upper part of the intrusive/breccia complex may in part reflect destruction of chlorite and smectite during weathering. Illite indices above 95% primarily occur in narrow subvertical structures displaying pervasive illite-pyrite alteration. The illite index in the basaltic wall rock generally exceeds that of the breccia complex, and exceptionally high relative abundances (>75%) occur in the volcanic breccia facies of the Bacuag Formation. (C) Smectite index ($100^{\circ}\text{smectite}/[\text{illite} + \text{smectite} + \text{illite/smectite} + \text{chlorite}]$) as determined by XRD and modeled using NewmodTM. Smectite and illite/smectite are most abundant in the western high-grade zone. (D) Occurrence of chlorite. In porphyritic intrusions, chlorite has replaced mafic phenocrysts and hydrothermal biotite as a selective pervasive alteration. The degree of selective replacement by chlorite is based on visual estimate in polished thin sections. In the fine-grained basaltic wall rock, chlorite occurs as a pervasive replacement of groundmass. Epidote and calcite occur with chlorite in the pyritic halo on the eastern margin. Chlorite is absent from the intensely weathered portions of the deposit and from the deepest intersections of the intermineralization diorite porphyry.

smectite alteration through the Boyongan complex. The smectite index exceeds 75% in the western high-grade zone, where it occurs in association with interstratified illite/smectite. High smectite indices also characterize the northern and southern margins of the diatreme breccia complex. In one such zone,

veinlets of stellerite (a Ca-rich zeolite) were identified in an area of intense smectite alteration within the intermineralization diorite porphyry stock (TSD27, 660 m).

Chlorite alteration intensity: In the intrusive complex, the proportion of all mafic minerals selectively replaced by

chlorite (based on thin-section description) provides a measure of the intensity of this style of alteration. At Boyongan, selectively pervasive chloritization exceeds 25% in and around the upper portions of the early-mineralization diorite stocks and diminishes laterally and at depth (Fig. 23D; App. 1, Figs. A26D, A27D). At Bayugo, selectively pervasive chloritization exceeds 25% in the bird's-eye porphyry, medium-grained diorite porphyry, DIO3, and DIO4 intrusions and is weakest in the DIO2 stock (App. 1, Fig. A28D).

The presence of illite and smectite in association with chlorite and the general absence of epidote and calcite distinguish illite-smectite-chlorite alteration from the propylitic assemblage commonly described for porphyry systems (e.g., Sillitoe, 2000). Outside the skarn zones, the assemblage of chlorite + calcite + epidote ± illite has only been encountered within and outboard of the pyritic fringe on the eastern side of Boyongan, where chlorite occurs as a pervasive alteration of the Bacuag Formation basalts (Fig. 23D).

Illite-pyrite alteration assemblage

The illite-pyrite assemblage overprinted the K silicate alteration assemblage, occurring as a pervasive replacement of all aluminosilicates by mixtures of fine-grained illite + pyrite ± quartz. The assemblage varies from thin sulfide veinlets with discrete illite alteration halos (Fig. 24A, B) to zones of intense, texturally destructive illite-altered rock with up to 30% disseminated pyrite. The latter typically occur in narrow (0.2–10 m), structurally controlled or brecciated zones and commonly contain clasts of K silicate-stage vein quartz in a fragmental matrix replaced by illite and pyrite (Fig. 24C–E). Accessory minerals in the illite-pyrite assemblage include chalcocite, tetrahedrite-tennantite, sphalerite, galena, and locally siderite (Fig. 24F–J). These phases contribute to the anomalous levels of Cu, arsenic, antimony, silver, lead, and zinc common in illite-pyrite zones. Assays also indicate anomalous tellurium and Au in some illite-pyrite intervals, but the mineralogical residence of these elements remains unclear.

Illite-pyrite alteration occurred along narrow structures throughout Boyongan and Bayugo but has affected relatively discrete volumes of rock (Fig. 23B; App. 1, Figs. A26B, A27B, A28B, D). The volumetrically most significant illite-pyrite domain is present in the shallow portion of the eastern high-grade zone at Boyongan, where a diffuse envelope of illite occurs around a narrow (10 cm) sulfide-rich vein (App. 1, Fig. A27B). In intensely weathered zones, illite-dominated intervals lacking kaolinite, chlorite, and smectite are inferred to represent vestigial illite-pyrite alteration.

Extensive illite (and minor kaolinite)-pyrite alteration affected clasts in debris flows interbedded with fluviolacustrine sediments in the Tugunan Formation overlying Boyongan and Bayugo (Fig. 6A; App. 1, Figs. A4–A6). These debris flows contain intensely illite-pyrite-altered clasts supported in a matrix of pyritic white clay. Accumulations of these debris flows are thickest on the south and west margins of Boyongan (App. 1, Fig. A3D), suggesting local derivation.

Quartz-alunite-clay alteration assemblage

Regional sampling in the Bagacay and Magpayang areas adjacent to Boyongan and Bayugo (Fig. 4) identified numerous float blocks with alteration assemblages characteristic of

low-pH environments, although no such alteration has been identified in situ. Petrographic, XRD, and SWIR studies have identified assemblages including pyrophyllite ± illite ± dickite ± alunite that replaced the aluminosilicate component of diorite porphyry cobbles discovered in these areas (I. Bogie, unpub. report, 2000; P. White, unpub. report, 2002; Braxton, 2007). Many of these altered cobbles display stockworks of sucrosic quartz veins containing finely disseminated bornite and chalcocite, which are similar in texture and morphology to K silicate vein stages 2 and 3 described from Boyongan and Bayugo (Fig. 25A). At least one cobble has quartz-vein-stockworked breccia clasts in a fragmental matrix, in which the aluminosilicates in both the clasts and matrix were pervasively replaced by alunite (Fig. 25B, E). This relationship demonstrates that quartz-alunite-clay alteration postdated the K silicate-style quartz veining in these samples.

Rocks displaying a skeletal or vuggy quartz texture (Fig. 25A, B; e.g., White and Hedenquist, 1990) were identified in float overlying the Bayugo deposit and as subcrop at Paragayo Hill east of Boyongan (Figs. 5A, 2A). Fine-grained quartz has replaced the groundmass of these rocks, while leaching of phenocryst and/or clasts has produced vuggy cavities reflecting vestigial textures of the protolith (Fig. 25C). Masses of subhedral-euhedral quartz have filled many of these vugs (Fig. 25D, F), locally displaying realgar overgrowths (Fig. 25H). Fine disseminated rutile crystals occur throughout the quartz-flooded groundmass and have locally replaced phenocrysts (Fig. 25G–I).

Despite occurring as float, the textural preservation of vuggy quartz alteration can enable recognition of the original rock type in cases where the primary textures are distinctive. Figure 25C depicts a coarse-grained feldspar-phyric rock that is texturally similar to the bird's-eye diorite porphyry encountered during drilling (cf. App. 1, Fig. A7A).

Supergene Profiles

Paragenesis and spatial zonation of supergene copper phases

Braxton et al. (2009), drawing on Ignacio (2005) and Braxton (2007), documented the nature of the supergene profiles affecting the Boyongan and Bayugo deposits following exhumation. A synopsis of that work is presented here.

Supergene Cu phases at Boyongan and Bayugo fall into three distinct groups: sulfide phases, native Cu, and oxide phases. Supergene Cu sulfides developed at the base of the supergene zone, where they consist primarily of sooty chalcocite and subordinate covellite and digenite. These sulfides replaced hypogene pyrite, chalcocite, and bornite, commonly as a corrosive patina on the surface or along fractures within hypogene sulfides (Fig. 15C, D).

Native Cu occurs near the base of the supergene Cu zone and is widespread at Boyongan but only locally present at Bayugo. Where native Cu occurs with chalcocite, it is as a replacement of the supergene Cu sulfide.

The most important Cu oxide phases at Boyongan and Bayugo are cuprite (commonly as chalcotrichite), malachite, and azurite. Subordinate Cu oxide phases at Boyongan comprise chrysocolla, pseudomalachite ($\text{Cu}_5[(\text{OH})_2(\text{PO}_4)]_2$), and pseudoneotocite ($[\text{Mn,Cu}]_2[\text{CO}_3]_2$). All oxide Cu phases occur as near in situ oxidation products in hydrothermal quartz ±

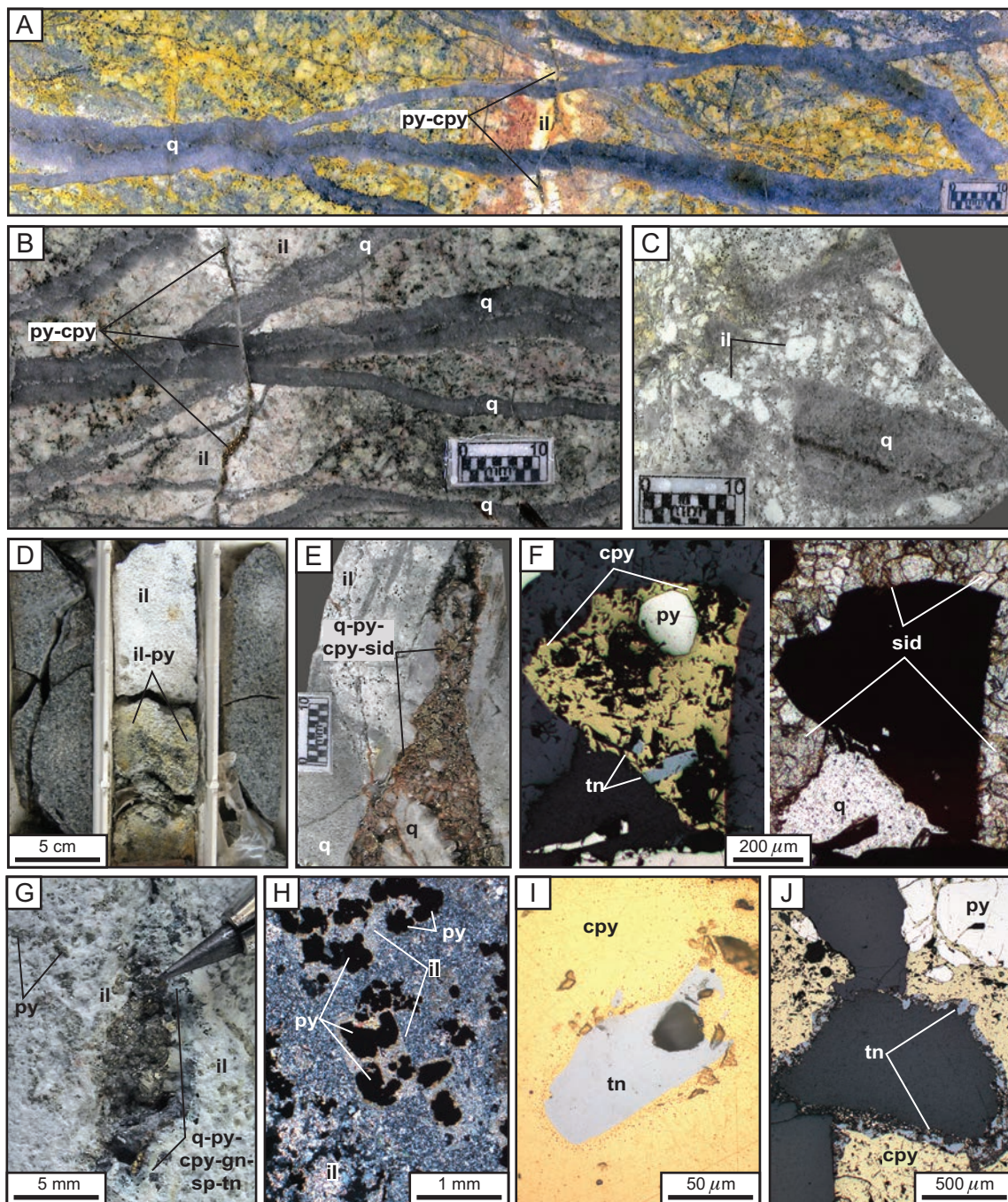


Fig. 24. Character and mineralogy of illite-pyrite alteration. (A) Intensely quartz-stockworked interval of DIO3 porphyry with associated K-feldspar alteration (yellow staining). A narrow pyrite-chalcopyrite veinlet with an intense white illite alteration halo has cut the older quartz vein stages. Sample: 815082. Diamond drill hole TSD75, 714.52 m. (B) Detail of unstained face of (A) showing the sulfide veinlet cutting and displacing the older K silicate-stage quartz veins. The intense illite alteration halo has not affected the quartz veins. (C) Narrow brecciated zone in DIO2 with fragments of K silicate stage vein quartz in intensely illite-pyrite-altered fragmental matrix. Sample: 815064. Diamond drill hole TSD73, 573.25 m. (D) Typical expression of narrow illite-pyrite-altered structure cutting the medium-grained diorite porphyry. Diamond drill hole TSD51, 600 m. (E) Quartz-pyrite-chalcopyrite-siderite structure with intense illite-pyrite alteration halo cutting DIO2. Sample: 815072. Diamond drill hole TSD73, 731.95 m. (F) Photomicrographs of the vein in (E) showing sulfide clast containing pyrite, chalcopyrite, and tennantite cemented by siderite. (G) Quartz-pyrite-chalcopyrite-galena-sphalerite-tennantite vein with an intense halo of illite and disseminated pyrite cutting the medium-grained diorite porphyry. Sample: 819537. Diamond drill hole TSD69, 405.72 m. (H) Cross-polarized photomicrograph of (G) showing intense illite and pyrite replacement of plagioclase phenocrysts. (I) Reflected-light photomicrograph of (G) showing tennantite bleb in chalcopyrite. (J) Reflected-light photomicrograph showing pyrite brecciated and cemented by chalcopyrite with tennantite lining vugs in chalcopyrite. Sample: 814794. Diamond drill hole TSD15, 427.48 m. Abbreviations: cpy = chalcopyrite, gn = galena, il = illite, py = pyrite, q = quartz, sid = siderite, sp = sphalerite, tn = tennantite.

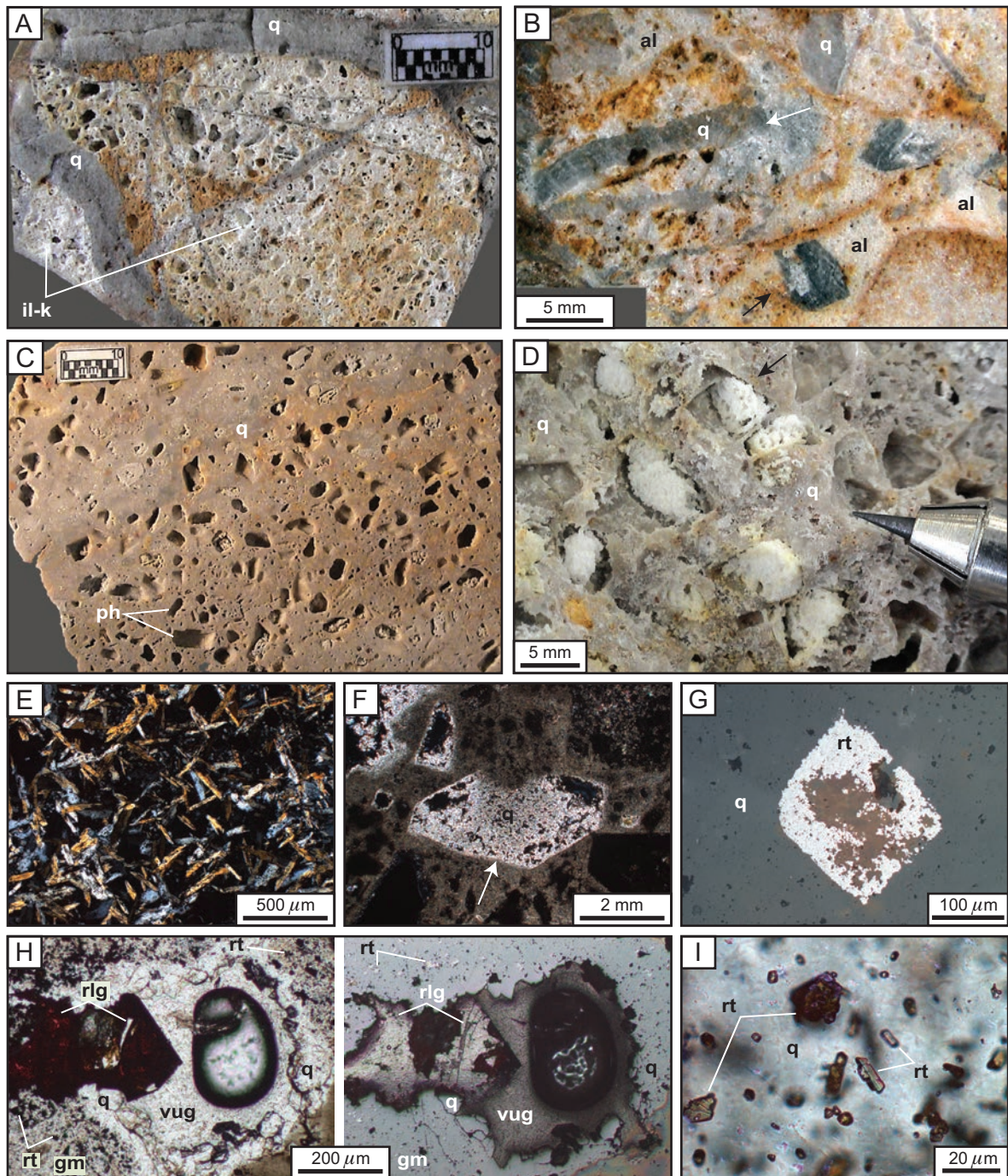


Fig. 25. Character and mineralogy of quartz-alunite-clay alteration. (A) Medium-grained porphyritic rock cut by irregular quartz-vein stockwork containing fine disseminated bornite and chalcopyrite. An intense, pervasive assemblage of illite and kandite has replaced all primary phenocrysts. Void spaces at former phenocryst sites formed by flushing of clay during sample sawing. Sample: 815116. Float from Bagacay boulder field. (B) Breccia with quartz-vein-stockworked clasts (arrows) containing fine disseminated chalcopyrite. Alunite has pervasively replaced lithic clasts and fragmental matrix. Sample: 815178. Float from Pista creek, Bagacay boulder field. (C) Bird's-eye diorite porphyry displaying vuggy quartz texture. Phenocrysts have been leached and locally filled by skeletal quartz (D, F), while the groundmass has been replaced by fine quartz. Sample: 819906. Float from upper Bayugo creek. (D) Detail of skeletal quartz in (C) filling former phenocryst sites. (E) Cross-polarized photomicrograph of (B) showing alunite replacement of fragmental breccia matrix. (F) Cross-polarized photomicrograph of (C) showing skeletal quartz in (C) filling former phenocryst site. (G) Reflected-light photomicrograph of sample in (C) showing rutile replacement of phenocryst. (H) Plane-polarized and reflected-light photomicrograph of vuggy quartz rock similar to (C) showing vug lined with euhedral quartz overgrown by realgar. The groundmass is a mixture of fine quartz with disseminated rutile and pyrite. Sample: 819905. Grab sample from exploration trench at Paragayo Hill. (I) Cross-polarized photomicrograph of sample in (H) showing replacement of groundmass by rutilated quartz. Abbreviations: al = alunite, gm = groundmass, il = illite, k = kandite, ph = phenocryst site, q = quartz, rl = realgar, rt = rutile.

sulfide veins and in open fractures of posthydrothermal origin. In addition, malachite, azurite, and chrysocolla commonly occur as finely disseminated grains within supergene kaolinite.

Contrasting supergene profiles

Significant differences in the character and extent of supergene profile development exist between Boyongan and Bayugo (Figs. 11–13; App. 1, Figs. A13–A17, A29, A30). Oxide Cu phases at Boyongan are present throughout a vertical interval locally exceeding 600 m below the paleosurface, whereas at Bayugo, the oxide zones are generally less than 70 m thick. Boyongan lacks broad enrichment domains or blankets dominated by supergene Cu sulfides, whereas at Bayugo, supergene sulfides are more widely distributed, with a tabular zone exceeding 100 m in thickness.

Discussion

The spatial and temporal relationships between intrusive activity, veining, and alteration presented in this study demonstrate the intimacy of magmatism and Cu-Au mineralization at Boyongan and Bayugo. Figure 26 summarizes the lateral and temporal distribution of veining and alteration events that characterized the evolution of fluid conditions within the intrusive complex.

Magmatic-hydrothermal cycles and superior grade development

Although the early diorite stocks (bird's-eye porphyry, medium-grained diorite porphyry, and fine-grained diorite porphyry) may have formed in association with some early formed calc-silicate alteration, these intrusions appear to have acted primarily as passive hosts to mineralizing fluids introduced during the emplacement of the synmineralization intrusions (early-mineralization diorite series, intermineralization diorite porphyry, and late-mineralization diorite porphyry at Boyongan, DIO series at Bayugo).

Truncated veins, vein-quartz xenoliths, and abrupt changes in vein abundance and grade at intrusive contacts all support a model for multiple discrete magmatic events during the evolution of the hydrothermal system (Fig. 19). A similar progression of K silicate-related alteration and veining followed the emplacement of each synmineralization intrusion. At Bayugo the fertile hydrothermal cycle was associated with the DIO2 stocks, while at Boyongan most of the Cu and Au was introduced during the magmatic-hydrothermal cycles associated with the ECD1 and ECD2 stocks. Superposition of these two magmatic-hydrothermal cycles in the shallow eastern high-grade zone at Boyongan is considered to account for the superior hypogene grades (locally exceeding 2% Cu and 3 g/t Au) in this area (Figs. 7, 11; App. 1, Figs. A13, A14). Vein quartz abundance and Cu-Au introduction attenuated progressively with successive magmatic-hydrothermal cycles associated with intermineralization (intermineralization diorite porphyry and DIO3) and late-mineralization (late-mineralization diorite porphyry and DIO4) intrusions.

Post-K silicate alteration

The timing of magmatism and K silicate alteration relative to the peripheral illite-chlorite-epidote-calcite assemblage

within and beyond the pyrite halo remains unclear. However, within the intrusive complex widespread chloritization of mafic minerals and weak illite-smectite alteration clearly followed the K silicate alteration stages as the hydrothermal system cooled.

The illite-smectite-chlorite assemblage described herein is similar in mineralogy and relative timing to the sericite-clay-chlorite assemblage of Sillitoe and Gappe (1984). These authors described an assemblage of sericite (fine-grained white mica), clay (kaolinite and smectite), and chlorite that overprinted earlier K silicate alteration in more than half of the 48 Philippine porphyry systems that they studied. Veinlets of pyrite ± chalcopyrite are common in sericite-clay-chlorite-altered rocks, but in many deposits it is difficult to assess the importance of the sericite-clay-chlorite alteration in modifying the earlier Cu-Au mineralization introduced during K silicate alteration (Sillitoe, 2000). At Boyongan, there is no evidence to suggest that fluids responsible for illite-smectite-chlorite alteration had any measurable impact on the concentration or distribution of Cu or Au.

The structural control of illite-pyrite alteration at Boyongan and Bayugo is typical for sericitic or phyllic alteration described from many Philippine porphyry deposits. In contrast to many of the Cu porphyries of the American southwest and the Andes, broad (>250 m) annular zones of intense sericitic alteration around a K silicate core are present in only a small proportion of the Philippine deposits (Sillitoe and Gappe, 1984). Instead, sericitic alteration occurs more commonly in narrow, structurally controlled zones as alteration halos to late pyrite-quartz ± chalcopyrite ± molybdenite veins ("D" veins of Gustafson and Hunt, 1975) or to quartz-calcite-pyrite-sphalerite-galena veins. Sericitic alteration zones are typically pyrite-rich. Sillitoe and Gappe (1984) documented sulfide contents of >5% for the sericitic alteration zones in their Philippines study, with pyrite/chalcopyrite ratios varying from 3:1 to 10:1. These characteristics are similar in mineralogy and timing but greater in intensity than the illite-pyrite alteration assemblage developed at Boyongan.

Some cobbles derived from debris flows at Bagacay and Magpayang have quartz-alunite-clay assemblages that have overprinted K silicate-style veining and alteration. This raises intriguing questions as to their potential relationships to Boyongan and/or Bayugo. The overprinting alteration relationships document the influx of low-pH hydrothermal fluids into a porphyry system. Despite the inherent uncertainty of provenance, the proximity of these boulder fields to the Boyongan and Bayugo deposits and the similarity of veining and related K silicate alteration styles to those observed in situ suggest that these boulders were derived from Boyongan and/or Bayugo as they were exposed by exhumation and erosion. Vuggy quartz alteration in float resembling recognizable intrusions such as the bird's-eye porphyry (Fig. 25C) also supports the case for a quartz-alunite-clay overprint in the Boyongan/Bayugo complex, even though no such assemblage has been recognized in situ.

Domains of quartz-alunite-clay alteration are spatially associated with many Philippine porphyry deposits, including Far Southeast, Guinaoang, Batao Tabio, Pisumpan, San Antonio (Marcopper), Tapian, Balak-5, Hinobaan, Labangan, Salatan, Batong Buhay, and Tampakan (Sillitoe and Gappe, 1984;

Arribas et al., 1995; Hedenquist et al., 1998; Rohrlach, 2002). In most of these cases, the quartz-alunite-clay alteration zone occurs above and is laterally displaced from the porphyry systems (e.g., Far Southeast-Lepanto: Arribas et al., 1995). In other cases (e.g., Tampakan: Rohrlach, 2002) relict porphyry-style quartz veins occur in pervasively quartz-alunite-clay-altered rock, providing evidence for overprinting of earlier K silicate assemblages. Where evidence of both K silicate and quartz-alunite-clay alteration is preserved in the same rock, the quartz-alunite-clay assemblage formed later (Sillitoe, 2000), consistent with observations in the float samples from Bagacay and Magpayang.

Timing and duration of the magmatic-hydrothermal systems

Braxton et al. (2012) presented the results of a high-resolution geochronological study on magmatism and hydrothermal activity at Boyongan and Bayugo. Through absolute dating of igneous zircon from the earliest premineralization stocks and late-mineralization dikes these authors bracketed the timing and duration of magmatism and K silicate-stage alteration at Boyongan and Bayugo to between 2.3 ± 0.1 and 2.1 ± 0.2 Ma (at 2σ uncertainty). Coupled with mean Re-Os age determinations for K silicate-stage quartz-molybdenite veining (2.120 ± 0.007 and 2.115 ± 0.008 Ma), mean K-Ar dates of illite (2.12 ± 0.06 and 2.09 ± 0.06 Ma), and of alunite (2.1 ± 0.1 Ma) alteration, Braxton et al. (2012) presented a coherent, internally consistent history of multiphase magmatism and related hydrothermal alteration at Boyongan and Bayugo, probably occurring over approximately 200,000 years, although analytic uncertainties on age determinations allow a maximum lifespan of 500,000 years. These results are consistent with numerical models describing the convective cooling rates of porphyry stocks of comparable size and emplacement depth (e.g., Norton, 1982; Cathles et al., 1997), which demonstrate cooling to $<200^\circ\text{C}$ over intervals of less than 100,000 years. Other geochronological studies focusing on the duration of porphyry formation have presented findings consistent with those in the current study (e.g., Chiaradia et al., 2014; Mercer et al., 2015, and references therein).

Many Philippine districts display a spatial relationship between porphyry systems and illite- and/or alunite-altered lithocaps (Sillitoe and Gappe, 1984; Arribas et al., 1995; Chang et al., 2011). Detailed radioisotopic dating from these systems reveals that some alteration systems were contemporaneous or nearly so, suggesting a common origin. In a seminal study in the Pleistocene Mankayan district of northern Luzon, Arribas et al. (1995) demonstrated that age determinations for alunite associated with the Lepanto high-sulfidation deposit (1.6–1.2 Ma) were indistinguishable from those for hydrothermal biotite (1.5–1.3 Ma) and illite (1.4–1.2 Ma) associated with the subjacent Far Southeast porphyry Cu-Au deposit. On the basis of these close spatial and temporal relationships, these authors interpreted a genetic link between the two alteration styles, suggesting that porphyry and quartz-alunite-clay alteration styles represented distinct products of a single hydrothermal system. The age determinations for illite and alunite in the current study show that this alteration immediately followed the final intrusive event. These findings are consistent with porphyry emplacement, illite-pyrite alteration, and quartz-alunite-clay

formation from a single evolving magmatic-hydrothermal system at Boyongan and Bayugo.

Exhumation, deep oxidation, and preservation by burial

Braxton et al. (2012) presented thermochronological data from apatite (U-Th)/He dating that constrain the timing and rate of exhumation of Boyongan and Bayugo. That study presented evidence for exhumation rates exceeding 2.5 km/m.y., with weathering of the currently preserved paleosurface beginning by approximately 1.6 Ma. Physiographic reconstructions based on the topography of the paleosurface and on stable isotope paleoaltimetric constraints (Braxton et al., 2009) suggest that the weathering profiles of the two deposits formed in an environment of high topographic relief immediately east of a prominent (>550 m) escarpment at elevations between 750 and 1,050 m a.s.l.

Pronounced differences in the bedrock permeability and hypogene pyrite/Cu sulfide ratios are implicated in the contrasting supergene profiles of the adjacent Boyongan and Bayugo deposits. In the immediate vicinity of Boyongan, a high permeability contrast between the diatreme breccia complex and the surrounding wall rocks, coupled with the proximity of the breccia complex to the escarpment to the west, is inferred to have led to a depressed groundwater table and a vertically extensive unsaturated zone. Positioned farther from the escarpment and outside the diatreme breccia complex, Bayugo's vadose zone was commensurately restricted.

Low hypogene pyrite/Cu sulfide ratios (0.6) at Boyongan contrast with more elevated ratios (2.3) at Bayugo (Braxton et al., 2009). These characteristics suggest that limited acid-generating capacity at Boyongan, essential for supergene Cu remobilization (e.g., Emmons, 1917; Locke, 1926; Blanchard, 1968; Sillitoe, 2005), promoted largely in situ oxidation of Cu-bearing sulfides and modest supergene remobilization of Cu. Thus the superior grades encountered in Boyongan's eastern and western high-grade zones are attributed almost exclusively to hypogene processes. Higher hypogene pyrite/chalcopyrite ratios at Bayugo likely led to greater acid production during weathering and more complete leaching of Cu above the base of oxidation. These conditions enabled local supergene Cu enrichment to develop at Bayugo (Braxton and Mathur, 2011) and also promoted significant (600 m) lateral dispersion of Cu to form the exotic Cu deposit between Bayugo and the diatreme breccia complex (App. 1, Figs. A29, A30).

As early as the late Pleistocene, transtensional movement along strands of the Philippine fault zone (Fig. 1) contributed to local extension in northeast Mindanao. Braxton et al. (2012) presented geochronological evidence for subsidence rates exceeding 0.34 km/m.y. within the Mainit graben. These processes culminated in final burial of the Boyongan and Bayugo deposits beneath fluviolacustrine and volcanic facies of the Tugunan Formation by 1.6 ka (App. 1, Fig. A31).

Conclusions

Exploration following the emerging genetic link between epithermal Au and porphyry Cu deposits led to the discovery of two porphyry Cu-Au mineral deposits (Boyongan and Bayugo) concealed beneath postmineralization cover in the Surigao Au district.

Emplacement of a polyphase, silt-sand matrix breccia complex preceded Cu and Au introduction at Boyongan. The emplacement of this diatreme may have provided conduits for subsequent ascent of magmatic-hydrothermal fluids. In both deposits, auriferous bornite and chalcopyrite were concentrated in quartz-vein stockworks mantling the upper portions of small (200–300 m diam), high aspect-ratio, pencil-shaped diorite porphyry stocks. These mineralized stocks are part of a multiphase diorite intrusive complex that includes a pre-mineralization early-diorite complex, the aforementioned diatreme, and a series of early-, inter-, and late-mineralization porphyry intrusions.

A characteristic progression of K silicate alteration and veining followed the emplacement of each synmineralization intrusion. Copper-gold introduction occurred principally during the K silicate veining and alteration cycles of the early-mineralization and the DIO2 stocks (at Bayugo) and the ECD1 and ECD2 stocks (at Boyongan). At Boyongan, Cu-Au introduction accompanying overprinting K silicate-stage events contributed to (spatially restricted) superior grade development, locally exceeding 2% Cu and 3 g/t Au.

The history at Boyongan and Bayugo of porphyry emplacement (from 2.3–2.1 Ma), exhumation (by 1.6 Ma), supergene oxidation (approaching 600-m depth at Boyongan), and final burial (by 1.6 ka) attests to the geologically short time scales and transient geodynamic environments that can govern porphyry formation and preservation. With the industry turning ever more toward exploration under cover, the nuanced understanding of the anatomy, processes, pathways, and environments of porphyry formation and preservation derived from such studies will contribute to the concepts guiding future discovery.

Acknowledgments

The geologic framework presented was developed as part of the first author's doctoral research at the Centre of Excellence in Ore Deposits (University of Tasmania). This framework emerged in collaboration with the Anglo American (Philippines) exploration team and built upon the early geologic model developed for Boyongan by R. Sillitoe (unpub. report, 2001). Professor Erich Petersen's collaboration in clay mineral separation and XRD analysis was essential in enabling the understanding of alteration in the district. The authors also wish to thank Anglo American for the generous financial support of this project and in particular acknowledge that company's Philippine exploration staff for the indispensable logistical support provided. Likewise, the authors are grateful to Philex for enabling the study's publication. Constructive reviews by Richard Sillitoe, Donald Singer, and the editorial staff at *Economic Geology* enhanced significantly the clarity and content of the manuscript.

REFERENCES

American Geological Institute, 1996, Dictionary of mining, mineral, and related terms, 2nd ed.: Alexandria, Virginia, American Geological Institute in cooperation with the Society for Mining, Metallurgy, and Exploration, Inc., 646 p.

Anglo American, 2004, Geological and geochemical results of the drilling program at Boyongan and Bayugo: Anglo American Exploration (Philippines) Inc., unpublished database.

Arancibia, O.N., and Clark, A.H., 1996, Early magnetite-amphibole-plagioclase alteration-mineralization in the Island Copper porphyry

copper-gold-molybdenum deposit, British Columbia: *Economic Geology*, v. 91, p. 402–438.

Arribas, A., Hedenquist, J.W., Itaya, T., Okada, T., Concepcion, R.A., and Garcia, J.S., 1995, Contemporaneous formation of adjacent porphyry and epithermal Cu-Au deposits over 300 Ka in Northern Luzon, Philippines: *Geology*, v. 23, p. 337–340.

Atkinson, W.W., and Ware, H., 2002, Comb quartz layers in the porphyry copper deposit at Yerington, Nevada: Geological Society of America (GSA) annual meeting: Geological Society of America, Corvallis, Oregon, May 13–15, 2002, Abstracts with Programs, 15 p.

Aurelio, M.A., 2000a, Shear partitioning in the Philippines: Constraints from Philippine fault and global positioning system data: *Island Arc*, v. 9, p. 584–597.

—2000b, Tectonics of the Philippines revisited: *Journal of the Geological Society of the Philippines*, v. 55, p. 119–183.

Bellon, H., and Yumul, G.P., Jr., 2000, Mio-Pliocene magmatism in the Baguio mining district (Luzon, Philippines); age clues to its geodynamic setting: *Comptes Rendus de l'Academie des Sciences, Serie II., Sciences de la Terre et des Planetes*, v. 331, p. 295–302.

Bignall, G., Tsuchiya, N., Browne, P.R.L., Garg, S.K., and Hiriart, G., 2001, Use of illite crystallinity as a temperature indicator in the Orakei Korako geothermal system, New Zealand: *Transactions—Geothermal Resources Council*, v. 25, p. 339–344.

Blanchard, R., 1968, Interpretation of leached outcrops: Nevada Bureau of Mines, Bulletin 66, 196 p.

Bragg, W.L., 1912, The specular reflection of X-rays: *Nature*, v. 90, p. 410.

Braxton, D.P., 2007, Boyongan and Bayugo porphyry Cu-Au deposits, NE Mindanao, Philippines: Geology, geochemistry, and tectonic evolution: Ph.D. thesis, Hobart, Australia, University of Tasmania, 277 p.

Braxton, D.P., and Mathur, R., 2011, Exploration applications of copper isotopes in the supergene environment: A case study of the Bayugo porphyry copper-gold deposit, southern Philippines: *Economic Geology*, v. 106, p. 1447–1463.

Braxton, D.P., and Waters, P.J., 2012, Discovery of the Boyongan and Bayugo porphyry copper-gold deposits, Mindanao, Philippines, in Austen, S., Sillitoe, D., Naicker, T., and Brown, G., eds., *Anglo American Exploration: Decade of Discovery*: London, Anglo American, p. 96–102.

Braxton, D.P., Cooke, D.R., Ignacio, A.M., Rye, R.O., and Waters, P.J., 2009, Ultra-deep oxidation and exotic copper formation at the late Pliocene Boyongan and Bayugo porphyry copper-gold deposits, Surigao, Philippines; geology, mineralogy, paleoaltimetry, and their implications for geologic, physiographic, and tectonic controls: *Economic Geology*, v. 104, p. 333–349.

Braxton, D.P., Cooke, D.R., Dunlap, J., Norman, M., Reiners, P., Stein, H., and Waters, P.J., 2012, From crucible to graben in 2.3 Ma: A high-resolution geochronological study of porphyry life cycles, Boyongan/Bayugo copper-gold deposits, Philippines: *Geology*, v. 40, p. 471–474.

Brindley, G.W., 1952, Structural mineralogy of clays: *Clays and Clay Minerals*, v. 1, p. 33–43.

Bryner, L., 1970, Geology of the Sto. Nino copper prospect area: *Journal of the Geological Society of the Philippines*, v. 24, p. 33–40.

Bureau of Mines and Geosciences (BMG), 1983, Geology of the Taganaan and Ana-aon quadrangles: Philippine Bureau of Mines and Geosciences, two maps, scale 1:50,000.

Camacho, A., 2001, Ar-Ar age determinations of hornblende samples from Mindanao: Report prepared for Anglo American Philippines Inc., December 19, 2001, Research School of Earth Sciences, Australian National University, Canberra, Australia, 26 p.

Cannell, J., Cooke, D.R., Walshe, J.L., and Stein, H., 2005, Geology, mineralization, alteration, and structural evolution of the El Teniente porphyry Cu-Mo deposit: *Economic Geology*, v. 100, p. 979–1003.

Carman, G., 1994, Genesis of the Landolam gold deposit, Lihir Island, Papua New Guinea: Ph.D. thesis, Melbourne, Australia, Monash University, 381 p.

Cas, R.A.F., and Wright, J.V., 1987, Volcanic successions, modern and ancient; a geological approach to processes, products, and successions: London, Allen and Unwin, 528 p.

Cathles, L.M., Erendi, A.H.J., and Barrie, T., 1997, How long can a hydrothermal system be sustained by a single intrusive event?: *Economic Geology*, v. 92, p. 766–771.

Chang, Z., Hedenquist, J.W., White, N.C., Cooke, D.R., Roach, M., Deyell, C.L., Garcia, J., Jr., Gemmill, J.B., McKnight, S., and Cuisson, A.L., 2011, Exploration tools for linked porphyry and epithermal deposits: Example from the Mankayan intrusion-centered Cu-Au district, Luzon, Philippines: *Economic Geology*, v. 106, p. 1365–1398.

- Chiaradia, M., Schaltegger, U., and Spikings, R., 2014, Time scales of mineral systems—advances in understanding over the past decade: Society of Economic Geologists, Special Publication 18, p. 37–58.
- Clark, A.H., and Arancibia, O.N., 1995, Occurrence, paragenesis, and implications of magnetite-rich alteration-mineralization in calc-alkaline porphyry copper deposits: Giant Ore Deposits 2, Kingston, Ontario, Canada, April 25–27, 1995, Proceedings, p. 511–581.
- Conde, F.C., 2014, Preliminary report on exploration results on Manila Mining Corporation's deep-seated porphyry Cu-Au prospect, Placer, Surigao del Norte, Mindanao, Philippines: Competent person exploration results and mineral resource estimation: Lepanto Consolidated Mining Company, April 25, 2014, Surigao City, Philippines, 36 p., www.manilamining.com/docs/2016/MMC%20Prelim%20Report%20on%20Deep-Seated%20Porphyry%204-25-2014.pdf.
- Cooke, D.R., Hollings, P., and Walshe, J.L., 2005, Giant porphyry deposits: Characteristics, distribution, and tectonic controls: *Economic Geology*, v. 100, p. 801–818.
- Cooke, D.R., Hollings, P., and Chang, Z., 2011, Philippine porphyry and epithermal deposits: An introduction: *Economic Geology*, v. 106, p. 1253–1256.
- Davies, A.G.S., 2002, Geology and genesis of the Kelian gold deposit, east Kalimantan, Indonesia: Ph.D. thesis, Hobart, Australia, University of Tasmania, 404 p.
- Definiens, 2005, eCognition 3.0, Object-oriented image classification software: www.definiens-imaging.com/ecognition/pro/index.htm.
- Eberl, D.D., Srodon, J., Lee, M., Nadeau, P.H., and Northrop, H.R., 1987, Sericite from the Silverton caldera, Colorado: correlation among structure, composition, origin, and particle thickness: *American Mineralogist*, v. 72, p. 914–934.
- Emmons, W.H., 1917, The enrichment of ore deposits, U.S. Geological Survey Bulletin 625, 530 p.
- Fernandez, J.C., 1981, Geology and mineral resources of the Philippines: Manila, Philippines, Bureau of Mines and Geosciences, Ministry of Natural Resources, v. 1, 406 p.
- Gervasio, F.C., 1966, The age and nature of orogenesis of the Philippines: *Philippine Geologist*, v. 20, p. 121–140.
- Giese, R.F., Jr., 1988, Kaolin minerals: Structures and stabilities: *Reviews in Mineralogy*, v. 19, p. 29–66.
- Greene-Kelly, R., 1952, Irreversible dehydration in montmorillonite: *Clay Minerals Bulletin*, v. 1, p. 221–227.
- 1953, Irreversible dehydration in montmorillonite; part II: *Clay Minerals Bulletin*, v. 2, p. 52–56.
- Grimm, R.E., 1952, Objectives on the first national conference on clays and clay technology and definitions of terms used in the industry: *Clays and Clay Minerals*, v. 1, p. 13–15.
- Gustafson, L.B., and Hunt, J.P., 1975, The porphyry copper deposit at El Salvador, Chile: *Economic Geology*, v. 70, p. 857–912.
- Güven, N., 1988, Smectites: *Reviews in Mineralogy*, v. 19, p. 497–559.
- Harris, A.C., Cooke, D.R., White, N.C., Danyushevsky, L.V., and Gilbert, S.E., 2005, Volatile loss from high-level magmas at Bajo de la Alumbrera porphyry Cu-Au deposit, NW Argentina: Geological Society of America (GSA) Annual Meeting, Geological Society of America, Salt Lake City, Utah, October 16–19, 2005, Abstracts with Programs, 163 p.
- Hawkins, J.W., More, G.F., Villamor, R., Evans, C., and Wright, E., 1985, Geology of the composite terranes of east and central Mindanao, in Howell, D., ed., Tectonostratigraphic terranes of the circum-Pacific: American Association of Petroleum Geologists (AAPG) Earth Science Series 1, Houston, Texas, American Association of Petroleum Geologists, p. 437–466.
- Hedenquist, J.W., Arribas, A., and Reynolds, T.J., 1998, Evolution of an intrusion-centered hydrothermal system: Far Southeast-Lepanto porphyry and epithermal Cu-Au deposits, Philippines: *Economic Geology*, v. 93, p. 373–404.
- Hollings, P., Wolfe, R., Cooke, D.R., and Waters, P.J., Cousens, B., 2011, Igneous geochemistry of mineralized rocks of the Baguio district: Implications for tectonic evolution and the genesis of porphyry-style mineralization: *Economic Geology*, v. 106, p. 1317–1333.
- Ignacio, A.M., 2005, Supergene mineralisation of the Boyongan porphyry copper-gold deposit, Surigao del Norte, Philippines: Master of Economic Geology thesis, Hobart, Australia, University of Tasmania, 163 p.
- Imai, A., 2001, Generation and evolution of ore fluids for porphyry Cu-Au mineralization of the Santo Tomas 2 (Philex) deposit, Philippines: *Resource Geology*, v. 51, p. 71–96.
- Kerntke, M., Tarkian, M., and Baumann, A., 1991, Geochemie und Geochronologie der Magmatite von Lutopan und Talamban, Cebu/Philippinen. Geochemistry and geochronology of magmatite from Lutopan and Talamban, Cebu, Philippines: *Mitteilungen aus dem Geologisch-Palaeontologischen Institut der Universität Hamburg*, v. 71, p. 93–120.
- Kirkham, R.V., and Sinclair, W.D., 1988, Comb quartz layers in felsic intrusions and their relationship to porphyry deposits: Canadian Institute of Mining and Metallurgy, Special volume 39, p. 50–71.
- Knittel, U., and Burton, C.K., 1985, Polillo Island (Philippines); molybdenum mineralization in an island arc: *Economic Geology*, v. 80, p. 2013–2018.
- Locke, A., 1926, Leached outcrops as a guide to copper ore: Baltimore, Williams and Wilkins, 166 p.
- Maglambayan, V.B., Montes, S., Hipol, K., Mamitag, M., Pineda, R.P., Rodolfo, R., Oliveros, N., and Sy, A., 2005, Carlin-type gold prospects in Surigao del Norte, Mindanao Island, Philippines: Their geology and mineralization potential: *Resource Geology*, v. 55, p. 145–154.
- Maliha, T.D., 1982, Geology of the Dizon porphyry copper-gold orebody: Seminar on developing new open pit mines in the Philippines: First University of the Philippines Geology Alumni Association lectures, Manila, Philippines, October 1982, p. 27–49.
- McPhie, J., Doyle, M., and Allen, R., 1993, Volcanic textures, a guide to the interpretation of textures in volcanic rocks: Hobart, Australia, Centre for Ore Deposit and Exploration Studies (CODES), University of Tasmania, 198 p.
- Mercer, C.N., Reed, M.H., and Mercer, C.M., 2015, Time scales of porphyry Cu deposit formation: Insights from titanium diffusion in quartz: *Economic Geology*, v. 110, p. 587–602.
- Merry, N., Pontual, S., and Gamson, P., 1999, The Spectral Geologist users manual v2.0: AusSpec International Pty Ltd., 146 p.
- Meyer, C., and Hemley, J.J., 1967, Wall rock alteration, in Barnes, H.L., ed., Geochemistry of hydrothermal ore deposits, 1st ed.: New York, Holt, Rinehart and Winston, p. 166–235.
- Mitchell, A.H.G., and Balce, G.R., 1990, Geological features of some epithermal gold systems, Philippines: *Journal of Geochemical Exploration*, v. 35, p. 241–296.
- Mitchell, A.H.G., and Leach, T.M., 1991, Epithermal gold in the Philippines; island arc metallogenesis, geothermal systems, and geology: London, Academic Press, 457 p.
- Moore, D.M., and Reynolds, R.C., Jr., 1989, X-ray diffraction and the identification and analysis of clay minerals: New York, Oxford University Press, 332 p.
- Norman, M.B., II, 1974, Improved techniques for selective staining of feldspar and other minerals using amaranth: *Journal of Research of the U.S. Geological Survey*, v. 2, p. 73–79.
- Norton, D.L., 1982, Fluid and heat transport of phenomena typical of copper-bearing pluton environments, in Titley, S.R., ed., Advances in geology of porphyry copper deposits; southwestern North America: Tucson, University of Arizona Press, p. 59–72.
- Philex, 2011, Philex announces PMRC compliant mineral resource estimate for Silangan project: News release by Philex Gold Corporation, August 5, 2011.
- Proffett, J.M., 2003, Geology of the Bajo de la Alumbrera porphyry copper-gold deposit, Argentina: *Economic Geology*, v. 98, p. 1535–1574.
- Pubellier, M., Quebral, R., Defontaine, B., and Rangin, C., 1993, Neotectonic map of Mindanao (Philippines): Asia Geodyne Corporation, scale 1:800,000 with explanatory notes.
- Red 5, 2005, Annual report to shareholders: West Perth, Australia, 64 p.
- 2012, Annual report to shareholders: West Perth, Australia, 56 p.
- 2015, Annual report to shareholders: West Perth, Australia, 64 p.
- 2016, Annual report to shareholders: West Perth, Australia, 64 p.
- Redmond, P.B., and Einaudi, M.T., 2001, Temporal evolution of the intrusive-hydrothermal system at the Bingham porphyry Cu-Au-Mo deposit, Utah: Goldschmidt Conference, 11th annual, Hot Springs, Virginia, May 20–24, 2001, Abstracts.
- 2010, The Bingham Canyon porphyry Cu-Mo-Au deposit. I. Sequence of intrusions, vein formation, and sulfide deposition: *Economic Geology*, v. 105, p. 43–68.
- Redmond, P.B., Landtwing, M.R., and Einaudi, M.T., 2001, Cycles of porphyry dike emplacement, veining, alteration and mineralisation in the Bingham porphyry Cu-Au-Mo deposit, Utah: Joint sixth biennial meeting, Society for Geology Applied to Mineral Deposits (SGA) and Society of Economic Geologists (SEG), Cracow, Poland, August 26–29, 2001, Abstracts, p. 473–476.
- Redmond, P.B., Einaudi, M.T., Inan, E.E., Landtwing, M.R., and Heinrich, C.A., 2004, Copper deposition by fluid cooling in intrusion-centered

- systems; new insights from the Bingham porphyry ore deposit, Utah: *Geology*, v. 32, p. 217–220.
- Reynolds, R.C., Jr., and Reynolds, R.C., III, 1996, Newmod for Windows: Software for the calculation of one-dimensional X-ray diffraction patterns of mixed-layered clay minerals.
- Rohrlach, B.D., 2002, Tectonic evolution, petrochemistry, geochronology, and paleohydrology of the Tampakan porphyry and high-sulfidation epithermal Cu-Au deposit Mindanao, Philippines: Ph.D. thesis, Canberra, Australia, Australia National University, 499 p.
- Sajona, F.G., Bellon, H., Maury, R.C., Pubellier, M., Quebral, R.D., Cotten, J., Bayon, F.E., Pagado, E., and Pamatian, P., 1997, Tertiary and Quaternary magmatism in Mindanao and Leyte (Philippines); geochronology, geochemistry and tectonic setting: *Journal of Asian Earth Sciences*, v. 15, p. 121–153.
- Sawkins, F.J., O'Neil, J.R., and Thompson, J.M., 1979, Fluid inclusion and geochemical studies of vein gold deposits, Baguio district, Philippines: *Economic Geology*, v. 74, p. 1420–1434.
- Shannon, J.R., Walker, B.M., Carten, R.B., and Geraghty, E.P., 1982, Unidirectional solidification textures and their significance in determining relative ages of intrusions at the Henderson Mine, Colorado: *Geology*, v. 10, p. 293–297.
- Sillitoe, R.H., 1985, Ore-related breccias in volcanoplutonic arcs: *Economic Geology*, v. 80, p. 1467–1514.
- 2000, Gold-rich porphyry deposits: descriptive and genetic models and their role in exploration and discovery: *Reviews in Economic Geology*, v. 13, p. 315–345.
- 2005, Supergene oxidized and enriched porphyry copper and related deposits: *Economic Geology 100th Anniversary Volume*, p. 723–768.
- 2010, Porphyry copper systems: *Economic Geology*, v. 105, p. 3–41.
- Sillitoe, R.H., and Angeles, C.A., Jr., 1985, Geological characteristics and evolution of a gold-rich porphyry copper deposit at Guinaoang, Luzon, Philippines, *Asian Mining '85*: London, Institution of Mining and Metallurgy, p. 15–26.
- Sillitoe, R.H., and Gappe, I.M., Jr., 1984, Philippine porphyry copper deposits; geologic setting and characteristics: United Nations Coordinating Committee for Geoscience Programmes in East and Southeast Asia and Economic and Social Commission for Asia and the Pacific (CCOP-ESACP), Technical publication 14, 89 p.
- Singer, D.A., Berger, V.I., Menzie, W.D., and Berger, B.R., 2005a, Porphyry copper deposit density: *Economic Geology*, v. 100, p. 491–514.
- Singer, D.A., Berger, V.I., and Moring, B.C., 2005b, Porphyry copper deposits of the world: Database, map, and grade and tonnage models: U.S. Geological Survey Open-file Report 2005–1060, 9 p., www.pubs.usgs.gov/of/2005/1060/.
- 2008, Porphyry copper deposits of the world: Database, map, and grade and tonnage models, U.S. Geological Survey Open-file Report 2008–1155, 45 p., www.pubs.usgs.gov/of/2008/1155/.
- Titley, S.R., 1982, The style and progress of mineralization and alteration in porphyry copper systems; American Southwest, *in* Titley, S.R., ed., *Advances in geology of porphyry copper deposits; southwestern North America*: Tucson, University of Arizona Press, p. 93–116.
- United Nations Development Program, 1984, *Geology of northern Agusan, Mindanao*: Technical report 2, DP/UN/PHI-79-004/6, New York, United Nations, 36 p.
- 1987, *Geology and Gold Mineralization of Surigao del Norte*: Technical report 4, DP/UN/PHI-85-001/4, Manila, United Nations, 60 p.
- Walker, G.P.L., 1971, Grain-size characteristics of pyroclastic deposits: *Journal of Geology*, v. 79, p. 696–714.
- Walther, H.W., Foerster, H., Harre, W., Kreuzer, H., Lenz, H., Mueller, P., and Raschka, H., 1981, Early Cretaceous porphyry copper mineralization on Cebu Island, Philippines, dated with K-Ar and Rb-Sr methods: *Geologisches Jahrbuch. Reihe D: Mineralogie, Petrographie, Geochemie, Lagerstättenkunde*, v. 48, p. 21–35.
- Waters, P.J., Cooke, D.R., Gonzales, R.I., and Phillips, D., 2011, Porphyry and epithermal deposits and $^{40}\text{Ar}/^{39}\text{Ar}$ geochronology of the Baguio district, Philippines: *Economic Geology*, v. 106, p. 1335–1363.
- White, N.C., and Hedenquist, J.W., 1990, Epithermal environments and styles of mineralization; variations and their causes, and guidelines for exploration: *Journal of Geochemical Exploration*, v. 36, p. 445–474.
- Wilson, A.J., Cooke, D.R., and Harper, B.L., 2003, The Ridgeway gold-copper deposit; a high-grade alkalic porphyry deposit in the Lachlan fold belt, New South Wales, Australia: *Economic Geology*, v. 98, p. 1637–1666.
- Wolfe, R.C., and Cooke, D.R., 2011, Geology of the Didipio region and genesis of the Dinkidi alkalic porphyry Cu-Au deposit and related pegmatites, Northern Luzon, Philippines: *Economic Geology*, v. 106, p. 1279–1315.
- Wormald, P.J., Orr, T.O.H., and Hodgkinson, I.P., 1993, The Mount Leyshon gold mine (NE Queensland), and intrusive breccia and igneous complex, *in* Henderson, R.A., ed., *Field Excursion Guidebook, Charters Towers, June 12–14, 1993*, Geological Society of Australia, Queensland Division: Townsville, Australia, James Cook University, Australia, p. 61–74.



David Braxton is the head of discovery strategy for Anglo American plc, a role linking his profound minerals systems interests to systems-wide value drivers in the natural resources sector. His responsibilities include setting the strategic framework and portfolio management for global discovery and leading the global generative group. He holds three geology degrees including a Ph.D. degree (CODES, University of Tasmania, Australia, 2007), an M.Sc. degree (University of Utah, Utah, 1997), and a B.A. degree (Earlham College, Indiana, 1992). David has had the privilege of sharing discovery success with leading teams, working in more than 30 countries on some of Earth's most significant mineral deposits.

